



UNIVERSITÀ DI NAPOLI “FEDERICO II”

DOTTORATO DI RICERCA

IN

“RISCHIO SISMICO”

XXI CICLO

Tesi di Dottorato

Development and test of tunable mechanical
monolithic horizontal accelerometer
for low frequency seismic noise measurement

Dr. Gerardo Giordano

2008



UNIVERSITÀ DI NAPOLI “FEDERICO II”

DOTTORATO DI RICERCA

IN

“RISCHIO SISMICO”

XXI CICLO

Tesi di Dottorato

Development and test of tunable mechanical
monolithic horizontal accelerometer
for low frequency seismic noise measurement

Dr. Gerardo Giordano

Advisors

Prof. Fabrizio Barone (Tutor)

Prof. Leopoldo Milano (Referee)

Coordinator of the Ph.D. course

Prof. Paolo Gasparini

2008

A S. Maria Regina Pacis

In teoria, non c'è differenza tra pratica e teoria.

In pratica, la teoria è diversa dalla pratica.

In theory, there is no difference between practice and theory.

In practice, theory is different from practice.

Jan LA van de Snepscheut

Contents

Introduction	1
1 Seismic waves	4
1.1 Stress and strain tensor	4
1.1.1 The Hooke's law	7
1.2 The equation of the seismic wave	9
1.2.1 The seismic wave equation	10
1.2.2 The P- and S- waves	12
1.2.3 Surface waves	15
1.3 Seismic sensor	21
1.3.1 Accelerometer	22
1.3.2 Different type of sensors	23
1.3.3 Low frequency sensor	25
2 Mechanics of the accelerometer	27
2.1 Mechanical model	28
2.1.1 Introduction	28
2.1.2 Folded pendulum	29
2.1.3 Open loop mechanical transfer function	31
2.1.4 Potential energy of a folded pendulum	36

2.1.5	Thermal noise	39
2.1.6	The calibration mass	40
2.2	Mechanical design	44
2.2.1	Mechanical requirements	45
2.2.2	Material choice	46
2.2.3	Elliptical hinges	46
2.3	Realized prototype	53
2.3.1	Measured open loop transfer function	55
2.4	Q, mechanical quality factor	59
2.4.1	Measured quality factor in air	60
2.5	Quality factor with different weights	62
2.5.1	Measured quality factor in vacuum	68
2.6	Simulation	69
3	Readout	72
3.1	General schema of the readout system	72
3.2	Light sources	74
3.3	Choice of the position sensor	77
3.3.1	Quadrants photodiodes sensitivity	77
3.3.2	Position sensing devices sensitivity	79
3.3.3	Quadrant photodiodes and PSD sensitivity comparison	80
3.4	Position Sensing Device	82
3.4.1	PSD noise	84
3.4.2	PSD signal to noise ratio	86
3.5	Power supply	87
3.6	Reading amplifier	90
3.6.1	Generality on noise reduction	90
3.6.2	Amplifier noise	91

3.6.3	Operational amplifier noise	93
3.6.4	Transimpedance amplifier	99
3.6.5	Inverting amplifier	103
3.6.6	Differential amplifier	104
3.6.7	Divider	105
3.7	The better choice	108
4	The accelerometer	110
4.1	Force balanced accelerometer	110
4.2	Digital and analog controller	113
4.2.1	Open-loop transfer function analysis	116
4.3	Feedback control design	117
4.3.1	Corrector	119
4.3.2	PID control design	119
4.4	Calibration of the accelerometer	123
4.5	Sensitivity Curve	125
4.5.1	Interferometric readout	126
	Conclusions	131
	Bibliography	137
A	Work hints	141
A.1	Structural specification of the folded pendulum	141
A.2	Spot light waist	141
A.3	Cross talk of the electronic circuit	143
A.4	Acronyms	146

B	Mathematical hints	147
B.1	Transfer function of a PID feedback control	147
B.2	Quality factor: an electric approach	149
B.3	The dB unity	150
B.4	Equivalent noise band	151

Introduction

Seismic Hazard is a physical process or an event that describes the potential for dangerous, earthquake-related natural phenomena such as ground shaking, fault rupture, or soil liquefaction. These phenomena could cause adverse consequences to society such as loss of life, destruction of buildings, properties or threat to human society or its well-being. *Seismic Risk* is the probability of a specific loss as consequence of a seismic hazard.

The output of the seismic hazard analysis could be a description of the intensity of shaking of a nearby magnitude eight earthquake or a map which shows levels of ground shaking in different regions of a country having equal chance of being exceeded, while the output of the seismic risk analysis could be the probability of damage from a nearby magnitude eight earthquake or the probability of fatalities due to seismically induced buildings accidents.

For a correct evaluation of the seismic hazard we have to consider several aspects:

- the characterization of the source or sources of the hazard, in terms of size, spatial location, orientation, slip type, probability of rupture, etc.;
- the characterization of the seismic wave propagation until a particular location;
- the site response to a particular earthquake, in terms of peak ground acceleration (PGA) or in term of response spectra (relation between amplitude of the ground accelerations and its frequency): in fact the amplitude of earthquake

ground motion can be increased or decreased by both the properties and the configuration of the near surface material through which seismic waves propagate. For this reason the same earthquake, at the same distance from the source, can produce different ground acceleration in function of the site response.

By considering the approach to seismic zonation of a country, characterized by ground motion, slope instability and liquefaction, we can divide the knowledge level in three parts which are more and more accurate:

- Grade 1: the only knowledge we have is from historical earthquakes, from interviews with local residents and from geological and geomorphological maps; the typical scale of this mapping is $1 : 1\,000\,000 \div 1 : 50\,000$.
- Grade 2: the knowledge is from simplified geotechnical studies, from air photos, from field studies and from remote sensing; the typical scale of this mapping is $1 : 100\,000 \div 1 : 10\,000$.
- Grade 3: this level of knowledge is the more accurate and it is based on geotechnical investigation and analysis of recorded data of ground motion; the typical scale of this mapping is $1 : 25\,000 \div 1 : 1 : 5\,000$.

From this, it is clear that for a more accurate mapping of seismic hazard it is necessary to have a kind of sensors which can record with high accuracy and in a broad frequency band, in particular at low frequency, because much of the energy released during an earthquake results in teleseismic signals with periods ranging from hours to seconds.

The work we present is related to the development of a new kind of seismic sensor, optimized for very low frequency and having a sensitivity best of the actual commercial instrument and very little dimensions. It is based on the schema of the

folded pendulum and it is monolithical, so we can have a great sensitivity in low frequency because of the little contribution due to the thermal noise. This work describe how we have implemented this sensor to use as an accelerometer and the various hints to reach some original results. This thesis work is organized in the following parts:

- in the chapter 1 we will discuss about seismic signals and about the instruments used to measure them.
- the chapter 2 is dedicated to the mechanics of the sensor, and it is presented an analytical discussion of the folded pendulum, followed by our implementation and the most significative measurement on the mechanical part;
- in the chapter 3 is discussed the readout of the system, with a little description of the optical readout, the electronic implementation and the measurement of the electronic noise;
- in the chapter 4 we will present the feedback control necessary to use the system as an accelerometer and so the improvement in sensitivities as seismometer and as accelerometer with different readout systems and configuration, in comparison with commercial products;
- in the last chapter are exposed the conclusion of the this work and a little discussion on the possible development of the system.

Chapter 1

Seismic waves

A description of seismic waves requires the characterization of the internal forces and deformations in solid materials. We'll show a brief review of the theory of stress and strain and how they are linked through the constitutive relationships that describe the nature of the elastic solids. Then, by using this theory we construct the seismic wave equation for elastic wave propagation in uniform whole space and, by solving this equation, we obtain the solutions, that are plane waves called *body waves*, and, if in the medium there is a free surface, we'll show that exists other solutions, called *surface waves*.

1.1 Stress and strain tensor

The mechanical response of a material can be characterized with some parameters related to the internal force (stress) and deformation (strain); some relations can be used to relate the stress parameters to the the strain ones.

The stress tensor

The stress tensor describes internal forces in a solid volume. Let's consider a small volume inside of a solid body; the external forces that act on this block are called *body forces*: they are originated outside the block and act on every molecule within the block. The existence of a surface on the volume generate the *surface forces*, which are forces that act on the surface of the block through surrounding molecules, through atomic and molecular bonding. Principally, these forces are between neighbors and next-nearest neighbors. The surface force on the unit area of the surface is called the stress [21].

Let's consider an infinitesimal plane of arbitrary orientation within an homogeneous elastic medium in a static equilibrium. Let be \hat{n} the unit normal vector that specify the orientation of the plane. The force on the unit of area exerted by the side in the \hat{n} direction across this plane is called *traction* and is represented by a vector $\vec{t}(\hat{n})$. The component of \vec{t} normal to the plane is termed *normal stress*; the parallel component is called *shear stress*. Note that in the case of a fluid, there is no shear stress and $\vec{t} = -P\hat{n}$, where P is the pressure.

By indicating with n_1 , n_2 and n_3 the component of \hat{n} normal to the planes $x_2 x_3$, $x_1 x_3$ and $x_1 x_2$ respectively, we can define the stress tensor T_{ij} in Cartesian coordinates system by the traction across this planes as:

$$T_{ij} = \begin{bmatrix} t_1(n_1) & t_1(n_2) & t_1(n_3) \\ t_2(n_1) & t_2(n_2) & t_2(n_3) \\ t_3(n_1) & t_3(n_2) & t_3(n_3) \end{bmatrix}$$

Because the stress tensor is symmetric, it contains only six independent components. The traction across any arbitrary plane of orientation defined by \hat{n} , may be obtained by multiplying the stress tensor with \hat{n}

$$\vec{t}(\hat{n}) = T \hat{n}$$

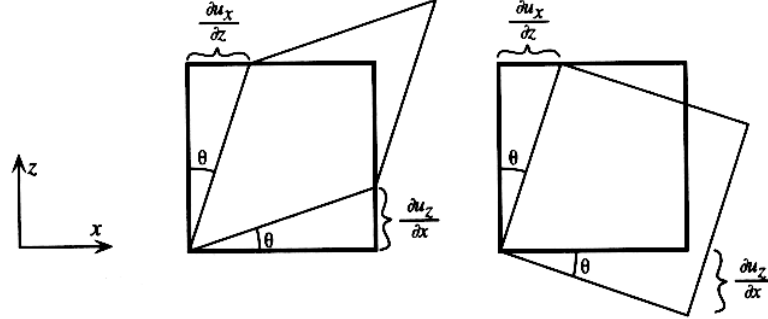


Figure 1.1: *The effects of the strain tensor E (on the left) and the rotation tensor W (on the right) with respect of the deformation of a square in a bidimensional cartesian reference system (x, z) .*

The stress tensor is a linear operator which produces the traction vector \vec{t} from normal \vec{n} , so it exists independently of any particular coordinate system. The stress tensor generally varies with position in a material; it is a measure of the force acting on infinitesimal planes at each point in the solid. The stress provides a measure only of the forces exerted across these planes and has units of force on unit of area; other forces may be present (for example the gravity), termed body forces, that have dimension of forces on unit of volume or mass.

The strain tensor

If we consider a volume in a three dimensional space, we can identify any point with a vector $\vec{r} = (x_1, x_2, x_3)$. If there is a deformation, the point \vec{r} can be indicated with a new vector $\vec{r}' = (x'_1, x'_2, x'_3)$, and we can define the deformation vector $\vec{u} = \vec{r}' - \vec{r}$. In this way the coordinates x'_i depend on the coordinates x_i and so the deformations u_i depend on x_i . Consider an infinitesimal deformation, the differential $d\vec{u}$ is

$$du_i = \partial_j u_{ij} dx_j + O(dx_j^2)$$

where we adopt the Einstein's convention (a repeated index means the sum over this index) and the convention that $\partial_j u_{ij} = \frac{\partial u_i}{\partial x_j}$. The matrix $\partial_j u_{ij}$ is the Jacobian matrix J (displacement gradient matrix) associated with the displacement field \vec{u} in the Cartesian coordinate system.

The matrix J can be written as a sum of a symmetric matrix E and a skew-symmetric matrix W , where $E = (J + J^T)/2$ and $W = (J - J^T)/2$. The elements of E and W are

$$\begin{aligned} E_{ij} &= \frac{1}{2} (\partial_j u_{ij} + \partial_i u_{ji}) \\ W_{ij} &= \frac{1}{2} (\partial_j u_{ij} - \partial_i u_{ji}) \end{aligned} \quad (1.1)$$

The symmetric matrix E represents a second order symmetric tensor (the irrotational strain sensor) and W matrix a second order skew-symmetric rotation matrix [21].

Consider an infinitesimal cube like that shown in figure 1.1. The off-diagonal elements of E cause shear strain; for example, in two dimension, if $W = 0$ and there is no volume change, then

$$J = E = \begin{bmatrix} 0 & \theta \\ \theta & 0 \end{bmatrix} = \begin{bmatrix} 0 & \partial_3 u_{13} \\ \partial_1 u_{31} & 0 \end{bmatrix}$$

where θ is the angle (in radians) through which each side rotates. Note that the total change in angle between the sides is 2θ . The W tensor, instead, causes rigid rotation, so, if $E = 0$, then

$$J = W = \begin{bmatrix} 0 & \theta \\ -\theta & 0 \end{bmatrix} = \begin{bmatrix} 0 & \partial_3 u_{13} \\ \partial_1 u_{31} & 0 \end{bmatrix}$$

1.1.1 The Hooke's law

In elastic media stress and strain are related by a stress-strain relationship (constitutive relationship). The most general linear relationship between stress and strain

tensor is the *Hooke's law* [21]:

$$T_{ij} = c_{ijkl}E_{kl} \quad (1.2)$$

where c_{ijkl} is the *elastic tensor*. The equation 1.2 assumes perfect elasticity, so there is no energy loss as the material deforms in response to applied stress. The elastic tensor is a fourth-order tensor with 81 components: because of the symmetry of the stress and strain tensor, only 21 of these components are independent.

By assuming isotropy (that is c_{ijkl} invariant with respect to rotation), it can be shown that the number of independent parameters can be reduced to two and

$$c_{ijkl} = \lambda\delta_{ij} + \mu(\delta_{il}\delta_{jk} + \delta_{ik}\delta_{jl})$$

with λ and μ called *Lamé parameters* of the material and δ_{ij} the Kronecker's delta. Then the stress-strain relationship 1.2 for an isotropic solid is [8]:

$$\begin{aligned} T_{ij} &= [\lambda\delta_{ij} + \mu(\delta_{il}\delta_{jk} + \delta_{ik}\delta_{jl})]E_{kl} \\ &= \lambda\delta_{ij}E_{kk} + 2\mu E_{ij} \end{aligned} \quad (1.3)$$

The Lamé parameters completely describe the linear stress-strain relationship within an isotropic solid:

μ is termed the *shear modulus* and it is a measure of the resistance of the material to shearing;

λ does not have a simple physical explanation.

Other commonly used elastic constants for describing isotropic solids are:

- E , the *Young modulus*: the ratio of extensional stress to the resulting extensional strain for a cylinder being pulled on both ends:

$$E = \frac{(3\lambda + 2\mu)\mu}{(\lambda + \mu)}$$

- k , the *bulk modulus*: the ratio of hydrostatic pressure to the resulting volume change, a measure of the incompressibility of the material:

$$k = \frac{\lambda + 2\mu}{3}$$

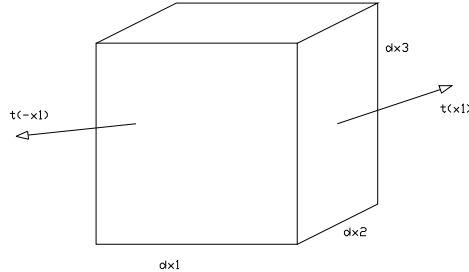


Figure 1.2: *Picture of the force on the x_2-x_3 face of an infinitesimal cube in (x_1, x_2, x_3) cartesian space.*

- σ , the Poisson's ratio: the ratio of the lateral contraction of a cylinder (being pulled on its ends) to its longitudinal extension:

$$\sigma = \frac{\lambda}{2(\lambda + \mu)}$$

1.2 The equation of the seismic wave

In the last section we have considered the stress, strain and displacement field in a static equilibrium and constant in time; because seismic waves are time-dependent phenomena that involve velocities and accelerations, we need to account for the effect of momentum, so we must apply dynamic's law to a continuous medium.

Let's consider the force on an infinitesimal cube $dV = dx_1 dx_2 dx_3$ in (x_1, x_2, x_3) coordinate system, as shown in figure 1.2. The surface forces on each surface of the cube are given by the product of the traction vector and the surface area:

$$F_i^S = T_{ij} n_j$$

and, integrating over all the face

$$F^S = \int_S T \cdot \hat{n} dS \quad (1.4)$$

There may also exist a net body force on the cube that acts proportionally to the volume of material, that, for all the volume, is

$$F^B = \int_V \vec{f} dV \quad (1.5)$$

By indicating with ρ the density, the mass of an infinitesimal cube is $dm = \rho dV$. The acceleration of the cube $\vec{a} = \ddot{\vec{u}}$ is given by the second time derivative of the displacement \vec{u} .

By substituting the equations 1.4 and 1.5 into $\vec{F} = m \vec{a}$ we obtain

$$\int_S T \cdot \hat{n} dS + \int_V \vec{f} dV = \rho \vec{a} \quad (1.6)$$

Applying the theorem of the divergence to the tensor

$$\int_S T \hat{n} dS = \int_V \nabla \cdot T dV \quad (1.7)$$

the equation 1.6 becomes

$$\int_V [\nabla \cdot T + \vec{f} - \rho \vec{a}] dV = 0 \quad (1.8)$$

The equation 1.8 is valid for arbitrary volume V , so the integrand function vanishes everywhere and we obtain the momentum equation [8]

$$\nabla \cdot T + \vec{f} - \rho \vec{a} = 0 \quad (1.9)$$

With no body forces, we have the homogeneous equation of motion

$$\nabla \cdot T - \rho \vec{a} = 0 \quad (1.10)$$

that describes the seismic wave propagation outside source regions.

1.2.1 The seismic wave equation

To solve the equation 1.10, we require a relationship between stress and strain, and we can express T in terms of displacement \vec{u} . By using the linear, isotropic

stress-strain relationship 1.3 and the definition of strain tensor 1.1 we have:

$$T_{ij} = \lambda \delta_{ij} \partial_k u_k + \mu (\partial_i u_j + \partial_j u_i) \quad (1.11)$$

If we substitute the equation 1.11 in the equation 1.10 we can write

$$\rho \vec{a} = \nabla \lambda (\nabla \cdot \vec{u}) + \nabla \mu \cdot [\nabla \vec{u} + (\nabla \vec{u})^T] + (\lambda + \mu) \nabla \nabla \cdot \vec{u} + \mu \nabla^2 \vec{u}$$

and by using the vector identity

$$\nabla^2 \vec{u} = \nabla \nabla \cdot \vec{u} - \nabla \times \nabla \times \vec{u}$$

we obtain the seismic wave equation [22]:

$$\rho \vec{a} = \nabla \lambda (\nabla \cdot \vec{u}) + \nabla \mu \cdot [\nabla \vec{u} + (\nabla \vec{u})^T] + (\lambda + 2\mu) \nabla \nabla \cdot \vec{u} - \mu \nabla \times \nabla \times \vec{u} \quad (1.12)$$

By considering the first two terms on the right-hand side of the equation, we see that they involve gradients in the Lamé parameters themselves and are non-zero whenever the material is non-homogeneous. Furthermore, we can consider the velocity as a function only of the depth, so the material can be modeled as a series of homogeneous layers. Within each layer, there are no gradient in the Lamé parameters and so these terms go to zero. The different solutions of each layer are linked by calculating the reflection and transmission coefficients for waves at both sides of the interface separating the layers. The effects of a continuous velocity gradient can be simulated increasing the number of layers. Then, if we ignore the gradient terms, the momentum equation for homogeneous media becomes:

$$\rho \vec{a} = (\lambda + 2\mu) \nabla \nabla \cdot \vec{u} - \mu \nabla \times \nabla \times \vec{u} \quad (1.13)$$

that is the standard form for seismic wave equation [21] [8] [22]. However, it is important to remember that it is an approximate equation, which neglects the gravity and the velocity gradient terms and assumes a linear, isotropic Earth model.

Rock/Soil Description	Average S-wave velocity (m/s)
Hard Rock	> 1500
Rock	760-1500
Very dense soil/soft rock	360-760
Stiff soil	180-360
Soft soil	< 180
Rock/Soil Description	Average P-wave velocity (m/s)
Air	330
Water	1450-1530
Sand (dry, loose)	200-1000
Sand (water saturated, loose)	1500-2000
Sand and gravel	400-2300
Clay	1000-2500
Sandstone	2500-4500
Limestone (soft)	1700-4200
Limestone (hard)	2800-7000
Dolomites	2500-6500
Shales	2000-4100
Granites	4600-6200
Basalts	5500-6500
Serpentinite	5500-6500
Gneiss	3500-6500
Concrete	3000-3500

Figure 1.3: *P- and S- wave velocities for some different materials.*

1.2.2 The P- and S- waves

We can separate the equation 1.13 into solution for P-waves and S-waves by taking the divergence and the curl, respectively. Taking the divergence of equation 1.13 and using the vector identity $\nabla \cdot \nabla \times \vec{\psi} = 0$, we obtain

$$\nabla^2(\nabla \cdot \vec{u}) - \frac{1}{\alpha^2} \frac{\partial^2(\nabla \cdot \vec{u})}{\partial t^2} = 0 \quad (1.14)$$

where the P-wave velocity, α , is given by

$$\alpha^2 = \frac{\lambda + 2\mu}{\rho}$$

Taking the curl of equation 1.13 and using the vector identity $\nabla \times \nabla \phi = 0$, we obtain

$$\nabla^2(\nabla \times \vec{u}) - \frac{1}{\beta^2} \frac{\partial^2(\nabla \times \vec{u})}{\partial t^2} = 0 \quad (1.15)$$

where the S-wave velocity, β , is given by

$$\beta^2 = \frac{\mu}{\rho}$$

A table of typical seismic waves velocities is shown in table 1.3.

Potentials

The vector \vec{u} is often expressed in terms of the P-wave scalar potential ϕ and S-wave vector potential $\vec{\psi}$, using the Helmholtz decomposition theorem (Each differentiable field can be expressed as the gradient of scalar field plus the curl of vectorial field):

$$\vec{u} = \nabla\phi + \nabla \times \vec{\psi} \quad (1.16)$$

with $\nabla \cdot \vec{\psi} = 0$, so we have:

$$\nabla \cdot \vec{u} = \nabla^2\phi \quad (1.17)$$

$$\nabla \times \vec{u} = -\nabla^2\vec{\psi} \quad (1.18)$$

being $\nabla \cdot \vec{\psi} = 0$. Substituting into 1.14 and 1.15, we may obtain

$$\nabla^2\phi - \frac{1}{\alpha^2} \frac{\partial^2\phi}{\partial t^2} = 0 \quad (1.19)$$

$$\nabla^2\vec{\psi} - \frac{1}{\beta^2} \frac{\partial^2\vec{\psi}}{\partial t^2} = 0$$

The P-wave solution is given by the scalar wave equation for ϕ ; the S-wave solution is the vector wave equation for $\vec{\psi}$.

The polarization of P- and S- waves

The general solutions of equations 1.19 are plane waves described by the general function:

$$\vec{u}(\vec{r}, t) = \vec{A}(\omega)e^{i(\vec{k}\cdot\vec{r}-\omega t)}$$

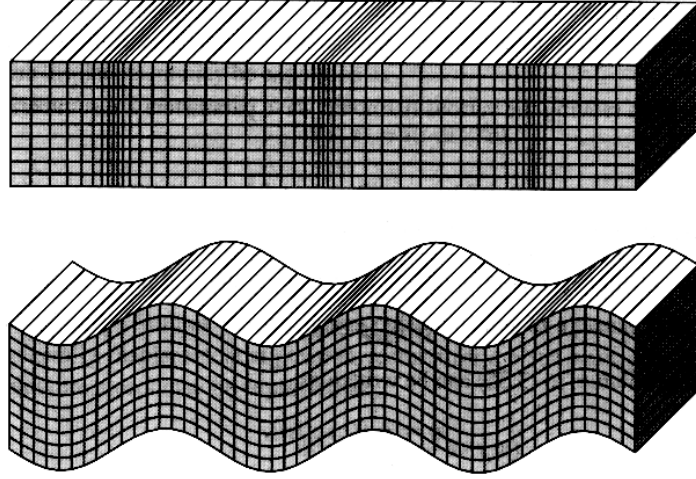


Figure 1.4: *Displacement due to an harmonic plane P-wave (top) and S-wave (bottom) traveling along the horizontal direction.*

where $\vec{k} = (\omega/c) \hat{k}$ is the wave vector and c the phase velocity of the wave. Other parameters and their relationship are shown in table 1.1.

By considering the equation for P-wave, because $\vec{u} = \nabla\phi$, we have $u_x = \partial_x\phi$, $u_y = 0$ and $u_z = 0$. Note that for a plane wave, propagating in the \hat{x} direction, there is no change in the \hat{y} and \hat{z} directions, so the spatial derivative ∂_y and ∂_z are zero. For P-waves, the only displacement occurs in the direction of propagation

Name	Symbol	Relationship
Period	T	$T = \frac{1}{f} = \frac{2\pi}{\omega} = \frac{\lambda}{c}$
Frequency	f	$f = \frac{\omega}{2\pi} = \frac{1}{T} = \frac{c}{\lambda}$
Angular frequency	ω	$\omega = 2\pi f = \frac{2\pi}{T} = c \vec{k} $
Velocity	c	$c = \frac{\lambda}{T} = f \lambda = \frac{\omega}{ \vec{k} }$
Wavelength	λ	$\lambda = \frac{c}{f} = cT = \frac{2\pi}{ \vec{k} }$
Wave vector	\vec{k}	$\vec{k} = \frac{\omega}{c} \cdot \hat{k} = \frac{2\pi}{\lambda} \cdot \hat{k} = \frac{2\pi f}{c} \cdot \hat{k}$

Table 1.1: Harmonic wave parameters

along the \hat{x} axis; such wave is termed longitudinal. Because $\nabla \times \nabla\phi = 0$, the motion is curl-free or irrotational. Since P-waves introduce volume changes in the material ($\nabla \cdot \vec{u} \neq 0$), they can also be termed compressional or dilatational. However, note that P-waves involve shearing as well as compression; this is why the P velocity is sensitive to both the bulk and shear moduli.

Consider a plane S-wave propagating in the positive \hat{x} direction. The displacement is

$$\begin{aligned} u_x &= (\nabla \times \vec{\psi})_x = \partial_z \psi_y - \partial_y \psi_z = 0 \\ u_y &= (\nabla \times \vec{\psi})_y = \partial_x \psi_z - \partial_x \psi_z = \partial_x \psi_z \\ u_z &= (\nabla \times \vec{\psi})_z = \partial_y \psi_x - \partial_x \psi_y = -\partial_x \psi_y \end{aligned} \tag{1.20}$$

thus giving

$$\vec{u} = \partial_x \psi_z \hat{y} - \partial_x \psi_y \hat{z}$$

The motion is in the \hat{y} and \hat{z} directions, perpendicular to the propagation direction. S-wave particle motion is often divided in two components: the motion within a vertical plane through the propagation vector (SV-waves) and the horizontal motion in the direction perpendicular to this plane (SH-wave). Because $\nabla \cdot \vec{u} = \nabla \cdot (\nabla \times \vec{\psi}) = 0$, the motion is pure shear without any volume change.

Particle motion for harmonic P-wave and for harmonic shear wave polarized in the vertical direction (SV-wave) is illustrated in figure 1.4.

1.2.3 Surface waves

At this point our discussion has been limited to body waves, solutions to the seismic wave equation which exist in whole spaces. Because free surfaces exist in a medium, are possible other solutions, called *surface waves*. There are two types of surface

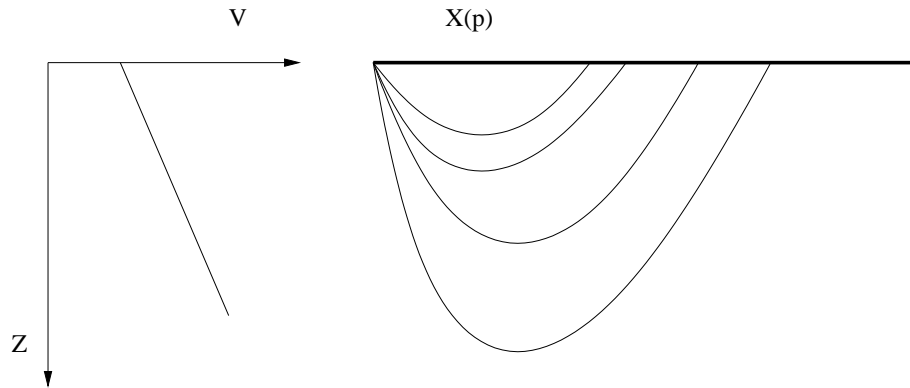


Figure 1.5: *A model with a continuous velocity increasing with depth (on the left) will curve back toward the surface the ray paths $T(p)$ (on the right).*

waves that propagate along Earth's surface, *Rayleigh waves* and *Love waves*. For laterally homogeneous models, Rayleigh waves are radially polarized (P/SV) and exist at any free surface, whereas Love waves are transversely polarized and require some velocity increase with depth (or a spherical geometry). Surface waves are generally the strongest arrivals recorded at teleseismic distances and they provide some of the best constraints on Earth's shallow structure and low-frequency source properties. They differ from body waves in many respects: they travel more slowly, their amplitude decay with range is generally smaller, and their velocities are strongly frequency dependent.

Love waves

This waves are formed through the constructive interference of high order SH surface multiples (i.e. SSS, SSSS, SSSSS, etc.), thus, it is possible to model Love waves as a sum of body waves. To see this, consider monochromatic plane wave propagation for the case of a vertical velocity gradient in a laterally homogeneous model. In this case, a plane wave defined by ray parameter p will turn at the depth where $\beta = 1/p$.

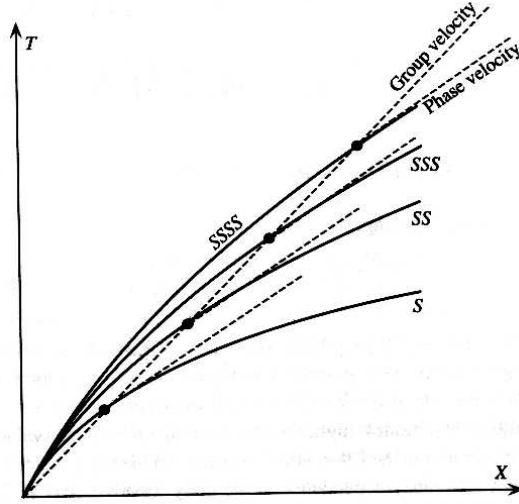


Figure 1.6: *The relationship between the phase velocity and the group velocity is shown. The dashed lines show the group and the phase velocities at a fixed value of the ray parameter p .*

Along the surface the plane waves will propagate with horizontal slowness defined by p . If the surface bounce points are separated by a distance $X(t)$, then the travel time along the surface between bounce points is given by $pX(p)$. This follows from our definition of a plane wave and does not depend upon the velocity model; in contrast, the travel time along the ray paths is given by $T(p)$ and is a function of the velocity-depth profile (see figure 1.5): if these travel times are not the same, as it generally happens, destructive interference will occur except at certain fixed frequencies. Along the surface, the phase (0 to 2π) of an harmonic wave will be delayed by $\omega p X(p)$, where ω is the angular frequency of the plane wave. The phase along the ray path is delayed by $\omega T(p) - \pi/2$, so the requirement for constructive interference is

$$\omega = \frac{n2\pi + \pi/2}{T(p) - pX(p)} \quad (1.21)$$

where n is an integer $n = 0, 1, 2, \dots$. The wave travels along the surface at velocity $c = 1/p$, thus the equation 1.21 defines the $c(\omega)$ function for the Love waves, often termed as dispersion curve. The values of ω given $n = 0$ are termed the fundamental modes; highest modes are defined by larger values of n . The frequency dispersion in the Love waves results from ray geometry and does not require any frequency dependence in the body wave velocity β .

c is defined as *phase velocity*, and it is the velocity with which the peaks and troughs at a given frequency move along the surface. When the phase velocity varies as a function of frequency, as in equation 1.21, the wave is spreaded and the *group velocity* U (the velocity with which the energy propagates) will be different from the phase velocity. In the Love waves, the energy must move along the actual ray path and thus the group velocity U is defined by

$$U = \frac{X(p)}{T(p)}$$

The relationship between the phase velocity and the group velocity is shown in figure 1.6 as a sum of SH surface waves.

Rayleigh Waves

The reflection coefficient of SH polarized waves at the free surface is equal to one, and the interference between the downgoing SH-waves and those turned back toward the surface, produces Love waves. The P/SV system is more complicated because the surface reflections involve both P- and SV-waves. In this case, the upgoing and downgoing body waves do not sum constructively to produce surface waves. However, a solution is possible for inhomogeneous waves trapped at the interface: the resulting surface waves are termed Rayleigh waves [8] [22].

Now we examine what occurs when P- and SV-waves interact with a free surface. For a laterally homogeneous medium, the displacements for harmonic plane waves

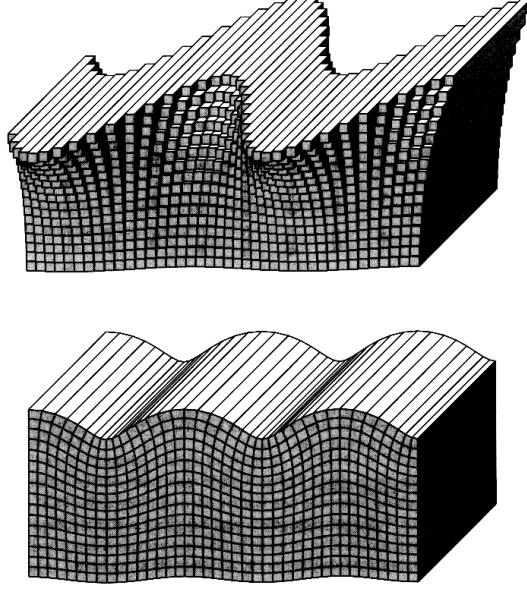


Figure 1.7: *Ground displacement occurring from a Love (top) and a Rayleigh (bottom) waves traveling horizontally.*

propagating in the $+\hat{x}$ direction are given by

$$\vec{u} = \mathbf{A}e^{-i\omega(t-px-\eta z)} \quad (1.22)$$

where p is the horizontal slowness and $\eta = \sqrt{1/c^2 - p^2}$ is the vertical slowness for the wave velocity c . Consider a plane wave solution for ϕ and ψ_y (the only component of $\vec{\psi}$ that produces SV motion for plane wave propagation in the \hat{x} direction):

$$\phi = Ae^{-i\omega(t-px-\eta_\alpha z)} \quad (1.23)$$

$$\psi_y = Be^{-i\omega(t-px-\eta_\beta z)} \quad (1.24)$$

where A and B are the amplitude of P- and SV-waves respectively, and the vertical slownesses are η_α and η_β . The ray parameter p is constant and both P- and SV are assumed to have the same horizontal slowness. By considering the boundary conditions at the free surface ($z = 0$), both the normal and the shear traction must

vanish, and, recalling the equation 1.3 it is possible to obtain a set of equations for the ray parameter and for the vertical slownesses:

$$A(2p\eta_\alpha) - B(p^2 - \eta_\beta^2) = 0 \quad (1.25)$$

$$A[\alpha^2(p^2 + \eta_\alpha^2) - 2\beta^2p^2] - B(2\beta^2\eta_\beta p) = 0$$

This coupled set of equations describes the free surface boundary condition for P- and SV-waves with horizontal slowness p . When $p < 1/\alpha$, there are two real solutions, a positive value of η_α for down-going P-waves and a negative value for up-going P-waves (assuming the z axis points down-going). Similarly, when $p < 1/\beta$, then η_β is real and there exist both down-going and up-going SV-waves. Our interest is in the case of $p > \beta^{-1} > \alpha^{-1}$ and both η_α and η_β are imaginary. In this case the equation 1.22 becomes

$$\vec{u} = \vec{A}e^{i\omega\eta z} e^{-i\omega(t-px)} \quad (1.26)$$

where we see that imaginary values of η will lead to real values in the exponents and so the wave amplitude decays exponentially as a function of depth. For $z = 0$ we have only single imaginary values of η and the linear system of equation for A and B given in 1.25 has a non trivial solution only when the determinant vanishes; substituting η_α and η_β , we can obtain an equation involving the ray parameter p and the body waves velocities α and β

$$\left(2p^2 - \frac{1}{\beta^2}\right)^2 - 2p^2 \left(p^2 - \frac{1}{\alpha^2}\right)^{1/2} \left(p^2 - \frac{1}{\beta^2}\right)^{1/2} = 0 \quad (1.27)$$

called the Rayleigh function, that has a single solution, with the exact value of p depending upon α and β . By using the solution for p we can obtain the relative amplitude of the P and SV components and so, using the relations 1.16, the vertical and horizontal displacements also.

Particle motion for both Love and Rayleigh waves are compared in figure 1.7, where

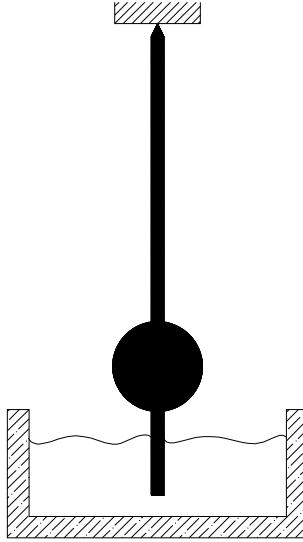


Figure 1.8: *A simple inertial seismometer for measuring horizontal motion.*

we see that Love waves are purely transverse motion, whereas Rayleigh waves contain both vertical and radial motion; in both cases, the wave amplitude decays strongly with depth..

1.3 Seismic sensor

In this first chapter we have discussed Earth's motion in terms of the displacement field $\vec{u}(\vec{x}, t)$, but we have not mentioned how these movements are actually recorded. A device that detects seismic wave motion is termed seismometer; the entire instrument package, including the recording apparatus, is called seismograph. The most common type of seismometer is based on the inertia of a suspended mass, which tends to remain stationary in response to external vibrations. As an example, figure 1.8 shows a simple seismometer scheme that will detect horizontal ground motion.

A mass is suspended with a wire and connected in a manner that it can move only in the horizontal direction (as a pendulum). The motion is damped using a *dash pot* to prevent excessive oscillations near the resonance frequency of the system. What is measured is the differential motion between the mass and the seismometer case, which is rigidly connected to the Earth (see figure 1.8). In alternative seismometer designs, the displacement or acceleration of the mass may be measured. Another scheme, which is similar to the one shown in figure 1.8, can be used to detect vertical ground motion; in this case, for example, a simple configuration can be a mass suspended with a spring, constrained to move along the vertical direction. Both vertical and horizontal instruments, based on a suspended mass, are called *inertial seismometers*.

1.3.1 Accelerometer

The best modern instruments are more sophisticated than the simple mechanical seismograph illustrated in figure 1.8. They are designed to achieve a linear response to Earth motion over a wide range of both amplitude and frequency. Mechanical non-linearity can arise from the finite length of the levers and springs used in the instrument's design. For example, the design shown in figure 1.8 will be linear only for excursions of the mass which are small compared to the length of the lever arm. Linearity is often maintained in modern instruments through the use of force-feedback designs in which the mass is maintained at a fixed point. The seismograph records a measure of the force that is required to keep the mass at rest, being the mass constant the force applied is directly proportional to the external acceleration, so this force is directly related to Earth's acceleration: by a measure of the applied force we can have a measure of the acceleration, so the same mechanical sensor (seismometer) became an accelerometer when we add a feedback control.

1.3.2 Different type of sensors

Modern seismometers can be roughly divided into three types by purpose of use: sensitivity seismometers for earthquake research observation, strong-motion seismometers for earthquake engineering, and control-type seismometers for secondary disaster prevention.

- Sensitivity seismometers for earthquake research observation: a typical sensitivity seismometer is an electrodynamic seismometer. This kind of seismometer measures micro earthquakes, that the human body cannot feel. This seismometer is required to detect the rising part of the waveform of P- and S-waves, which will be necessary for determining the hypocenter, and to record the exact times. To ensure this sensitivity observation, it is essential to eliminate miscellaneous man-made vibrations. Thus, sensitivity seismometers should be installed in earthquake observation stations distant from urban cities or in very deep underground observation bore.
- Strong-motion seismometers for earthquake engineering: a strong-motion seismometer mainly refers to a seismometer used to record how the ground under a structure responds to strong earthquake motions. Strong-motion seismometers start up only after they detect an earthquake greater than a preset level. They use their vertical movement components to detect the earliest P-waves, and this detection starts them up. They record waveform data with a delay circuit of ten seconds. It does take some time to cause the circuit to rise, but the seismometers can actually obtain the waveform that was generated earlier than the seismometers started recording. The earthquake data, including waveform, will be recorded; the data stored can be remotely accessed through the public telephone or data line. Thus, data from multiple locations can be collected and managed. Modern seismometers are computer systems with com-

munication capability and with internal sensitivity sensors, rather than mere mechanical seismometers. The conventional seismometers were used solely for recording waveforms. The combined use of high-performance sensors, such as servo acceleration sensors, and a microprocessor has changed this conventional seismometer into a new recording system equipped with multiple channels and functions. The new strong-motion sensor also collects wind direction and speed data along with seismic data. For this reason, the modern seismometer is also used as a disaster prevention system.

- Control-type seismometers for secondary disaster prevention: control-type seismometers issue an alarm signal immediately after an earthquake motion greater than a preset level occurs. These seismometers are not necessarily required to record seismic waves. However, they do need to offer accuracy and reliability that are different from those seen in other seismometers, since malfunction will directly cause huge economical loss or social disorder. These control-type seismometers are used to protect the infrastructure of our modern society, including railroads, nuclear plants, petrochemical complexes, and power and gas facilities. One of the familiar examples of use of the control-type seismometer is the emergency shut-down system to stop elevators in case of an earthquake. The simplified type is often interlocked with an automatic broadcast system in places where people gather, such as department stores and banks, in order to prevent panics in case of an earthquake. Display-type seismometers are used to display the extent of damage and the correct seismic intensity immediately after an earthquake. This information will be useful for evacuation and safety activities.

1.3.3 Low frequency sensor

As have we said a seismometer measure the oscillation of the ground, and it is based on the reading of the relative displacement of a suspended inertial mass with respect the ground. For an horizontal seismometer the motion of this mass is free, and the system can be schematized like a pendulum: in this way we can underline that it has a certain response frequency with a characteristic band of frequency.

Today's seismometers can be divided into three rough categories depending on their frequency band:

- Short-period (SP) seismometers measure signals in the range $[0.1, 250] Hz$
- Broadband sensors (BB) measure signals in the range $[0.01, 50] Hz$
- Very broadband (VBB) seismometers measure ground motion at frequencies from below $0.001 Hz$ to approximately $10 Hz$

For nearly a quarter of a century, the development of seismic sensors with low noise and high resolution in the low frequency band $[0.001, 10] Hz$ has languished. The choice of seismometer for this field of seismology is now over 20 years old, and is no longer being manufactured.

As we have introduced in section 1.3.1, in an accelerometer the ground acceleration on the sensor mass is *balanced* by a generated force in the opposite direction. The force can be generated by a current through a coil, that acts as a current-force transducer, and the current needed to balance the external force is linearly proportional (for little movement of the test mass) to the external acceleration, thus the sensor directly measures the acceleration.

The possible improvements on this type of sensor are related to:

- have a lower resonance frequency of the inertial part to relax of the specifications for the control in force-balanced configuration;
- have a monolithic design, to have an high mechanical quality factor, low hysteresis, low dissipation, low thermal noise, low coupling factor between different degrees of freedom;
- development of an optical readout, to get high sensitivity, low coupling with electromagnetic noise;
- development of the electronic part with low noise and high resolution ADC;
- a reduction of the cost of realization and maintenance.

In the next chapters we will discuss how we have realized an accelerometer and the original improvements for the development of the sensor, on the mechanical part and on the readout system.

Chapter 2

Mechanics of the accelerometer

An accelerometer is a seismic sensor to measure the ground motion when it is shaken by a perturbation. This motion is dynamic and the seismic sensor also has to give a dynamical physical variable related to this motion.

Our goal to reach is to measure the Earth's motion at a point with respect to this same point undisturbed; this measurement is done in a moving reference frame, in other words, the sensor is moving with the ground and there is not fixed undisturbed reference available to have a relative measure, so the displacement cannot be measured directly. According to the principle of inertia, we can only observe the motion if it has an acceleration; seismic waves cause transient motions and this implies that there must be acceleration.

So, because the measurements are done in a moving reference frame (the Earth's surface), the sensor is based on the inertia of a suspended mass, which will tend to remain stationary (according to the inertial principle) in response to external motion. The relative motion between the suspended mass and the ground then will be a function of the ground's motion.

For this reason our first attention is to realize a physical system whose mechanic can have a mass that tends to remain stationary when an external force acts on it,

like, for example, a suspended oscillating mass as a *pendulum*.

2.1 Mechanical model

To have an oscillating mass we need of a force that acts as function of the displacement, to restore the position of the mass when it move from the original (equilibrium) position. This force can be an elastic force, like a spring connected to the mass or a gravitational force like that of a simple pendulum.

Our system is monolithic so we have both the type of force.

2.1.1 Introduction

Each oscillating system has a first principal resonance frequency due to the oscillating mass and to restoring force that characterize the response of the system. The displacement of the ground can be obtained directly as the relative displacement between the mass and the Earth. Given a direction for the motion, if we imagine that the ground move in a versus, the oscillating mass move in the opposite versus, so we measure a phase shift of π in the measure of ground displacement. Similarly if the ground moves with a *very fast* sinusoidal motion (at frequency above the resonance frequency), we can expect that the mass remain stationary and thus the ground sinusoidal motion could be measured directly. The amplitude of the measurement would also be the Earth's amplitude and the seismometer would have a gain of 1. Thus the seismometer measures the relative displacement directly at high frequencies and we can say the seismometer response function (motion of mass relative to earth motion) is flat at high frequencies with a phase shift equal to π .

When we analyze the response in very low frequencies, the ground moves very slowly, the mass has “the time to *follow*” the ground motion and, in other words, there is a little relative motion and less phase shift, so the gain is low. This is also the reason

of the optimization of the system in low frequency: when the resonance frequency is very low, the corresponding gain at that low frequencies is high with respect to a system with higher resonance frequency, so we have a better mechanical sensitivity in that range of frequency; this permits a good sensitivity for the detection of the movement as input for the feedback control (and then a good sensitivity for the acceleration).

At the resonance frequency, if the damping is low, the mass could get a new push at the exact right time, like pushing a swing at the right time, so the mass would move with a larger and larger amplitude, thus the gain became larger than 1. For this to happen, the push from the Earth must occur when the mass is at an extreme position (top or bottom) and there must be a phase shift of $-\frac{\pi}{2}$.

By this short considerations we understand that the system must have the lowest possible resonance frequency and the lowest dissipation (that is a low viscosity). It is convenient that the restoring force is a gravitational force to minimize the thermal noise of the system, so we can imagine to realize a simple system by using a simple pendulum.

2.1.2 Folded pendulum

As explained in section 2.1.1 to have a good sensitivity in low frequency we need of a low resonance frequency. Considering the simple pendulum shown in figure 2.1; the resonance frequency is

$$f_r = \frac{1}{2\pi} \sqrt{\frac{g}{l}}$$

that we can rewrite as

$$\omega_r^2 = \frac{g}{l}$$

where $\omega_r = 2\pi f_r$. From this last equation we can see that if we want to have a resonance frequency of 500 mHz we need of a pendulum with an arm whose length

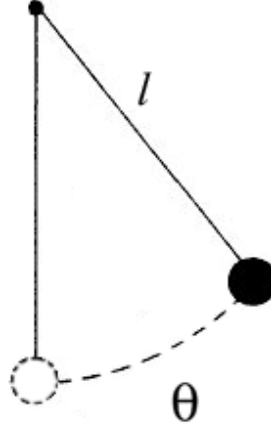


Figure 2.1: *Schema of a simple pendulum.*

is

$$l = \frac{g}{\omega_r^2} = \frac{9.8ms^{-2}}{(2\pi \cdot 0.5)^2s^{-2}} \approx 1m$$

and if we want a frequency of 50 mHz (equal to 20 seconds) we need of a length of 100 m .

The *folded pendulum*, called also Watt-linkage, is a system developed in 1962 [16], recently rediscovered for applications who require the study of ultra-low frequency phenomena [26]. In fact, a monolithic mechanical design has the great advantage of avoiding the shear effects at the contact surface among mechanical parts that can generate hysteresis and dissipation, resulting in a very compact sensor, with characteristics of thermal sensitivity and a Q-factor that assure a very good sensor directivity: coupling factors of less than 10^{-4} among the different degrees of freedom have been obtained in monolithic structures [11]. A broadband singleaxis monolithic folded pendulum of reasonable size with natural frequency of about 700 mHz has already been built [11]. Following this direction, we have developed an improved version of this monolithic seismic sensor, with good performances in terms of noise,

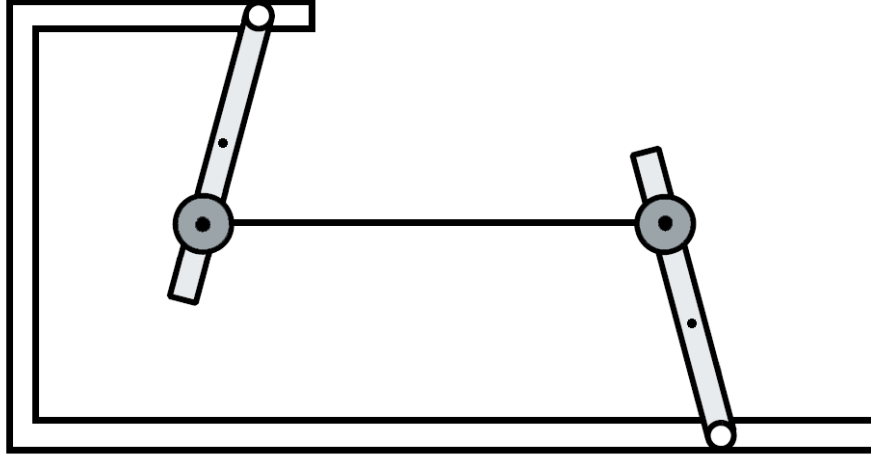


Figure 2.2: *Basic schema of the folded pendulum. Both the arm and the horizontal bar are considered with mass, the points represents the center of mass of the single elements.*

sensitivity and frequency band. In the following sections we will describe the status of the monolithic FP sensor prototype and its mechanical and optical performances.

The folded pendulum schema, shown in figure 2.2, is a configuration that allow an arbitrary low resonance frequency with little dimension of the system. It is constituted with a simple pendulum connected via a rigid massively bar to an inverted pendulum: theoretically with this configuration we have a stable equilibrium with no elastic restoring force (no material stress) and the only restoring force is the gravitational one.

2.1.3 Open loop mechanical transfer function

In figure 2.3 is shown the equivalent diagram of the folded pendulum; as we see, it consist of two arms, a pendulum of mass m_{a1} on the left and an inverted pendulum

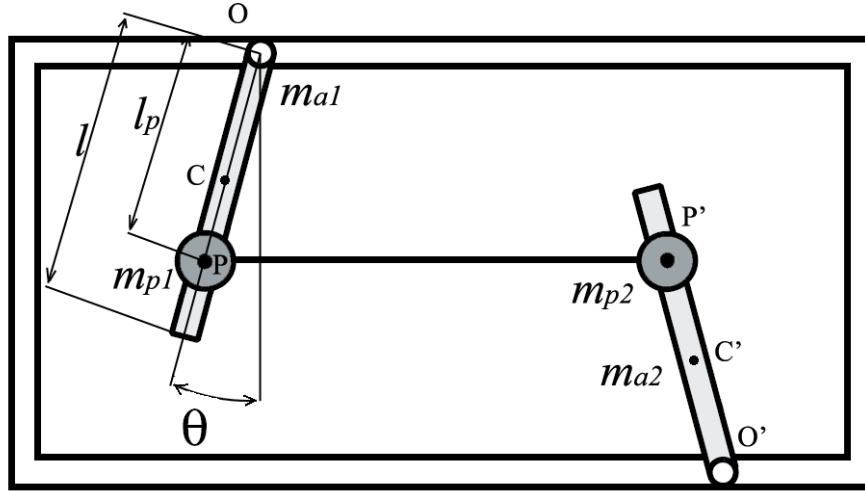


Figure 2.3: *Equivalent diagram of the folded pendulum.*

of mass m_{a2} on the right, connected with a rigid bar, whose mass, analytically, is divided into two equivalent mass approximated with the two point mass m_{p1} and m_{p2} , respectively placed on the pendulum arm and on the inverted pendulum arm (an accurate description of the analysis is given by Liu et al. [26]). The two arms have, as pivot point, the points O and O' , same length l , and the two mass m_{p1} and m_{p2} are at the same distance l_p from the points O and O' ; the points C and C' are the center of mass of the two arms. The bar is hinged to the two arms in the center of the two mass m_{p1} and m_{p2} , the points P and P' . The points O , O' , P , P' , C and C' have coordinates x_O , $x_{O'}$, x_P , $x_{P'}$, x_C and $x_{C'}$ respectively, while θ and θ' are the two angles from the vertical directions.

In the approximation of small oscillations (little angle of deflection of the vertical arms) we consider $\theta \approx \theta'$, $\dot{x}_C \approx \dot{x}_{C'}$ and $\dot{x}_P \approx \dot{x}_{P'}$.

To solve the Lagrange equation of the system we calculate the kinetic energy T and

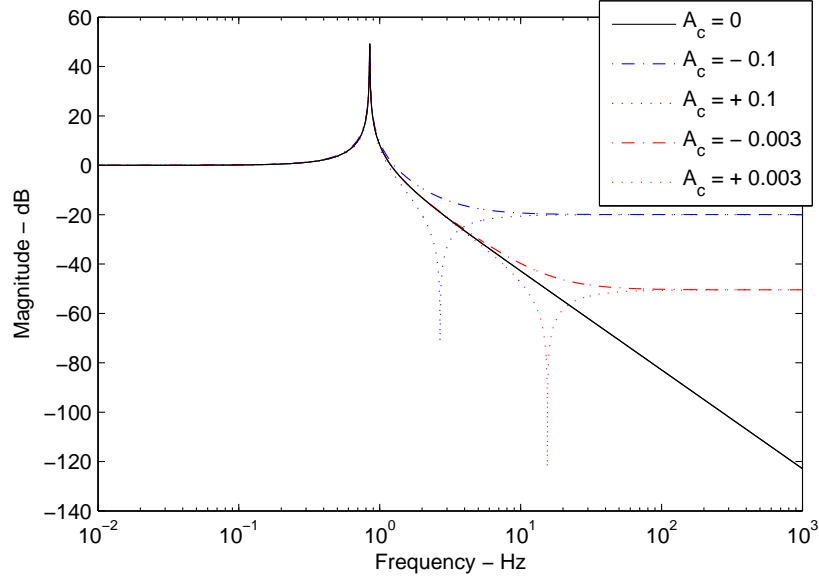


Figure 2.4: *Theoretical transfer function of the folded pendulum for resonance frequency of 721 mHz and different values of A_c .*

the potential energy V ,

$$T = \frac{1}{2}(I_1 + I_2)\dot{\theta}^2 + \frac{1}{2}(m_{a1} + m_{a2})\dot{x}_C^2 + (m_{p1} + m_{p2})\dot{x}_P^2 \quad (2.1)$$

$$V = \frac{1}{2}(2m_{p1} + m_{a1})lg - \frac{1}{2}(m_{a1} - m_{a2})lg \cos \theta - (m_{p1} - m_{p2})l_p g \cos \theta \quad (2.2)$$

where I_1 and I_2 are the moments of inertia of the two arms along the perpendicular axes through their center of mass C and C' respectively. Now we can suppose that a force f is applied directly on the pendulum platform in the x direction, and two forces, f_{x1} and f_{x2} are applied at the ends of the two pendula arms, in the pivot points O and O' , by the frame (an earthquake, for example); so the potential of the horizontal forces is

$$U = - \int (f_{x1} + f_{x2}) dx_O - \int f dx_P \quad (2.3)$$

The Lagrangian expression became $L = T - V - U$; to have L as a function of only two variable, x_O and x_P , we can introduce the following terms:

$$x_C = x_O - \frac{1}{2}l\theta \quad \theta = \frac{x_O - x_P}{l_P} \quad I_1 = \frac{1}{12}m_{a1}l^2 \quad I_2 = \frac{1}{12}m_{a2}l^2 \quad (2.4)$$

By solving the Lagrange equations

$$\frac{d}{dt} \frac{\partial L}{\partial \dot{x}_O} - \frac{\partial L}{\partial x_O} = 0 \quad \text{and} \quad \frac{d}{dt} \frac{\partial L}{\partial \dot{x}_P} - \frac{\partial L}{\partial x_P} = 0 \quad (2.5)$$

and merging the two equations into one to have $f_{x1} + f_{x2}$, by retaining the first order terms, we can express them as

$$\begin{aligned} & - \left[\frac{1}{3}(m_{a1} + m_{a2})\frac{l^2}{l_p^2} + (m_{p1} + m_{p2})l_p \right] \ddot{x}_P + \\ & + \left[\frac{1}{3}(m_{a1} + m_{a2})\frac{l^2}{l_p} - \frac{1}{2}(m_{a1} + m_{a2})l \right] \ddot{x}_O = \\ & = - \left[\frac{1}{2}(m_{a1} - m_{a2})\frac{l}{l_p} + (m_{p1} - m_{p2})l_p \right] \cdot (x_O - x_P)g - l_P f \end{aligned} \quad (2.6)$$

Now we assume that $f = Fe^{i\omega t}$, $x_O = X_O e^{i\omega t}$, $x_P = X_P e^{i\omega t}$ and set $x_O = 0$ and $f = 0$ respectively for force excitation and base excitation. We can choose to give the force excite and the base excite in a form similar to that of a simple pendulum, having the following transfer functions

$$\frac{X_P}{F} = \frac{1}{M_e \omega_0^2 \left(1 - \frac{\omega^2}{\omega_0^2}\right)} \quad (2.7)$$

$$\frac{X_P}{X_O} = \frac{1 - A_c \frac{\omega^2}{\omega_0^2}}{1 - \frac{\omega^2}{\omega_0^2}} \quad (2.8)$$

where

$$M_e = \frac{1}{3}(m_{a1} + m_{a2})\frac{l^2}{l_p} + (m_{p1} + m_{p2}) \quad (2.9)$$

$$\omega_0^2 = \frac{(m_{a1} - m_{a2})\frac{l}{2l_p} + (m_{p1} - m_{p2})g}{(m_{a1} + m_{a2})\frac{l^2}{3l_p^2} + (m_{p1} + m_{p2})l_p} \quad (2.10)$$

$$A_c = \frac{\left(\frac{1}{3l_p} - \frac{1}{2}\right)(m_{a1} + m_{a2})}{(m_{a1} + m_{a2})\frac{l}{l_p} + (m_{p1} + m_{p2})\frac{l_p}{l}} \quad (2.11)$$

in which we can see that if $A_c = 0$ the folded pendulum is equivalent to a simple pendulum with equivalent mass M_e and equivalent length

$$l_e = \frac{(m_{a1} + m_{a2})\frac{l^2}{3l_p^2} + (m_{p1} + m_{p2})}{(m_{a1} - m_{a2})\frac{l}{2l_p^2} + (m_{p1} - m_{p2})} l_p \quad (2.12)$$

A graph of the transfer function described by the equation 2.8 is shown in figure 2.4 where we have calculated the response to base excite with a mechanics with resonance frequency of 720 mHz . Note that the response of the mechanical system is flat for low frequency and decrease to the increasing of the frequency, showing a trend like that of a low-pass filter.

From the equation 2.10 we can see that with an opportune choice of the values of the mass m_{a1} , m_{a2} , m_{p1} and m_{p2} we can obtain any equivalent length, that is the same to say any arbitrarily low resonance frequency.

By considering two extreme cases of the folded pendulum, we can confirm these equations: in a first case, we can degenerate the folded pendulum to a simple pendulum by choosing the value for the mass m_{p1} as

$$m_{p1} \gg m_{a1}, m_{a2}, m_{p2} \quad (2.13)$$

that is a low value for the mass of the arm of the simple pendulum and both the mass of the inverted pendulum, obtaining the resonance frequency

$$\omega_0 = \sqrt{\frac{g}{l_p}} \quad (2.14)$$

the frequency of a simple pendulum; in a second case, the case of an inverted pendulum, with mass m_{a1} related to other mass as

$$m_{a1} \gg m_{a2}, m_{p1}, m_{p2} \quad (2.15)$$

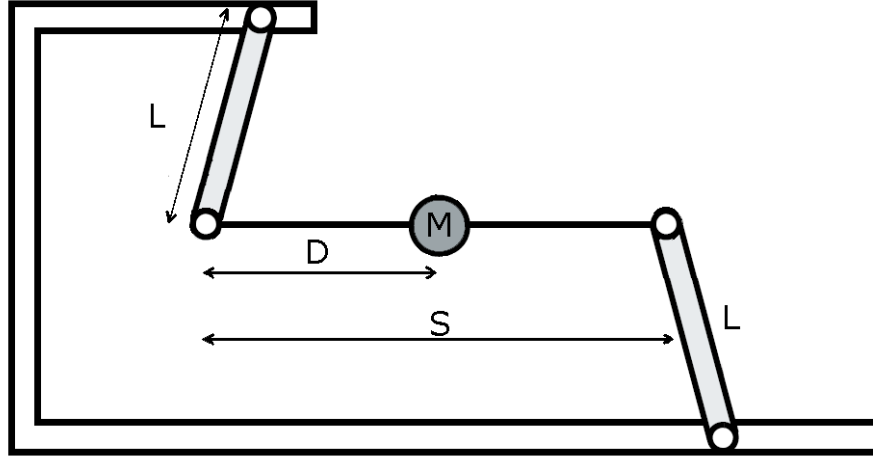


Figure 2.5: *Folded pendulum schema for the analysis of the potential energy.*

(that is equivalent to trascurate the oscillating mass of the inverted pendulum arm and both the mass of the simple pendulum) we obtain the frequency of a bar with a fixed extreme

$$\omega_0 = \sqrt{\frac{3g}{2l}} \quad (2.16)$$

As a final note, to optimize the schema of a folded pendulum, we can see, by analyzing the equation 2.12, that if we set $m_{a1} + m_{a2} = 0$ or $l_p = \frac{2}{3}l$ we have $A_c = 0$: setting $l_p = \frac{2}{3}l$ means that the points P and P' are on the center of percussion of the two arms, so if it is impossible to reduce to zero the mass af the two arms we can have the best isolations performance having the flexure hinge locate at the center of percussion of the two arm.

2.1.4 Potential energy of a folded pendulum

To evaluate the potential energy of the simple pendulum see the schema in figure 2.5, in which we consider all the arm to be massless and neglect the stiffness of the

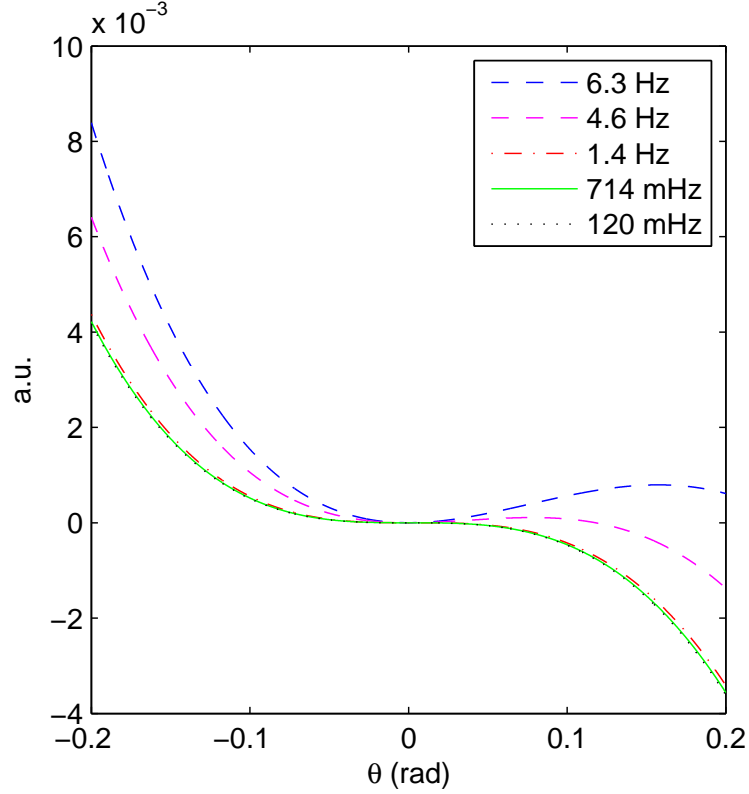


Figure 2.6: *Folded pendulum potential energy as function of the deflection angle θ .*

elastic flexure joint. The pendula's arm have the same length L and are at distance S each other; a mass M (the only massive element) is at distance D from the simple pendulum. With this schema the resonance frequency became

$$\omega_r^2 = \frac{g}{l} \left(1 - 2\frac{D}{S} \right) \quad (2.17)$$

and the potential energy is a function of the deflection angle θ and is

$$U_{pot}(\theta) = MgL(1 - \cos \theta) \left[1 - \frac{2}{S} \left(L \sin \theta + \sqrt{D^2 - L^2(1 - \cos \theta)^2} \right) \right] \quad (2.18)$$

As showed in the figure 2.6, we see that the folded pendulum has a well in $\theta = 0$ and a hill when $\theta > 0$, corresponding to a tilt towards the inverted pendulum arm.

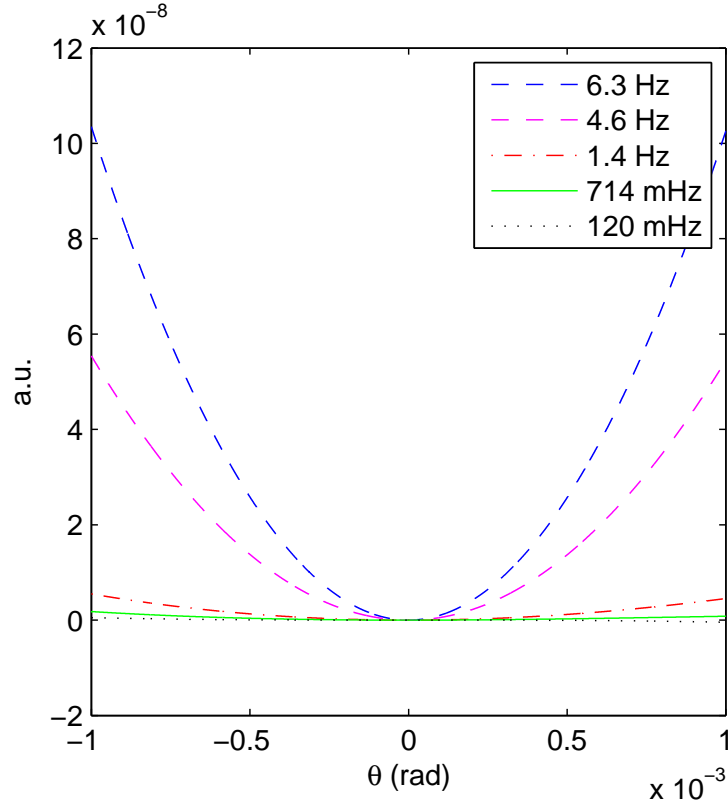


Figure 2.7: *Detail, for small angle, of the folded pendulum potential energy as function of the deflection angle θ .*

The graphs are been plotted with the length of both the arm $L = 81.5 \text{ mm}$ at a distance $S = 102 \text{ mm}$ each other, while the resonance frequency is being varied by moving position D , that is the center of mass of the horizontal bar.

The minimum of the potential energy is in the position $\theta = 0$, condition in which the two arm are parallel (vertical position of the arms). We note that if the center of mass (position of the mass M in figure 2.5) have a great displacement from its equilibrium position, we have a great value of θ : but if the value of θ is grater than the value of θ corresponding to the hill of the potential, the system will be instable. Experimentally this is one of limit condition to lower the resonance frequency of the system.

In the two figures 2.6 and 2.7 are shown different resonance frequencies and we can see (with magnifying of the second figure also) that the equilibrium condition (minimum of the potential) is more stable at high frequencies. In any case the stability in open loop is assured, with not too low frequency, because the fixed part of the structure of the system (solidal with the ground) limits the movement of the oscillating mass¹.

In literature [25] we can find that the maximal horizontal amplitude of the folded pendulum decrease with respect the resonance frequency as $\sim f^{1/2}$ and the depth of the potential well decrease as $\sim f^3$, so the lower is the resonance frequency the flatter is the bottom of the potential well as we can expect.

Considering the flexure joint's restoring force we can add a quadratic term $\kappa\theta^2/2$ to expression of the potential in the equation 2.18 being the the angular spring constant κ corresponding to a torque force equal to $\tau_{elastic} = -\kappa\theta$.

2.1.5 Thermal noise

To calculate the internal thermal noise, $Th_N(\omega)$, of FP we use the *Fluctuation Dissipation Theorem*:

$$Th_N^2(\omega) = \frac{4K_B T}{\omega^2} Re[Y(\omega)] \quad (2.19)$$

where K_B is the Boltzmann constant, T is the temperature and $Y(\omega)$ is the inverse of impedance $Z(\omega)$ defined as

$$F(\omega) = Z(\omega)i\omega x(\omega) \quad (2.20)$$

The internal thermal noise of a Folded Pendulum can be calculated introducing the complex equivalent spring constant $k(1 + i\phi(\omega))$, where the loss angle is equal to $\phi(\omega) = 1/Q$ [32]. If the FP dynamics shows small hysteresis, it is possible

¹Obviously we have a mechanical saturation of the dynamics when we reach this limit, with consequently discontinuity of the position signal

to measure the decay time τ to step response at resonance frequency f_0 and to calculate $Q = \pi f_0 \tau$. If the FP dynamics show considerable hysteresis (this happens at low frequency) it is necessary to measure the quality factor at several natural frequency and interpolate the function $Q = a f_0^2$. Defining

$$\begin{aligned} K_g &= (m_{a_1} - m_{a_2}) \frac{gl}{2l_p^2} + (m_{p_1} - m_{p_2}) \frac{g}{l_p} \\ K_e &= \frac{k}{l_p^2} \\ M_e &= (m_{a_1} + m_{a_2}) \frac{l^2}{3l_p^2} + (m_{p_1} + m_{p_2}) \end{aligned} \quad (2.21)$$

we can write the resonance frequency of a folded pendulum (equation 2.10) formally similar to that of a simple pendulum with resonance frequency

$$f_0 = \frac{1}{2\pi} \sqrt{\frac{K_g + K_e}{M_e}} \quad (2.22)$$

Using equation 2.22, the thermal noise of FP is

$$Th_N^2(\omega) = \frac{4K_B T}{\omega^2} \frac{\omega(K_g \phi_g + K_e \phi_e)}{[(K_g + K_e) - M_e \omega_0^2]^2 + K_g^2 \phi_g^2 + K_e^2 \phi_e^2} \quad (2.23)$$

Since the gravity is dissipative less, $\phi_g = 0$, the previous equation becomes

$$Th_N^2(\omega) = \frac{4K_B T}{\omega} \frac{K_e \phi_e}{[(K_g + K_e) - M_e \omega_0^2]^2 + K_e^2 \phi_e^2} \frac{[m]}{\sqrt{Hz}} \quad (2.24)$$

2.1.6 The calibration mass

Using a more accurate description of the dynamics of the folded pendulum that consider the effective mass of the single elements (see figure 2.8) and taking into account also the stiffness of the joints, as specified, assuming that the center of mass of the pendula is in $l_i/2$ and using the approximation of small angle deflection, the potential energy became:

$$U(\theta) = \frac{1}{2} \left(\frac{m_{a_1} g l_1}{2} - \frac{m_{a_2} g l_2}{2} + m_{p_1} g l_{p_1} - m_{p_2} g l_{p_2} + k \right) \theta^2 = \frac{1}{2} \mathcal{K}_{eq} \theta^2 \quad (2.25)$$

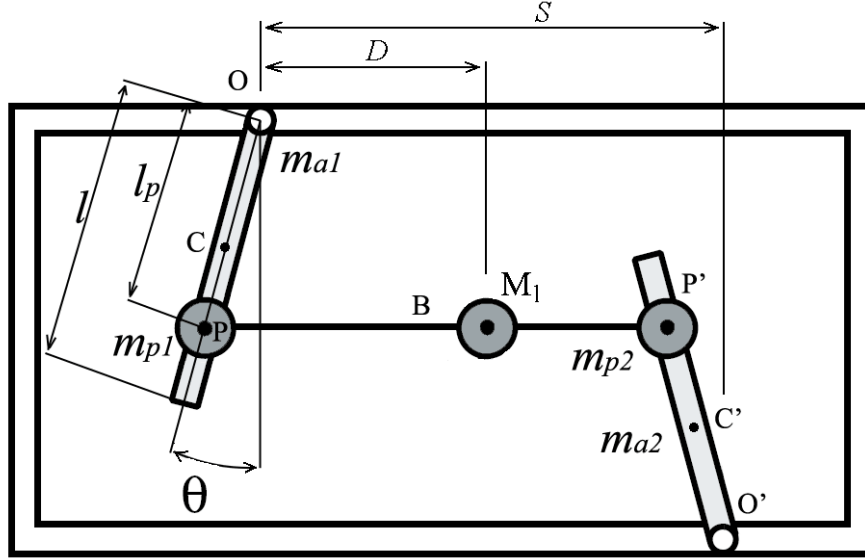


Figure 2.8: *Folded pendulum schema taking into account the mass of the single elements. Note the position of the calibration mass.*

where θ is the angle of deflection and k the cumulative stiffness of the joints. The mechanical characteristics of a FP can be changed by modifying the shape of the potential energy. It is sufficient, to change the values of the masses m_{p1} and m_{p2} , by adding an external mass (tuning mass), M_l , placing it at a distance D from the pendulum suspension point, as shown in figure 2.8. Defining S as the distance between the FP hinges points, then the values of the masses m_{p1} and m_{p2} change according to the relations

$$m_{p1_{new}} = m_{p1_{old}} + M_l \left(1 - \frac{D}{S}\right) \quad \text{and} \quad m_{p2_{new}} = m_{p2_{old}} + M_l \left(\frac{D}{S}\right) \quad (2.26)$$

Therefore, the new values of the masses m_{p1} and m_{p2} change the value of the equivalent stiffness \mathcal{K}_{eq} , and, as consequence, the value of the FP resonance frequency. Hence, as a conclusion, the FP resonance frequency can be easily modified by changing the value, M_l , and the position, D , of a tuning mass.

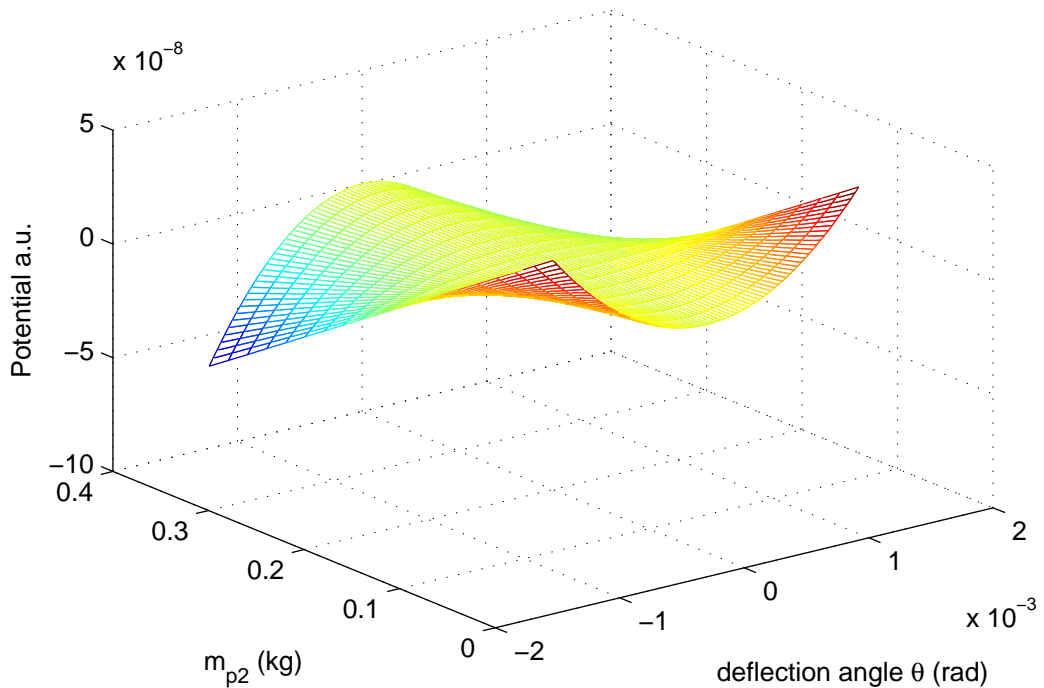


Figure 2.9: *Variation of the potential as a function of the mass m_{p2} . Note the instability over a certain value of m_{p2} .*

Theoretically the calibration of the resonance frequency can be lowered to an arbitrary value: in fact by analyzing the equation 2.10, relative to the resonance frequency, we note that with an opportune choice of the mass of the arm m_{a1} and m_{a2} , and the related suspended mass m_{p1} and m_{p2} (for example with the same value $m_{a1} = m_{a2}$ and $m_{p1} = m_{p2}$), we can have the theoretical frequency equal to zero, having the only limit on the elastic restoring force term k . But if we see the figure 2.9, we note that the potential can change its convexity (whose value is related to the frequency of oscillation), that is the system became instable, so if we choose an erroneous value for the calibration mass (that we remember that in our model is related to the absolute and relative value of m_{p1} and m_{p2}) we cannot have the oscillation of the system, and the value of the calibration mass cannot be greater as

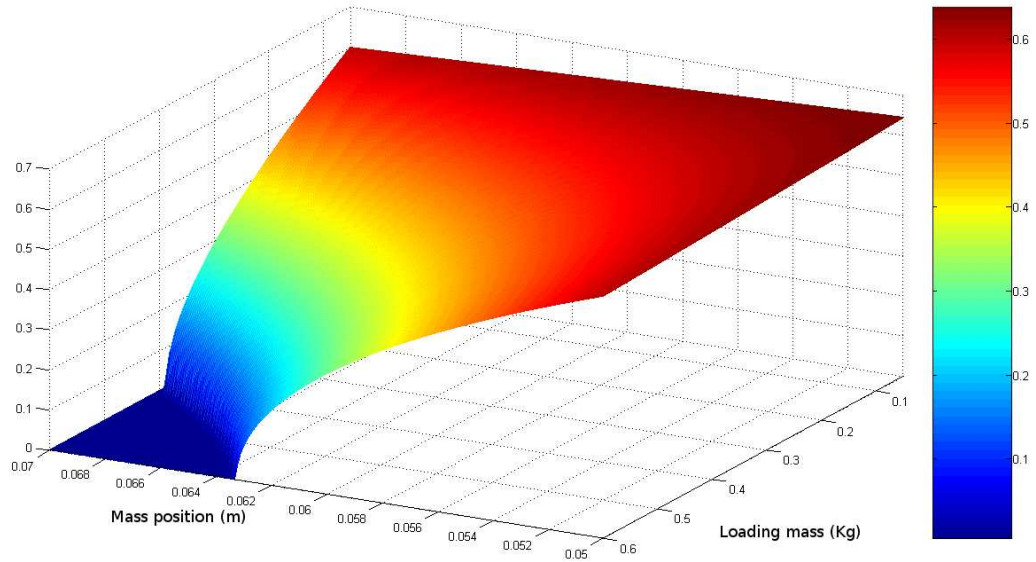


Figure 2.10: *Folded pendulum resonance frequency as a function of the value of the loading mass and the position of a tuning mass.*

you want.

In the figure 2.10 we have analytically evaluated the frequency versus the mass position and mass load to have an evidence of the instability region directly with the sperimental parameters.

To measure the variation of the frequency with respect to the variation of the geometry of the mass we have used a calibration mass constituted by a fixed mass of 336 g and two little masses (one for each side of the folded pendulum) of 40 g each for the fine tuning. The results are shown in the figure 2.11, where we can see the decreasing of the natural frequency when we increase the distance of the calibration mass from the simple pendulum; the red circle point is the lower measured frequency, in stability condition, corresponding to a frequency of 70 mHz [1].

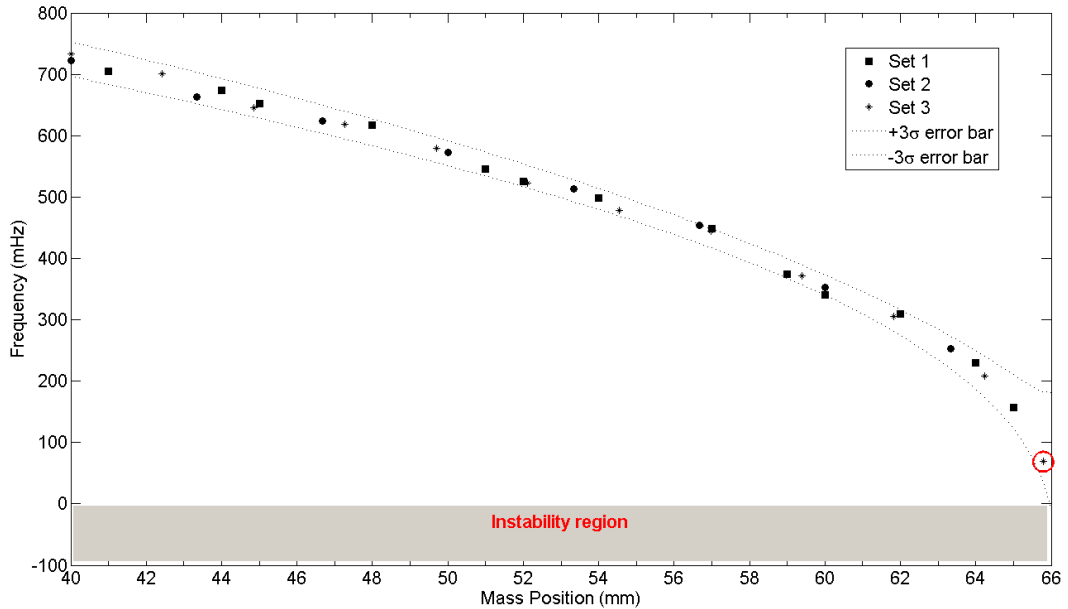


Figure 2.11: *Frequency versus mass calibration position. Red circle correspond to the frequency of 70 mHz.*

2.2 Mechanical design

To realize the folded pendulum we have used a monolithic structure to have low thermal noise. With a correct choice of the dimensions we have also a low coupling through the various degrees of freedom, that is important to have the certainty to measure the movement only in the direction of interest, make vanishing the spurious interaction both from the vertical than from the normal direction.

The system is obtained by machining an aluminum block whose external dimensions are $140 \times 134 \times 40 \text{ mm}^3$ by a wired electroerosion cut to get internal faces; the various cuts are made up with a $250 \mu\text{m}$ wire. Particular attention in machining it is used to

realize the *flexure hinges*, that, we remember, are also monolithic with the rest of the structure. The structure has an *external part* that is solidal with the ground and has various screw tip to fix several accessories (such as readout system, connector, etc.) and the structure itself to the ground. Through eight *flexure joints* (two for each extreme of each arm, to avoid interference with the normal horizontal direction) is suspended the *inertial mass*, that, by measuring the relative movement with respect the ground, is used as test mass. On the test mass there are some female screw to fix more weights, the *calibration mass*, to redistribute the center of mass of the oscillating mass, having different resonance frequency.

2.2.1 Mechanical requirements

To have a good system we need to satisfy same requirements like low thermal noise and low coupling to the transverse degree of freedom; to obtain this ones we have choose to use a *monolytich design* to have a great precision in the movements and avoid undesirable movement along the other direction together with the low thermal noise characteristics of a similar structure.

A good project give us also a great *robustness* (in all our experiments to torsion and load of great weights we haven't had no breakage).

The choice of the material, aluminum in the version used in our work, give to the system the *immunity to the magnetic field*, good *thermal conductivity*, with a *low cost material* that is also easy to machine.

Other requirements are the *easy construction procedure* (it is relatively simple to machine to obtain the system with the numerical machining instruments) and little total dimension to assure great *portability* to different work area.

2.2.2 Material choice

Because of his monolithic nature, the folded pendulum structure is greatly conditioned by the choice of the material that constitute it. In fact the material is important, for a given geometry, for the *specific weight* that determine the value of the oscillating mass, the elasticity of the material *Young's module* that determine the value of the elastic part of the restoring force, *thermal expansion* because the system has different z -dimension that imply different deformation with respect temperature variation, viscosity from which depends the *loss angle*.

The material under consideration had been the aluminum for its mechanical property than for is low cost and its good machining property; also the Cu-Be alloy has been considered for its good mechanical property, especially breaking strength (tensile) that permits to use a little thickness for joint realization, having a lower elastic restoring force.

A brief material characteristic are indicate in the following table:

	Al 7075-T6	Cu-Be C17200
Young's Module	72 GPa	131 GPa
Tensile Strength	570 MPa	1205 MPa
Thermal Expansion	23 ppm/C°	17 ppm/C°
Loss Angle	$4 \cdot 10^{-5} rad$	$4 \cdot 10^{-5} rad$

2.2.3 Elliptical hinges

The most critical part of the FP are the eight flex joints supporting the test mass, that we must remember is an integral part of the accelerometer because of his monolithic design. The upgrade, respect the older version, consists in the choice of the new geometrical design of the hinges: the older version in fact has a circular form,

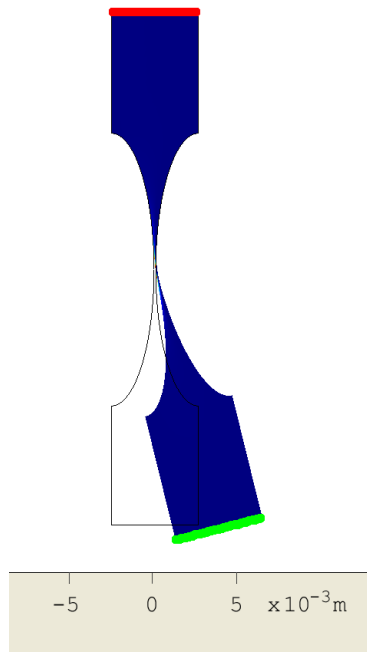


Figure 2.12: *Example of the deformation of the hinge with an horizontal displacement of $370 \mu\text{m}$. The deformation with respect the equilibrium position is enlarged by a factor 10.*

while the actual form is elliptical [3].

Because the eigenfrequency of the FP depends both by the gravity and by elastic restoring force of the hinges, to evaluate the frequency response of the hinge ellipticity we have simulated the first eigenfrequency (resonance frequency) of one hinge of the FP. Our goal is to verify that the higher is the ellipticity the lower is the frequency of the hinge, without evaluate quantitatively the contribution of the elastic force to the global eigenfrequency of the FP; in this way the valuation is focused on the single hinge response, to have a qualitatively ellipticity graph to minimize the contribution on the frequency due to the hinge presence. For these reason the absolute value of the frequency are not important for our goal, but it is of interest

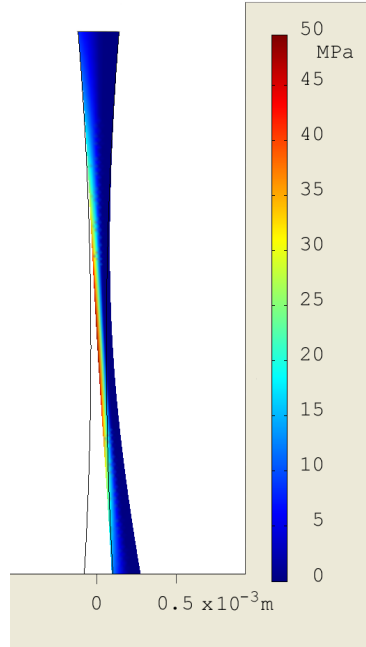


Figure 2.13: *By this figure we can see that the deformation is completely elastic, with the value of the stress always below the elastic limit of the material. The figure is relative to an hinge with ellipticity $\epsilon = 3.2$.*

only the variation of the frequency relatively to the variation of the ellipticity. To do this we have simulated, with a FEM application, the frequency of the hinge with no consideration of the gravity contribution. The shape of the hinge under study is drawn in figure 2.12, that has the same geometrical characteristic of the folded pendulum implemented hinge. For that system we have choose, as boundary condition, the upper face fixed (that is the horizontal red line in the upper of the hinge sketch, that being fixed it has no oscillations).

By seeing the figure relative to the deformation stress (figure 2.13), that shows the distribution of the first principal stress for the hinge implemented (with $\epsilon = 3.2$), we see that the stress of the material (on the right of the hinge, in blue color) is

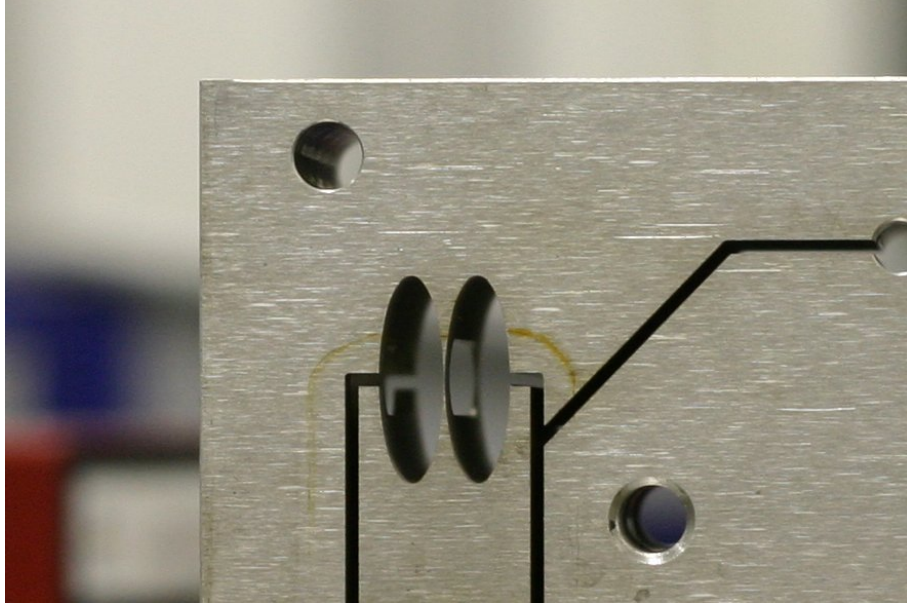


Figure 2.14: *Picture showing the elliptical hinge.*

very low, in contrast of the left part of the hinge (red color) that has the max of the deformation. However this is only the maximum stress of the external part (only the surface) of the hinge: in fact the central part of the hinge has always a stress whose value is under 550 MPa , the limit of the elastic stress, so we are always in the range of elastic deformation of the material.

To design the form of the hinge it is of primary importance to study analytically the stress to which the hinges is constrained, and the angular stiffness that, how we have seen in last section, give a contribute to the increase of the first natural frequency.

The angular stiffness can be modelled using the Tseytlin formula [34], that is

$$k = \frac{Eat^2}{16 \left[1 + \sqrt{1 + 0.215(2\epsilon R/t)} \right]} \quad (2.27)$$

where a is the width of the joint, t is the thickness at the center, R is the radius of curvature, E is the Young's modulus of the material and ϵ is the hinge ellipticity;

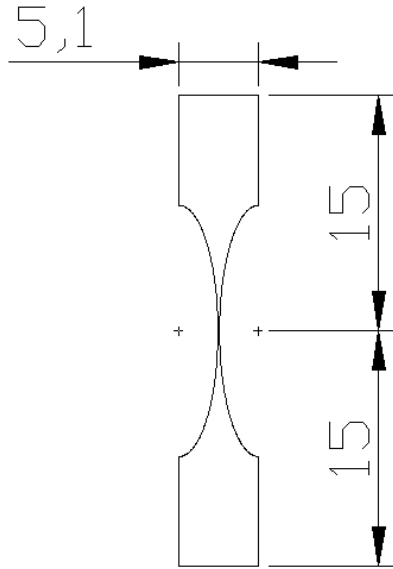


Figure 2.15: *Sketch of the hinge simulated with the finite element method; the quote value are in millimeters.*

the first series of monolithic FP sensors is characterized by circular notch hinges ($\epsilon = 1$) while the actual accelerometers have $\epsilon = 3.2$. An elliptical hinge (with the minor axis equal to the ratio of the circular hinge) gives to the system a lower stiffness, because the part of the material under stress have a greater length, so the stress is sharing out on a major surface. To calculate the correct ellipticity for the hinge we have used a simulation program based on the finite element analysis to characterize the stress and to evaluate that the deformation is under the elastic limit of the material.

As already mentioned, the geometry under study (shown with the implemented value in figure 2.15) has the major axis equal to 8 mm .

By taken fixed the minor axis of the ellipse (equal to 2.5 mm) we have varied the major axis, to have different ellipticity. In figure 2.16 we can see some of the elliptical hinges used; let's note that when the major axis has the value of 2.5 mm (with $\epsilon = 1$)

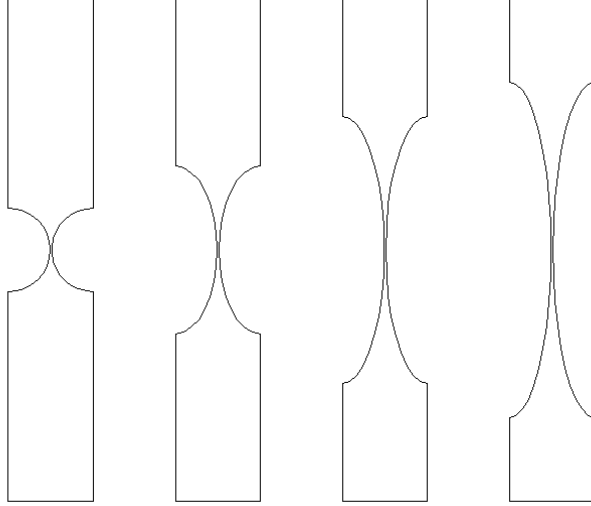


Figure 2.16: *Four shape of the 2D skecth of the joint with ellipticity $\epsilon = 1$, $\epsilon = 2$, $\epsilon = 3.2$ (implemented) and $\epsilon = 4$, from left to right.*

the hinge is circular, with the dimension of the radius equal to 2.5 mm .

Varying the ellipticity we have simulated the response of each type of hinge and analyzing with finite elements method, F.E.M., the characteristic of elliptical hinge, using the COMSOL[©] [15] simulation application, we have obtained the curves shown in figure 2.17, in which we see that the natural frequency of an hinge decrease to the increasing of the ellipticity of the hinge, as it is also clear from equation 2.27.

Stress evaluation

From the figure 2.17 we can also see the stress of the material. The boundary condition, used to calculate the stress, consist to fix the upper face of the structure (red line in the upper of the hinge in figure 2.12) and to move of a predefined distance the lower face (green line in the lower of the hinge): in this way we have measured

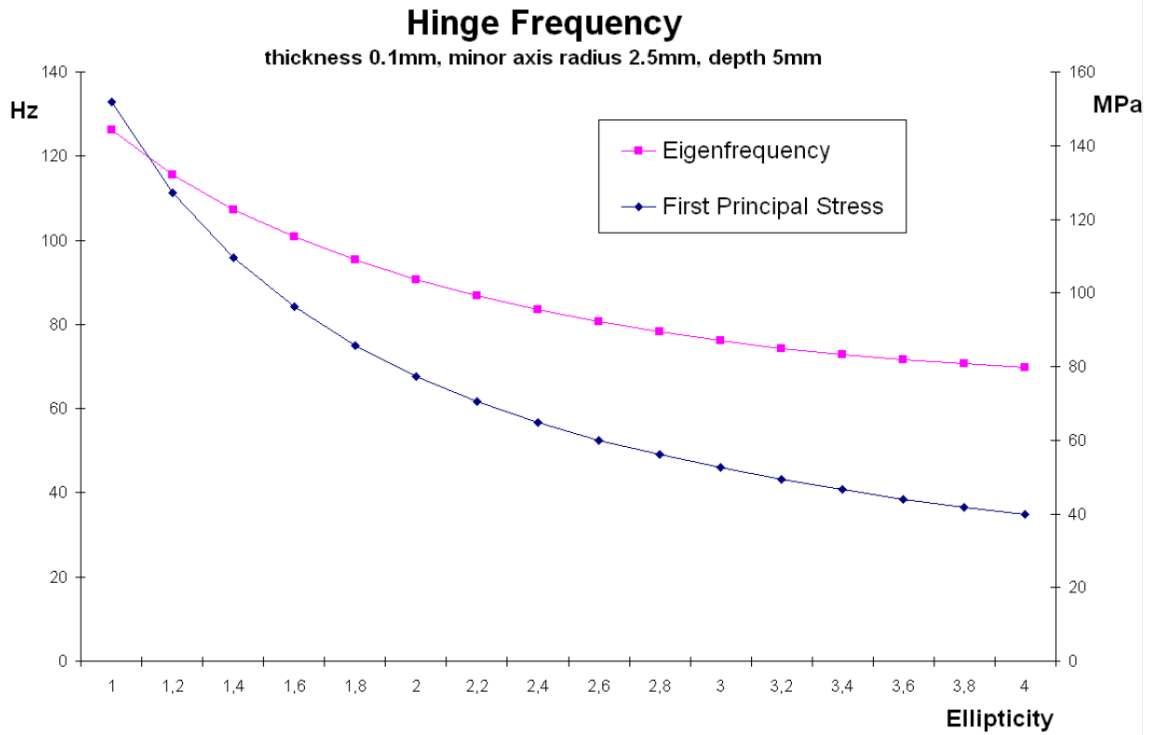


Figure 2.17: *Eigenfrequencies and the first principal stress of the hinge as function of ϵ , the hinge ellipticity.*

the stress of the material constituting the hinge under condition of stress and load similar to those existing on a hinge of the accelerometer in working conditions². The stress that we have taken under study is the bending stress, due to the deformation of the hinge when the suspended mass move from a equilibrium position to an ex-

² By analyzing the geometry of an arm we have evaluated that a displacement of the lower part of an arm (whose length is equal to about 80 mm) of 2 mm, given the lenght of the geometry under analysis, with similitude triangle, we obtain a displacement of the oscillating part of the hinge of figure 2.12 equal to 37 μm .

treme position³. The load has been chosen by dividing the total suspended mass by eight (do we remember that there are 8 flex joint constituting the accelerometer) so we have choose as value for the load a force of 1 N (we remember that the weight of the oscillating parts is about 800 g). For the stress due to the bending we have calculated a displacement of $37\text{ }\mu\text{m}$.

In the figure 2.17 we can see that the first principal stress of the hinge, with ellipticity varying in the interval $\epsilon \in [1, 4]$, is always below the limit of the elastic limit of 550 MPa of the material when the hinge has the maximum deformation (corresponding to an extreme position of the test mass), that is a warranty of robustness and long-term durability of the mechanics.

In conclusion we can say that the stress trend have also a recoil on the behavior of the frequency of an ideal hinge (the analysis is made only on an hinge whitout oscillating mass), demonstrating that the frequency contribution is minor with high ellipticity.

2.3 Realized prototype

The sketch of the mechanical part of the realized system is shown in figure 2.18, where we can see a schema of the folded pendulum with the pendulum arm on the left and the inverted pendulum on the right. In the central part we see the oscillating mass suspended to the two arms and in particular the calibration mass, that is not monolithic with the rest of the system, and can be moved in different position, and fixed with screw, to obtain different resonance frequencies. Note that

³ In a preliminar analysis on an hinge with ellipticity $\epsilon = 3.2$, we have evaluated the bending stress $\sigma_B = 49.9\text{ MPa}$ and tensile stress $\sigma_T = 2.1\text{ MPa}$ with the load and $\sigma_B = 47.6\text{ MPa}$ and $\sigma_T = 0\text{ MPa}$ without the load.

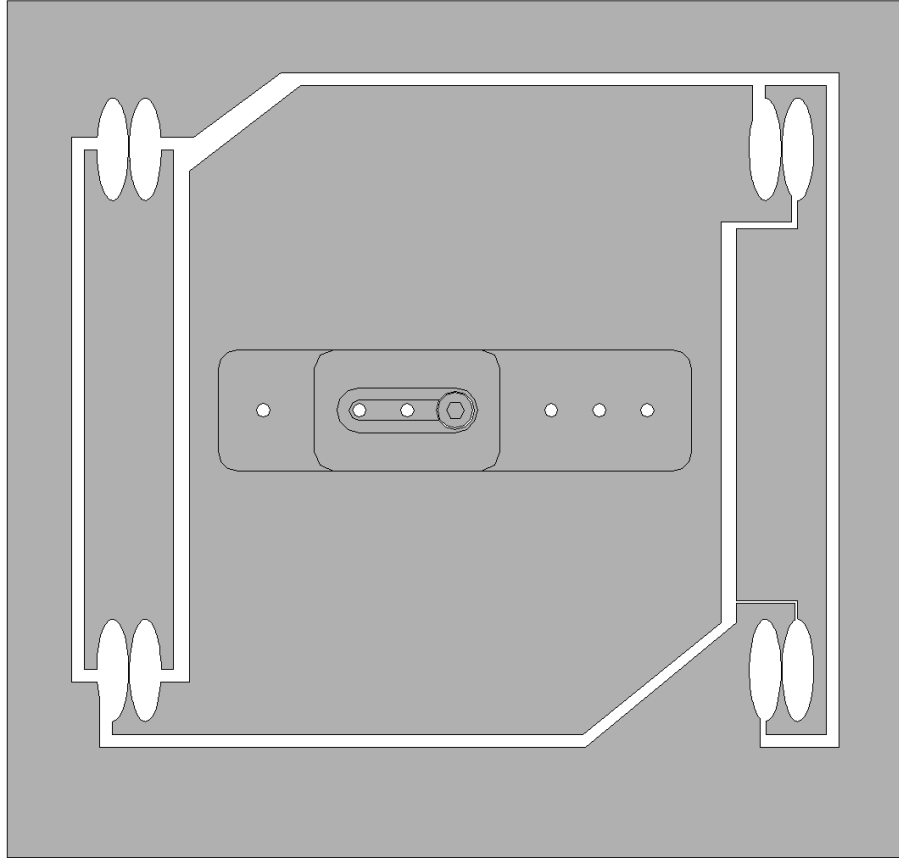


Figure 2.18: *Schema of the realized folded pendulum in a lateral projection.*

all the suspension are made up with the elliptical hinge, as already discussed the the section 2.2. In this figure we can see, from this perspective, four of the total eight joint.

A picture of the system is shown in figure 2.19, where the FP is completed with the readout system based on an optical lever (see section 3.1) and the actuator, all mounted on a metal base necessary to level it (the yellow cable is the optical fiber and the black cable the electrical connection of the actuator).

All the system can be covered with an apposite cup that can be fixed with screw to this base, to preserve it from dust, light (the light can introduce noise on the light

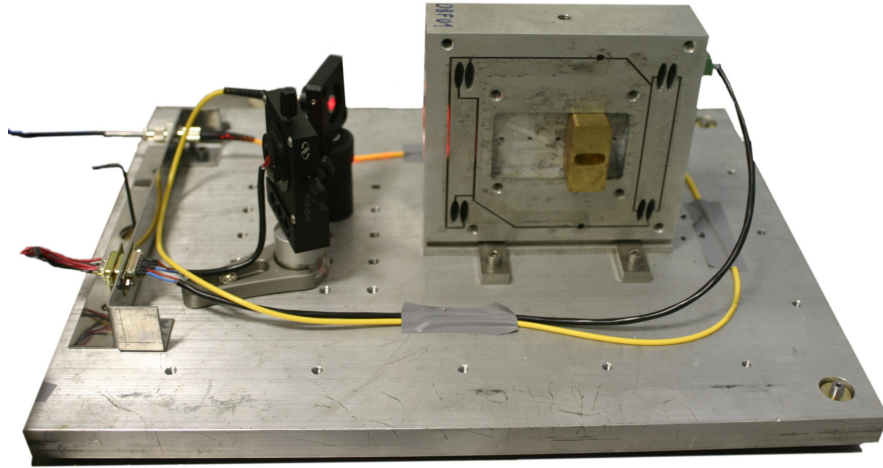


Figure 2.19: *Picture showing the realized mechanics and the optical lever readout.*

sensor) and wind.

2.3.1 Measured open loop transfer function

To measure the transfer function in open loop we need to excite the oscillating mass with an external force. We have different method, but obviously all are based on the measure of the value of the force and on the response of the mass. In a first elaborated method we have mounted the folded pendulum on a frame that we can move with a sliding stepper motor; we used two reading apparatus based both on the optical lever: a first one measure the displacement of the test mass with respect the moving frame (the base of the folded pendulum); a second apparatus is constituted by a mirror solidal with this frame and the laser of this apparatus is solidal with the ground. So when we move the frame we can measure the input signal (the motion of the frame) and the output (the movement of the test mass with respect the frame).

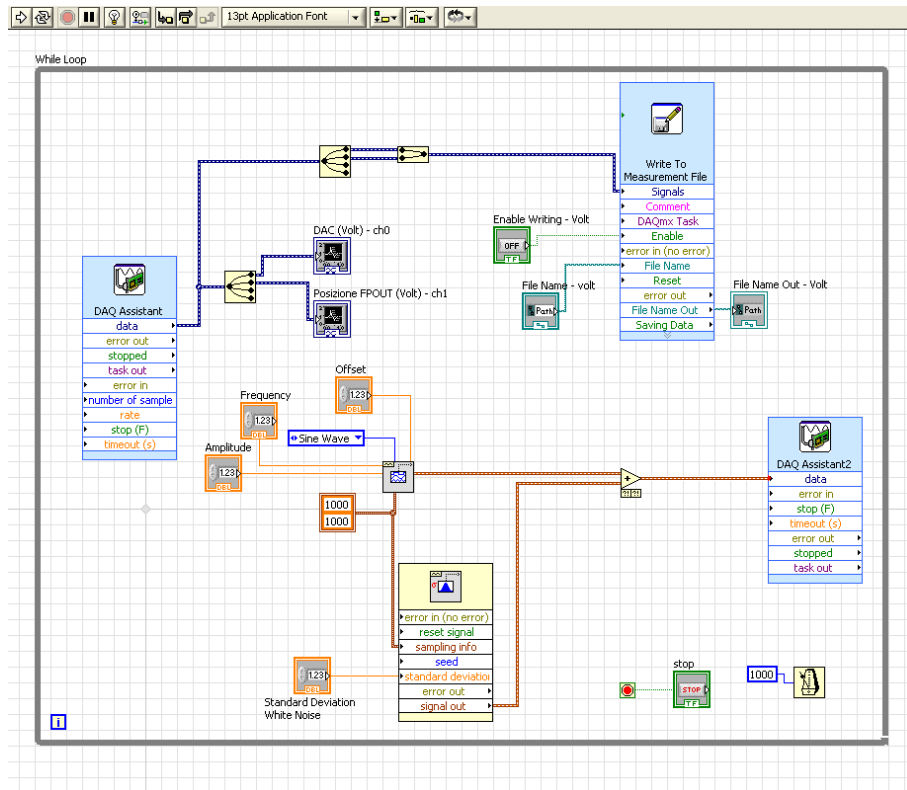


Figure 2.20: *Typical Labview programming screenshot to generate the input signal and to read the output signal to estimate the transfer function.*

This method is conceptually correct but it is not easy to perform: in fact the frame has a weight too high to move with the slider; because the slider has a motor that act via an elicoid in a versus and there is a spring that make the “return” in the opposite versus, we have that with at relatively high frequency (about $5 - 10 \text{ Hz}$) if we want to excite, for example, with a sine wave the motion of the frame is not described by a perfect sine wave, but there an hysteresis in the motion. This is not a problem because we measure also the motion of the frame so we can calculate the correct transfer function however, but we can't have a uniform ditribution in frequency.

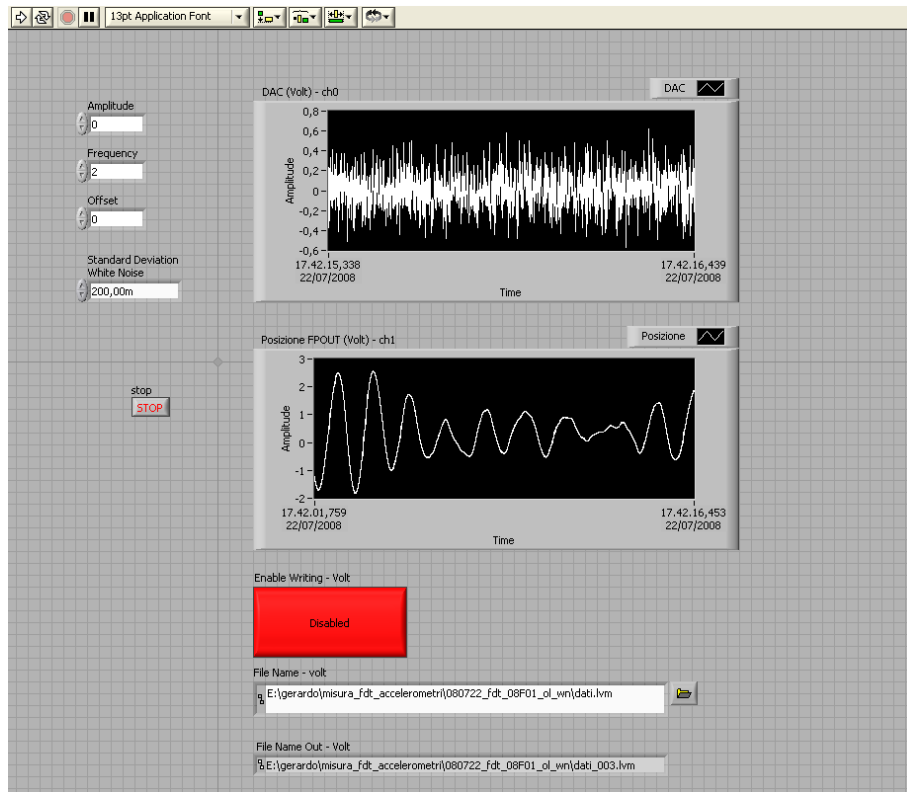


Figure 2.21: *Labview user interface of the programming screenshot shown in figure 2.20.*

An easy way to measure the transfer function is to excite directly the test mass with the voice-coil actuator. In this way we have that the frame is fixed to the ground (so there is no mechanical actuator) and the force is only electromagnetic: as input signal we use the voltage on the voice-coil and as output signal the motion measured with the optical lever. The input signal is generated with an opportune *Virtual Instrument*, VI, of *Labview*[©] [20] provided from the *National Instruments*, programmed to generate a white noise analog signal on the out and acquire the input and output signal from the folded pendulum (see figure 2.20 and 2.21). The output signal from the acquisition system is the signal that we send on the voice-coil: to avoid drop voltage (we remember that the voice-coil has a load of about one hundred

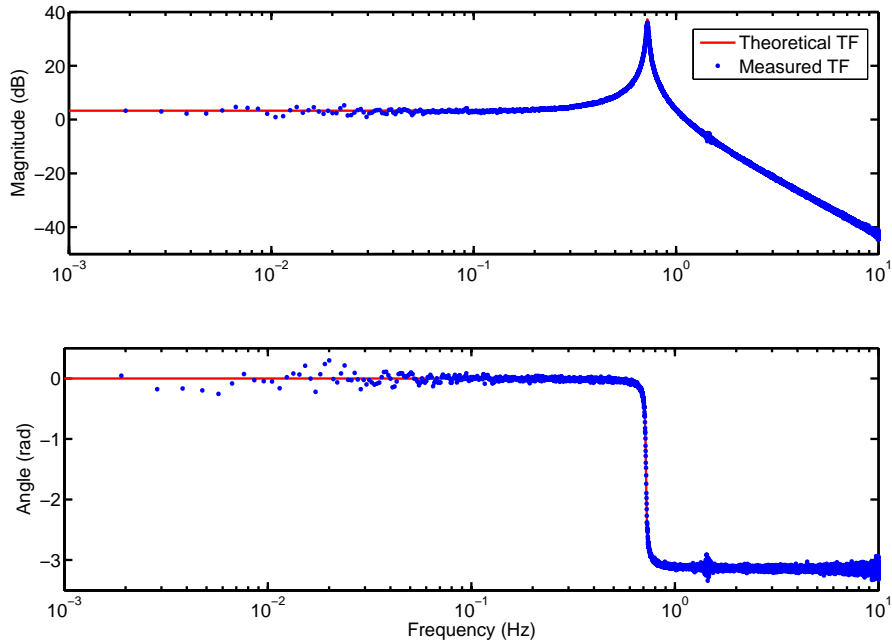


Figure 2.22: *Measured transfer function of the FP in open loop.*

ohms), in the circuital chain, before the voice-coil, we had insert an operational amplifier in a *buffer* configuration, to use it as current driver for the voice-coil⁴. During the measure all the system is covered with a metallic box to prevent light (for the photodiode) and wind (for the folded pendulum) disturb.

The measure is explained in the following. The system is being configurated in the operative configuration, with the voice-coil that work as actuator, a readout system constituted by an amplifier and a PSD (see section 3 for details). The open loop transfer function is evaluated as the response to an excitation. To have the response over all frequencies, we must actuate the excitation to the system with a signal having all the interest frequencies. To do this we have used a white noise signal with a filter to attenuate the high frequencies (in speciments a Butterworth filtering

⁴In our case we have used an *LT1028* [24] from *Linear Technology* [23]

with cutoff frequency at 100Hz). The transfer function that we have obtained is shown in figure 2.22.

2.4 Q, mechanical quality factor

As have seen in section 2.3.1 the lowest natural frequency measured is about 70 mHz with a $Q < 10$, which is a very good result for a monolithic FP sensor with these dimensions. Note that the position of the calibration mass has been fixed with an accuracy of about $\pm 1\text{ mm}$. In section 2.1.6 we have also seen that, to further decrease the natural frequency without reaching the FP instability, it is necessary to improve the tuning mass positioning system. As shown before, tuning the FP at its lowest possible natural frequency maximizes the sensor sensitivity at low frequencies, but at the same time reduces the restoring force of the pendulum to external perturbations, so that the test mass easily touches the frame, saturating the sensor. This may be a problem of dynamics for the FP as seismometer, that can be partially solved enlarging the gaps among the central mass-arms and arms-frame, (for another prototype we have reached the value of 2 mm): having more free space to oscillate the system can be kept in working more easily being less critical to individuate the point of the minimum of the potential; with this enlarging we have obtained an improvement for the quality factor because the larger air gap is a good help to evacuate the air inside cavity (formed by the arms and structure). In fact in previous version the air gap had a value of $250\ \mu\text{m}$ with a consequential low value for Q. When the FP is used as an accelerometer it would be not a problem, being the central mass kept in its rest position by a force feed-back control. But actually the real problem is the fact the FP quality factor Q decreases together with its natural frequency, so that the performances of the monolithic FP sensor decrease at low frequency. This effect is fully taken into account in equation 2.10, but what is still missing is the

theoretical prediction of the Q of the mechanical system.

The easiest way to overcome this problem is a direct measurement of the Q . For this task we performed a set of measurements in air in order to obtain an experimental curve expressing Q as function of the FP's resonance frequency, f_0 . We are well aware that these measurements are largely dependent also on the environmental conditions, but they are important to obtain an empirical physical law for our prototype, useful to predict the values of Q at different resonance frequencies.

For this task we have measured the quality factor with different resonance frequency. To vary the resonance frequency we have used the calibration mass (see section 2.1.6) in different position and weights: for a given weight of the calibration mass, we have measured the various quality factors versus the resonance frequency by varying the position of the weight, obtaining several set of measure (each set corresponding to a weight).

2.4.1 Measured quality factor in air

The measure is done with the system in open loop, by manually positioning the oscillating mass to an extreme (of the available space) and leaving it to oscillate: in this mode we have a free oscillation that is naturally damped according to the mechanical characteristic of the folded pendulum. If there is no damping, we obtain theoretically a sinusoidal signal, but, because of the damping, we obtain a sinusoidal wave form that is modulated (in amplitude) by an exponential factor related to the quality factor Q (see figure 2.23 and 2.24).

All the measurements were done using the readout system described in section 3.6, modified with substitution of the operational amplifier INA106 with INA105 to have more dynamic for the signal to detect the large signal of the system in open loop (we remember that the INA106 has same characteristic of the INA105 but have a

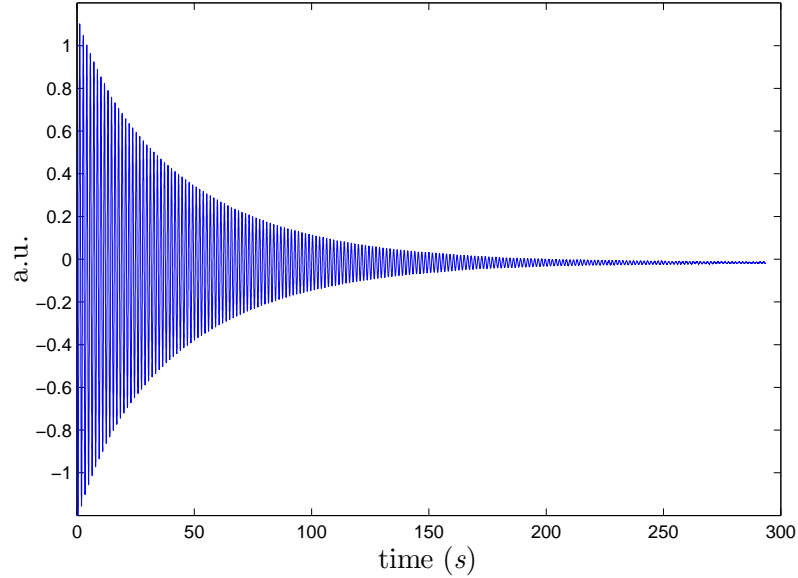


Figure 2.23: *Damping of the folded pendulum in free oscillation.*
Note the exponential decay of the amplitude of the sinusoid.

multiplier factor 10 instead of 1, gain of the INA105).

To fit the quality factor we used the analytical form for the signal⁵:

$$A \cdot \exp^{-\frac{t}{\tau}} \sin(2\pi f_0 t + \phi) + B \quad (2.28)$$

from which we have estimated the resonance frequency f_0 and the quality factor $Q = 1/2\xi$ (where $\xi = 1/(\omega_0\tau)$ being τ the time decay of the exponential and $\omega_0 = 2\pi f_0$ the pulsation), together with the time decay, τ , the phase ϕ , and the

⁵An analytical form that include directly the Q factor is of the type

$$A \cdot \exp^{-\frac{t \cdot Q}{f_0}} \sin(2\pi f_0 t + \phi) + B$$

but in this way we have a ratio of two unknown quantity (Q and f_0) in the argument of the exponential function that make the fit too difficult to realized, as more than one experiment has shown.

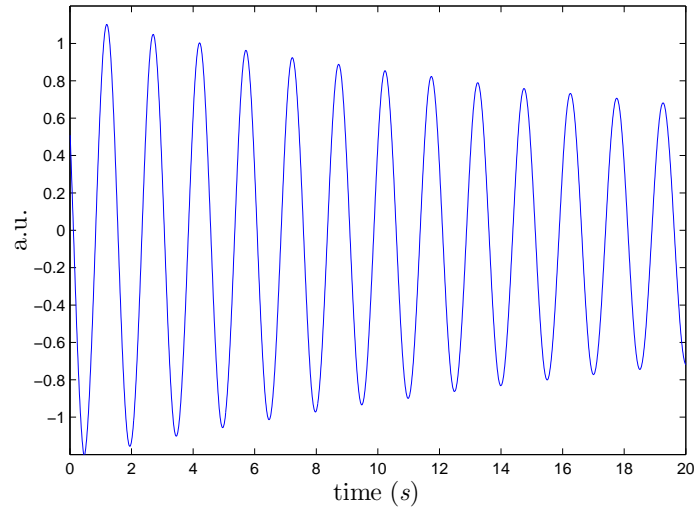


Figure 2.24: *Damping of the folded pendulum in free oscillation, first 20 seconds.*

known term B related to the offset.

2.5 Quality factor with different weights

It is interesting to measure the quality factor with respect the variation of the weight of the oscillating mass. The results are shown in the following sections, and a comparison of all the graphs is shown in figure 2.27. Note that for all the sets of measurements are indicated only the value of the weight of the calibration mass (the only that is variable) while the weight of the oscillating mass, fixed in the construction project, is equal to 760 g.

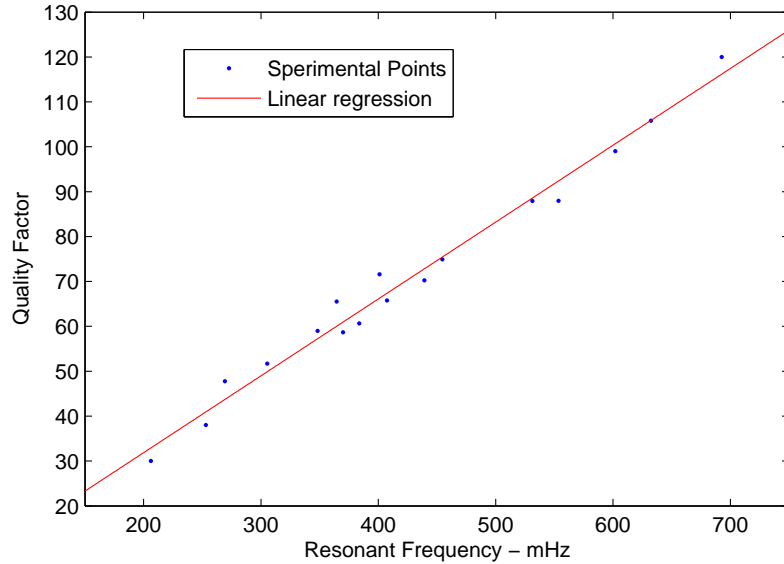


Figure 2.25: *Measured quality factor with calibration mass of 240 g in air.*

Calibration mass weight of 240 g in air

For the first set of measure we have used a tuning mass of $M_l = 240\text{ g}$, two mass of 120 g each⁶. The results of this set of measurement are reported in figure 2.25, where it appears evident that all the measurements follow a linear law⁷. In fact fitting the data we obtained

$$Q = a \cdot f_n + b = 170 \cdot f_n - 0.40 \quad (2.29)$$

⁶The calibration mass was constitute by two weigths of 118 g each one plus two screw driver whose weights was about 2 g each, for a total weight of calibration mass equal to $2 \times 118\text{ g} + 2 \times 2\text{ g} = 240\text{ g}$.

⁷ By considering the the internal friction (because of low frequency and amplitude) we must take into account the hysteresis versus the viscous phenomena: for the viscous damping $Q \propto f$ and for the hysteretic damping we have $Q \propto f^2$. In this case we are far from the frequency at which the hysteresis is prevalent on the viscous damping.

with a confidence factor equal to $R = 0.95$. Note that, according to equation 2.29 for $f_0 = 10 \text{ mHz}$ we have $Q = 1.3$, a very low value, that would prevent the use of the monolithic FP sensor at these low frequencies.

Our experimental tests have demonstrated that the values of the quality factor Q depends on the sum of the central mass and tuning mass weights. Increasing them, the Q at the same resonance frequencies should increase. Moreover, equation 2.29 describe also the performance of the monolithic FP in vacuum. In fact, a $Q \approx 3000$ was measured for a mechanical FP (Alloy 7075-T6 with $f_0 = 500 \text{ mHz}$) in vacuum at a pressure of the order of 10^{-2} mbar [11]. Therefore, if we extend this result to our monolithic FP prototype, that is $Q = 3000$ at a natural resonance frequency, $f_0 = 721 \text{ mHz}$, take into account that the material used is the same and assume the validity of equation 2.29 with $b = 0$, then at $f_0 = 10 \text{ mHz}$ and in vacuum we should get a quality factor of $Q \approx 40$. This implies that it is in principle possible to tune the monolithic FP at frequencies of the order of 10 mHz in moderate vacuum (10^{-2} mbar) acting on the positions and weights of the central and tuning masses, still having a Q enough high to use it as seismometer or as accelerometer.

Calibration mass weight of 100 g

This set of measure is being obtained by using a calibration mass whose weight is 100 g, two masses of 50 g each⁸.

By observing the figure 2.26 we note that the lower reachable resonance frequency is higher than the previous set of measure (see also figure 2.27); this is because a lower weight of the oscillating mass give us a not perfect sinusoidal signal, with an amplitude depending on the phase, having some problem to fit the data (see the equation 2.28), and we can't have a reasonable value for Q . The signal is more

⁸The calibration mass was constitute by two weights of 50 g each one plus two screw driver whose weights was about 2 g each, for a total weight of calibration mass equal to $2 \times 50 \text{ g} + 2 \times 2 \text{ g} \approx 100 \text{ g}$.

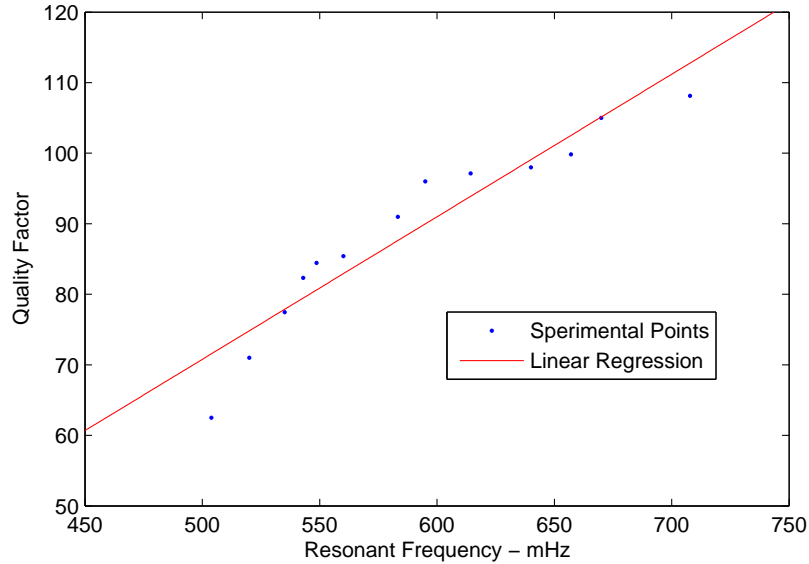


Figure 2.26: *Measured quality factor with calibration mass of 100 g.*

similar to a theoretical sine when the amplitude of the oscillation becomes smaller, but we can't make the measure with an arbitrary little oscillation because for very low amplitude the system is "auto-excited" by the ground noise and oscillations will be always present: so if we make measure in similare condition we'll obtain an infinite value for Q . For this reason we have omitted similar value of Q for these frequencies: incrementing the value of the weight can have a a signal "more" similar to a sinusoid at lower resonance frequency so we can show the values for Q until frequency of about 200 mHz .

Calibration mass weight of 350 g

It is interesting to evaluate how the quality factor Q vary to the variation of the values of the weights. A new set of measure is being obtained by using a calibration

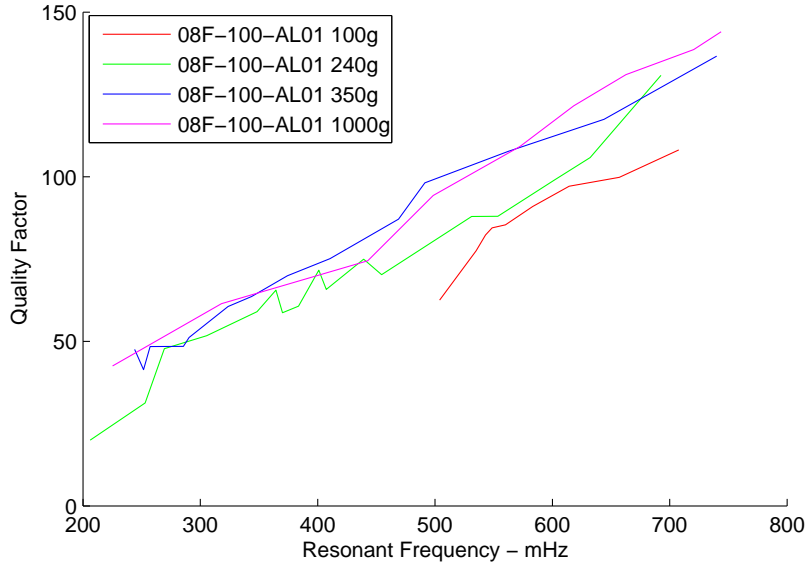


Figure 2.27: *Quality factor comparison of the folded pendulum with different resonance frequency and different weights of the calibration mass.*

mass whose weight is about⁹ 350 g and the results are shown in figure 2.27.

Calibration mass weight of 500 g

This set of measure is being obtained by using a calibration mass whose weight is about 500 g, four masses of about 120 g each¹⁰.

Definetively we can summarize in figure 2.27 all the measurement, in which we

⁹The calibration mass was constitute by two weights of 118 g each one, two weights of 50 g each one plus two screw driver whose weights was about 2 g each, for a total weight of calibration mass equal to $2 \times 118 g + 2 \times 50 g + 2 \times 2 g \approx 340 g$.

¹⁰The calibration mass was constitute by four weights of 118 g each one plus two screw driver whose weights was about 2 g each, for a total weight of calibration mass equal to $4 \times 118 g + 2 \times 2 g \approx 476 g$.

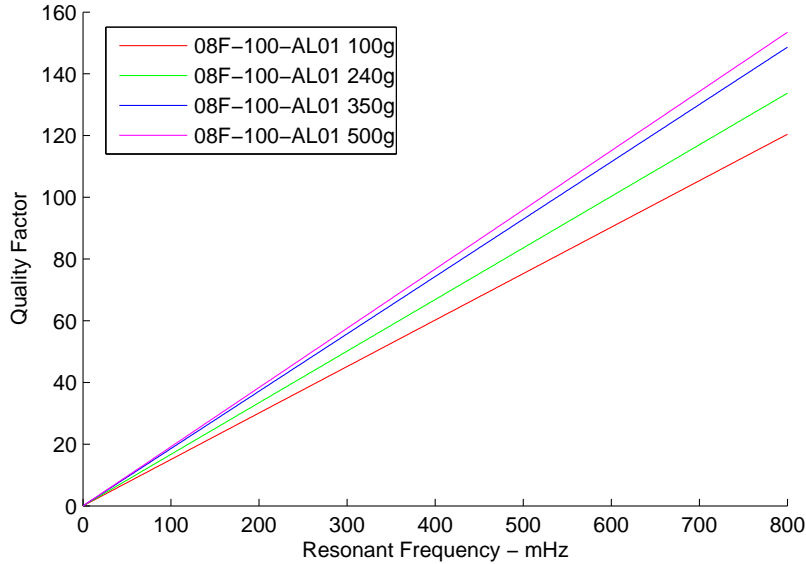


Figure 2.28: *Linear regression quality factor comparison of the folded pendulum with different resonance frequency and different weights of the calibration mass. See also table 2.1*

can see that the trend is linear, as the theory predict. In the figure 2.28 we have fit these data with a linear regression by fitting the function $Q = a \cdot f + b$, where a is angular coefficient, f the frequency and b is the known term, in which we have fixed $b = 0$ that is to impose that when the frequency is zero the quality factor must be zero. The table 2.1 shows the linear regression parameter of the quality factor measurements at different weights of the calibration mass; each value corresponds to a series of measures characterized by the same weight, where the *Weight* field is the weight of the calibration mass, and a is the fitted angular coefficient.

In particular we see that a more heavy oscillating mass, obtained in our measurement with a greater weight of the calibration mass, affect the value of the quality factor increasing it, so we conclude that to improve the quality factor, it is better to have an heavier oscillating mass.

Calibration mass weight	a
100 <i>g</i>	150
240 <i>g</i>	170
350 <i>g</i>	180
500 <i>g</i>	190

Table 2.1: Linear regression parameter of the quality factor measurement at different weights of the calibration mass.

2.5.1 Measured quality factor in vacuum

To have this set of measure we have inserted the folded pendulum with the same apparatus¹¹ (tilt plane, laser source) in a vacuum chamber¹². A first set of measure it has been useful to understand the behaviour of the quality factor with respect to the variation of the air pressure. We have chose different resonance frequency from 300 *mHz* to 450 *mHz* ¹³. The graphs are shown in figure 2.29 and, a comparison among different resonance frequenceis, in figure 2.30.

From the figures 2.29 and 2.30 we can see how the quality factor increase to the decreasing of the pressure: we note that in low pressure, about 10^{-4} *bar* (that is also the limit of the rotative pump that we have used), a little variation of the pressure can generate a great variation of the Q (for a given resonance frequency).

¹¹In the section A.3 we describe how we have modified the cabling with this readout to resolve some problem due to the cabling of the vacuum chamber.

¹²The vacuum instrumentation is constituite by a vacuum chamber with a rotative pump able to reach the pressure of about 10^{-4} *bar*, a pressure sensor Pfeiffer Vacuum Active Pirani transmitter TPR 280 and a display Pfeiffer Vacuum TPG 256 A MaxiGaugeTM measurement unit.

¹³Because it is very difficult to control the tilt of the system in the vacuum chamber, we have chose to limit our lower resonance frequency to 300 *mHz*. This limit is principally due to the deformation of the chamber when we pump out the air and to the impossibility to control externally the tilt in a micrometric way.

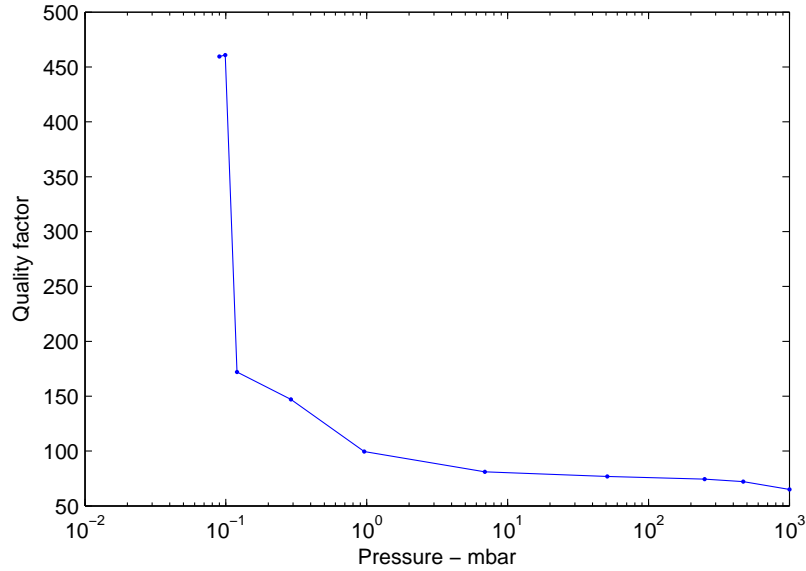


Figure 2.29: *Measured quality factor versus air pressure. Resonance frequency $f = 450 \text{ mHz}$.*

For this reason we must use care to set the correct pressure in vacuum chamber with a good precision. For these reason we have also great error in fixing the pressure to an assigned value (due to the fact that when we turn off the pump we have an increasing of the pressure, and when we turn on a decreasing), so we can obtain very different value for Q because of the high slope of the curve.

Theoretically by decreasing much more the pressure, we must observe a plateau for the curve that fix the highest quality factor, but to this it necessary to use a turbo pump to reach pressure under 10^{-4} bar .

2.6 Simulation

The simulation of the system can be done only with finite element analysis, FEM, because from an analytical point of view there are several problem due to the in-

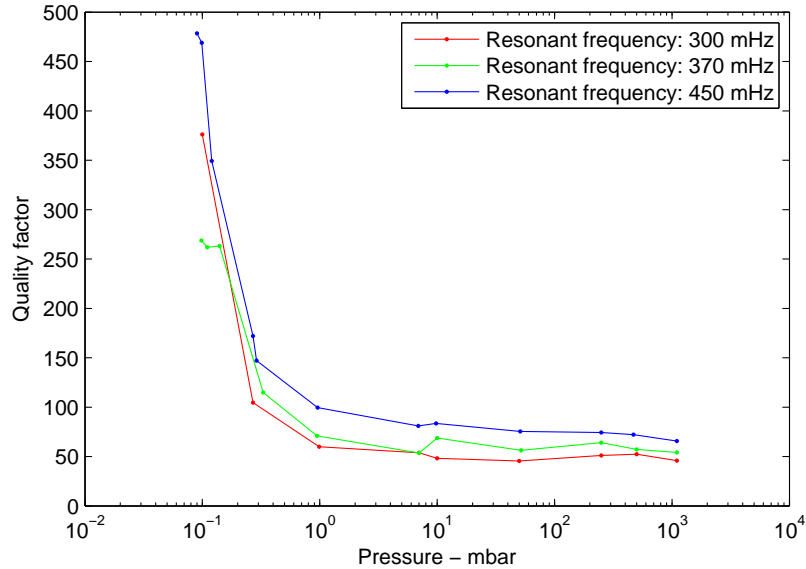


Figure 2.30: *Measured quality factor versus air pressure at different resonance frequency.*

evitable approximation that necessitate a similar type of analysis. In any case the analytical analysis of the approximated system has permitted a qualitatively study of the problem throughout we have identified some elements of the system on which we must focus a particular attention to reach some objective.

The finite element analysis of a similar system has several problems, the principal related to the mechanical dimensions of the object, that present great excursion in the dimensions of the various elements: infact we have value for the oscillating mass of the order of ten centimeter and for the thickness of the hinge of a tenth millimeter (we remember that the system is monolythical), having so a ratio of the dimension of about 10^3 ; a similar great difference is a problem for a correct FEM simulation due to the fact that the mesh that we use to discretize the system, must be dimensioned in a convenient manner for different parts of the system.

Another element, not usual for this type of analysis, is the gravity contribution for

the forces on the system that act as a restoring force: in fact, normally, in the FEM analysis the gravitational effects for the eigen-frequency analysis are not considered, because the effects related to the gravity are of the second order for the resonance frequency for commons objects, respect to the effects due to the elastic restoring forces, depending both from material than from the shape of the structure; if, in this consieration, we add the fact that the eigen-frequency of a similar system is less than $1 Hz$ with restoring gravitational forces comparable with restoring elastic forces we can imagine that the simulation can be particularly innovative and it is very hard to obtain consistent results.

The results of the simulation have never done good results: we have simulated the system with different application, that have done similar results, but always far from the real value¹⁴, probalby due to a not correct procedure of analysis. For this reason we have used the results of the simulations, as a qualitatively approach to find a best solution for a given project, having only an idea for the results, saving the time and cost of realization for bad test.

¹⁴We have simulated the first resonance frequency of the mechanical part, with the same mesh, with different finite elements analysis application like *Comsol*©, *Abacus*©and *Ansys*, and comparing the results of this various simulations, we have obtained very similar results each other, but very far from the real value, sperimentally evaluated.

Chapter 3

Readout

The readout system is based on the reading of a signal generated by a position sensing device (PSD) excited by a light beam whose direction is deviated by the mirror movement. This signal is a current signal, so we need of an amplifier to convert it in a tension signal; then we amplify this signal of a convenient ratio and we can read the position of the inertial mass.

We can decide to use directly this signal if we want to use the folded pendulum as a seismometer or to manipulate it in a convenient manner to have an accelerometer.

3.1 General schema of the readout system

In figure 3.1 we can see a sketch of the readout system. The general schema is based on an optical lever: a *light source*, solidal with the frame, generate a *beam*, that has the main characteristic to have a rectilinear propagation in space; this light beam is reflected by a *mirror* fixed on the *test mass*. When there is a perturbation of the ground we have a movement of the test mass (oscillating mass) with respect to the frame (seismometer principle), so we have that the reflected beam translate of a distance proportional to this displacement. To detect the movement there is

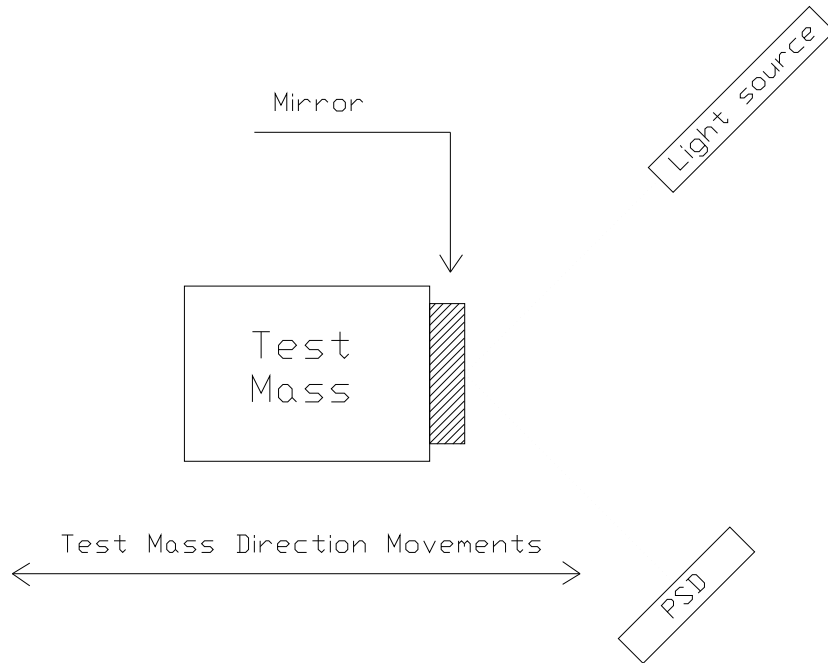


Figure 3.1: *Readout general schema. A light beam is reflected by a mirror and his displacement is red by a sensor.*

a *position sensing device*, *PSD*, based on a photodiode with a resistive layer, that has the capability to give the position of the center of the spot of the light beam with a sufficient resolution. So with this sensor we can generate a current signal proportional to test mass movement.

Analyzing this schema we can note that if we want a better performance we must increase the incidence angle θ of the light beam with respect to the mirror: in fact, as we can see in figure 3.2, if we consider two position of the test mass, A and B , given θ as the angle of the light beam with respect to the normal to the mirror, we observe that a variation of the position p (from A to B for example) give a variation

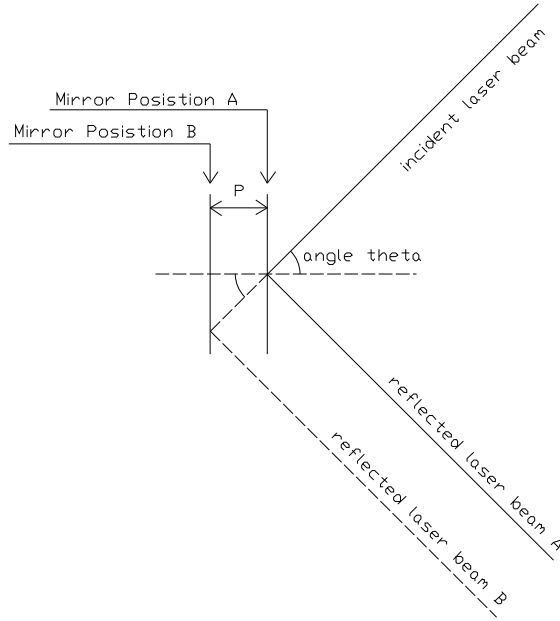


Figure 3.2: *Mirror movement and light beam displacement.*

s on the sensing device, equal to $p = s \cos \theta$, that is

$$s = \frac{p}{\cos \theta} \quad (3.1)$$

The equation 3.1 shows that with the same distance p , when the angle θ became greater (it assume a value near 90°), the cosine in the denominator became little and s gets the greater value. Obviously there is a limit to the angle θ depending on the dimension of the spot light of the beam and the dimension of the surface of the PSD.

3.2 Light sources

As we have described in the last section the measurement of the displacement is achieved with a light beam. We have tried different light sources to have the best performance. To have an easy positioning of the light beam it is of great utility to

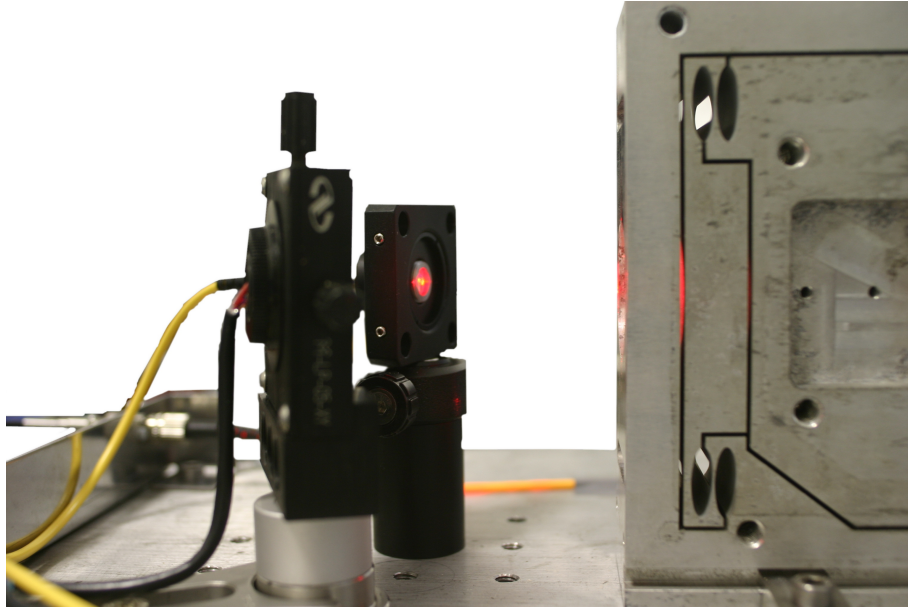


Figure 3.3: *Picture showing the optical lever.*

use the optical fibers that allow to have the light source far from the system and carry the light in a comfortable manner.

In our experiments we have used different type of light sources. The most valuable type are a red laser, OZ-2000-635-4 from OZ OPTICS LTD, with a wavelength of 635 nm and a power of 10 mW , and a second type is a Super Luminescent Light Emitting Diode, SLED, with wavelength of 830 nm (infrared) and a power of 1 mW . An high power is useful, but we must take into consideration that if the power is too high we have problem due to the saturation of the displacement sensor. When we used the red laser we have attenuated the power (often the laser source devices have a control electronics to regulate and stabilize the power) if we use it on a single system: in other case, when we used more than one system, by using a fiber beam splitter it is useful to have a great power available.

The SLEDs, compared to traditional LEDs, have a greater optical efficiency, and, in regard their optical characteristics, they are in between laser diodes and normal

LEDs. As laser diodes, they provide an almost monochromatic beam, but with a relatively short coherence length (well below 1 mm). On the other hand they are not lasing, so they are mode hopping free. The very short coherence length make the LEDs unsuited to cases in which coherent light is needed, as in interferometric optical readouts. For an optical level based readout there is no need of coherent light: on the contrary the use of incoherent light can be an advantage; in fact the short coherence length avoids the effect of ghost fringes, due to multiple reflections within optical components or windows, which can, in some cases, spoil the sensitivity of the readout system.

So a good idea is to use the SLED, but if we want a great improvement of the system, as we'll see later, we must abandon the optical lever readout principle and use an interferometric readout, for which it is necessary a laser source.

To carry out the light to the system, it is very useful to use optical fibers, that permits a comfortable way to assemble our readout system. In general we have adopted single mode, SM, fibers in order to get a good and stable beam quality and to filter out beam position and angular jitter that would otherwise be dominating for a free space sources.

It is important to point out that the fiber components must have small dimensions to fit into the box that cover the folded pendulum: they should be compact and the most simple as possible. Taking in account these requirements, the reference solution for the fiber focusers must be chosen among the pigtail style fiber collimators, which can be found on the market either in the aspherical micro-lens or graded index versions. At the extremity of any fiber we attached a focuser, simply constituted by an opportune convergent lens, whose utility is to focus the divergent light outcoming from the fiber. Although some fiber have integrated in the fibers the focuser, we have used fiber without this focuser to have a more modular system (in this way we can connect beam splitter, vacuum put through, extension cable, etc.).

It is worth noting that, differently from the traditional adjustable fiber couplers, which can be fixed to the relative support with screws, the pigtail collimators need suitable holders to be adapted to the interfaces of the support.

3.3 Choice of the position sensor

This sensor must be constituted on a system that can detect the presence of the light beam in space. A such sensor is based on the photodiode peculiarity to generate a current when it is excited by the light. In fact a similar transducer is very convenient for our scope because it generate electrical signal that can be manipulated in a very efficiency manner. So the choice is made by choosing on two different type of sensor: the *quadrant photodiode* sensor and the *PSD*, acronym of *Position Sensing Device*. In order to get the best choice among this two sensors, we make a comparison on the sensitivity [9].

3.3.1 Quadrants photodiodes sensitivity

A quadrant photodiodes is constituted by four square photodiodes disposed as shown in figure 3.4, each one labeled with the capital letter A , B , C and D ; the total sensing area is a square of dimension $2b \times 2b$ while the distance of the various photodiodes is $2a$ from each other. If we have a circular light beam whose diameter (waist) is w then, to detect correctly the position, must be $w > 2a$.

In a similar configuration, the response of the quadrant in the x direction is:

$$x = K \frac{(A + D) - (B + C)}{A + B + C + D}$$

while along the y direction

$$y = K \frac{(A + B) - (C + D)}{A + B + C + D}$$

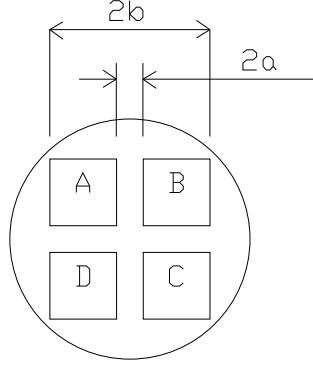


Figure 3.4: *Schematic of a quadrant photodiode.*

Because we are interested to the movement in one direction, we can considering only the x direction. By supposing a gaussian beam, we can define $f(x)$ as:

$$f(x) \doteq \frac{1}{w\sqrt{\pi}} e^{-\frac{x^2}{w^2}}$$

By defining $g(x)$ as

$$g(x) \doteq f(x) \cdot [H(b) + (H - b) - H(a) - H(-a)]$$

where $H(x)$ is the Heaviside distribution, so we have that $H(x + b) - H(x + a)$ represent the left quadrant area and $H(x - b) - H(x - a)$ the right quadrant area, we have that the current generated by the incident light is

$$I(x) = \frac{e\eta P}{h\nu} g(x)$$

If the center of the photodiode is located in the $x = 0$ position, the slope around the center is given by

$$g'(0) = f(b) + f(-b) - f(a) - f(-a)$$

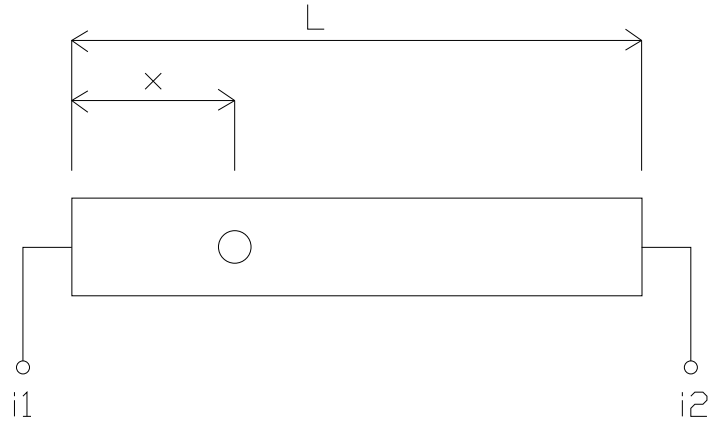


Figure 3.5: *Schematic of position sensing device: the circle represent the area of the laser beam at a x distance from one end.*

so the minimum detectable beam displacement (shot noise limited) is

$$\Delta x_{Qmin} = \sqrt{\frac{2h\nu}{\eta P}} \cdot \frac{1}{g'(x)} = \sqrt{\frac{2h\nu}{\eta P}} \cdot \frac{w\sqrt{\pi}}{2} \quad (3.2)$$

The dynamical range is defined as maximum detectable displacement of the beam, over the sensor, that can give a signal, that is the the diameter of the light beam (in fact to have a significative signal we must have that the laser beam cover at least two photodiodes in each instant, because when it cover only one photodiode we cannot have information about the effective position).

3.3.2 Position sensing devices sensitivity

Let's consider the figure 3.5 showing the schema of a PSD of length L , on which there is a circular laser beam at distance x from one extreme. The response of the PSD is given by

$$x = K \frac{I_1 - I_2}{I_1 + I_2}$$

where I_1 and I_2 are the current generated at the two end of resistive substratum of the sensor:

$$I_1 = \frac{e\eta P}{h\nu} \frac{x}{L}$$

and

$$I_2 = \frac{e\eta P}{h\nu} \frac{L-x}{L}$$

The slope of the signal, that has a linear trend along the beam displacement, is

$$\frac{dL}{dx} = \frac{2}{L} \frac{e\eta P}{h\nu}$$

so the minumum detectable displacement (also in this case shot noise limited) is

$$\Delta x_{Pmin} = \sqrt{\frac{2h\nu}{\eta P} \frac{L}{2}} \quad (3.3)$$

The dynamical range of the PSD has the whole length of the detector to which we must subtract the diameter of the spot size, that is exactly¹ $L - 2w$: if we use a little spot size we can approximate it to L .

3.3.3 Quadrant photodiodes and PSD sensitivity comparison

In the beginning of this section we have seen that (equations 3.2 and 3.3) the sensitivity and dynamical range of the quadrant photodiodes and the position sensing devices are

	Sensitivity	Dynamical range
Quadrant	$\sqrt{\frac{2h\nu}{\eta P} \frac{w\sqrt{\pi}}{2}}$	w
PSD	$\sqrt{\frac{2h\nu}{\eta P} \frac{L}{2}}$	$L - 2w$

¹ Practically is not possible to use the total PSD lenght, because there is a great non linearity response when the light beam is in the area near the electrodes.

To compare this quantity we define a merit factor as

$$m = \frac{\text{dynamical range}}{\text{sensitivity}}$$

So, for the quadrant we have

$$m_Q = \frac{w}{\frac{w\sqrt{\pi}}{2}\sqrt{\frac{2h\nu}{\eta P}}} = \frac{1}{\sqrt{\pi}} \cdot \frac{1}{\sqrt{\frac{h\nu}{2\eta P}}} \quad (3.4)$$

and for the PSD

$$m_P = \frac{L - 2w}{\frac{L}{2}\sqrt{\frac{2h\nu}{\eta P}}} \approx \frac{1}{\sqrt{\frac{h\nu}{2\eta P}}} \quad (3.5)$$

where we have used the approximation $L - 2w \approx L$ as explained in section 3.3.2. As we can see, the two merit factor has about the same value (they differ of a factor $\sqrt{\pi} \simeq 1.8$), but if we analyze the only contribution of the sensitivity, because we are interested to measure little displacement (for control application, to use the folded pendulum in closed loop as accelerometer, see chapter relative to the control design), we see that the ratio of the two sensitivities (from the equations 3.2 and 3.3) is:

$$\frac{\Delta x_{Qmin}}{\Delta x_{Pmin}} = \frac{w\sqrt{\pi}}{L} \quad (3.6)$$

From this equation we see that the quadrant can be more sensitive than the PSD: in particular if we calculate the numeric value of the sensitivities of the two sensor, with a light that have $w = 100 \mu m$, power of the incident light equal to $1 mW$ and a wavelength of $830 nm$ (note that the characteristics of the light sources have a contribution with the same value in the valuation of the sensitivity), we have that

$$\Delta x_{Qmin} = \sqrt{\frac{2h\nu}{\eta P}} w = 3.1 \cdot 10^{-8} w = 3.1 \cdot 10^{-12} m / \sqrt{Hz} \quad (3.7)$$

and, for a PSD of length $6 mm$

$$\Delta x_{Pmin} = \sqrt{\frac{2h\nu}{\eta P}} L = 3.1 \cdot 10^{-8} L = 1.9 \cdot 10^{-10} m / \sqrt{Hz} \quad (3.8)$$

From these equations we see that in our measurements the best sensitivity results were achieved with the quadrant photodiode sensor, gaining about one order of magnitude.

Although the best choice seems to be the quadrant photodiode, for practical motivation we have chosen the PSD.

The quadrant photodiode sensor is a good choice when the detectable displacement is very little, because this sensor shows a good linearity only for little displacement of the spot size, centered on the sensor; for this reason the quadrant can be used with no linearity problem only in the accelerometer setup.

Our choice is on the PSD, because in this configuration the sensitivity requested by our apparatus is limited by the electronics (ADC dynamical range, see section 3.4.2), and the sensitivity advantage of the quadrant is not crucial, so the sensitivity limit reachable with the PSD is lower than that offered by the readout. Moreover with the PSD we have a greater dynamics² that permits the use of the system as seismometer and as accelerometer.

3.4 Position Sensing Device

The position sensing device consists of a uniform resistive layer formed on the surface of a high resistive semiconductor substrate, having on the both ends of the resistive layer two electrodes to read the position signal. The active area is also a resistive layer that has a PN junction that generates a current when a spot light strikes on it (photocurrent). It is product either in the mono-dimensional than bi-dimensional

² This consideration is valid only in open loop, because when we use the system as an accelerometer the displacement is very reduced.

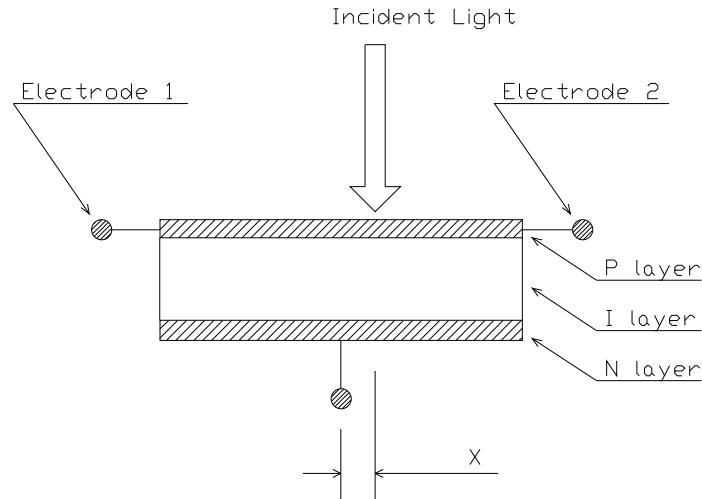


Figure 3.6: *Position sensing device schematic that showing a sectional view of the sensor.*

version³.

The figure 3.6 shows a schema that illustrates the operating principle of the monodimensional PSD, used in our system. The PSD has a P resistive layer on an N high-resistive silicon substrate: the P layer is the active area for the photoelectric conversion and the output electrode are connected to the ends of this layer. On the other side there is the silicon substrate type N connected to a common electrode. This is the same configuration of a PIN photodiode except for the P resistive layer on the surface. When a spot light strikes on the PSD, in that point (precisely on the area lightened) is generated an electric charge proportional to the light intensity that is propagated through the resistive layer until the two electrodes. The value of the current that is present on the two electrodes depends inversely by the distance of the electrode from the spot light: for example if the spot light is at the center

³The 2D version has one common electrode plus 4 electrodes, two for each directions.

between the two electrodes, we have that the resistive substrate offer a resistance that is equal for both the electrode, so the current is the same on the two ends; for example, if the spot is nearest the electrode 2 than electrode 1, we have that the current “see” a lower resistance versus the electrode 2, so we have that the current “produced” by the electrode 2 is larger than that relative to the electrode 1.

By indicating with X the distance from the center of the resistive substrate and the center of the spot light, L the length of the substrate (length of the active area of the PSD), I_1 the current on the electrode 1, I_2 the current on the electrode 2, and I_0 the total photocurrent generated by the spot light ($I_0 = I_1 + I_2$), we have the following relation to calculate the distance X measuring the current:

$$\begin{aligned} I_1 &= \frac{L/2-X}{L} \cdot I_0 \\ I_2 &= \frac{L/2+X}{L} \cdot I_0 \end{aligned} \quad (3.9)$$

and

$$\frac{I_2 - I_1}{I_2 + I_1} = 2 \frac{X}{L} \quad (3.10)$$

This last equation shows the relation that makes the intensity of the current independent from the light intensity, that we have used in our apparatus, making the system robust with respect the light oscillation intensity level.

The position sensing device used is the model S3931 from Hamamatsu[©] [18].

3.4.1 PSD noise

The noise that affect the PSD is a combination of thermal noise and shot noise, with regard of the electronics noise due to the amplifier that convert the current signal in tension signal.

The thermal noise, i_R , is given by the current, generated by the photodiode, flowing

through the resistance R of the sensor⁴:

$$\text{Thermal Noise} \quad i_R^2 = \frac{4K_B T}{R} \quad (A^2/Hz) \quad (3.11)$$

where K_B is the *Boltzmann constant* and T the temperature, so, if we work at a temperature of $20^\circ C$, the factor $4K_B T$ assume the value $4K_B T = 1.62 \cdot 10^{-20} \text{ m}^2 \text{ kg} / \text{s}^2$. The shot noise, i_{PhD} , is given by:

$$\text{Shot Noise} \quad i_{PhD}^2 = 2qI_{PhD} \quad (A^2/Hz) \quad (3.12)$$

where $q = 1.602 \cdot 10^{-19} C$ is electron charge and I_{PhD} is the combination of the *Photogenerated current*, I_{Ph} , and the *Dark current*, I_D , of the photodiode part of the PSD, that is $I_{PhD} = I_{Ph} + I_D$. The thermal noise and shot noise sources are not

correlated so we can add them obtaining the total current noise I_N as follows:

$$I_N = \sqrt{I_R^2 + I_{PhD}^2} \quad (A) \quad (3.13)$$

where

$$I_R = \sqrt{i_R^2 \cdot B} \quad I_{PhD} = \sqrt{i_{PhD}^2 \cdot B} \quad (3.14)$$

being B the bandwidth. Definitively we have

$$I_N(R, I_{PhD}, B) = \sqrt{i_R^2 \cdot B + i_{PhD}^2 \cdot B} = \sqrt{\left(\frac{4K_B T}{R} + 2qI_{PhD}\right) \cdot B} \quad (3.15)$$

expressed as root mean square value in ampere. Note that the total noise is given as specific values of construction of the sensor R , I_{PhD} and B .

⁴Note that the expression of the equation 3.11 can be expressed in volt as $v^2 = K_B T R$ being $v = R \cdot i$.

Noise evaluation

For our system the noise is summarized in the following:

Thermal noise	$i_R = 5.7 \cdot 10^{-13} A/\sqrt{Hz}$	from the eq. 3.11
Shot noise	$i_{PhD} = 1.33 \cdot 10^{-11} A/\sqrt{Hz}$	from the eq. 3.12
Total noise	$I_N = 1.33 \cdot 10^{-9} A$	from the eq. 3.15

where we used the parameters of our sensor as follows:

$R_{PSD} = 50 k\Omega$	PSD resistance
$T = 298.15^\circ K$	Temperature, $25^\circ C$
$I_D = 0.15 nA$	Dark current
$I_{Ph} = 550 \mu A$	Photogenerated current
$B = 10 kHz$	Bandwidth

3.4.2 PSD signal to noise ratio

To calculate the signal to noise ratio we define $I_{Ph} = \eta P$ as the photogenerated current caused by incident light on the sensor, where η is the sensitivity (efficiency) of the sensor and P the power of the light beam, so we have

$$SNR \doteq \frac{I_{Ph}}{I_N} = \frac{I_{Ph}}{\sqrt{\left[\frac{4K_B T}{R} + 2q(I_D + I_{Ph}) \right] \cdot B}} \quad (3.16)$$

with I_{Ph} and I_D defined in the previous subsection, and I_N evaluated via the eq. 3.15.

SNR evaluation

The signal to noise ratio that we obtain with our sensor is

Signal to noise ratio	$SNR = 410 \cdot 10^3$	from the eq. 3.16
-----------------------	------------------------	-------------------

where we have used the parameters given in the following

$\eta = 0.55$	Sensitivity at $\lambda = 830 \text{ nm}$
$P = 1 \text{ mW}$	Light power
$I_D = 0.15 \text{ nA}$	Dark current
$I_{Ph} = 550 \text{ } \mu\text{A}$	Photogenerated current
$I_N = 1.33 \cdot 10^{-9} \text{ A}$	Total noise

3.5 Power supply

From different test, we have seen that to achieve low noise measurement of the displacement signal it is necessary to have a correct power supply voltage. All the components necessitate of a supply voltage in the interval $V_{supply} \in [\pm 8, \pm 16] \text{ V}$ (some components, as the operational amplifier, has a large range, but other limite the range to this this interval). To have the best noise performance we must have a stable constant voltage of the power supply. In our first measurement we used a DC regulated power supply with a regulated voltage in the interval of our interest, with which we have made up several measurements at different voltages. To characterize the stability response of supply voltage, we have made some measurements in different conditions with two INA (integrated instrumentation amplifier) integrated circuit, INA105 [13] and INA106 [14]: this type of circuit amplify the relative voltage on the differential input and give on the output of the difference of the voltage on the input, offering a good CMRR. As power supply we have used the DC regulated power supply with the tension of $\pm 15 \text{ V}$ and $\pm 9 \text{ V}$, and, as stabilized

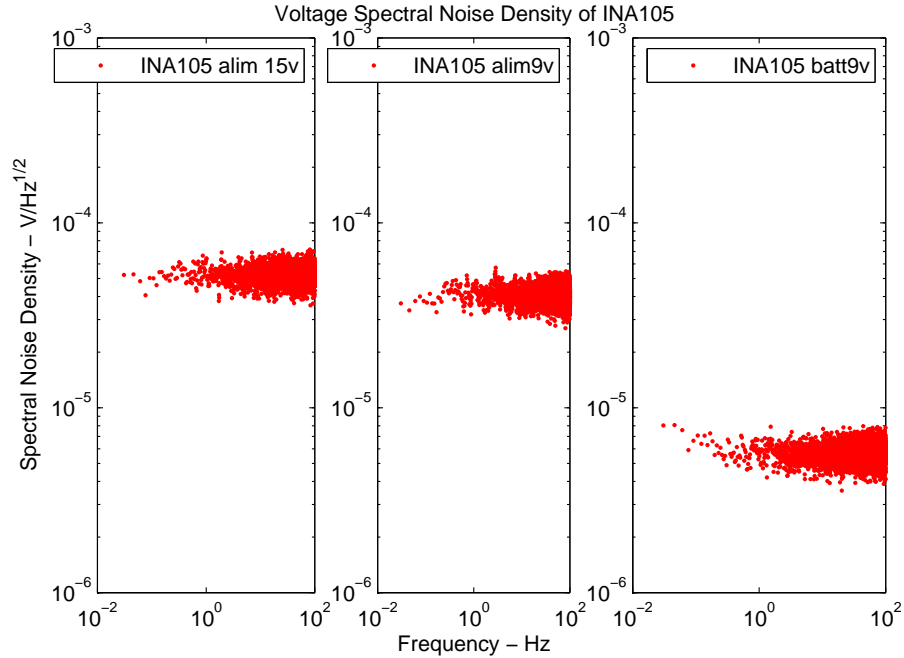


Figure 3.7: *Comparison of the noise generated from the IC INA105 with different type of voltage supply: note the best performance of the battery*

reference tension, two 9 Volt NiMh battery (with two battery we can have a dual supply voltage of $\pm 9V$). The results are shown in figure 3.7 and 3.8, where we can see the best performance of the battery.

Best performance in term of stability and durability (sufficient long durability is necessary for our application if we want to acquire signal for long time) can be obtained with common battery, as lead-acid battery. In their gel version, (also known as “gel cell”) are a rechargeable valve regulated lead-acid battery with a gelled electrolyte. This type of batteries virtually eliminate the electrolyte evaporation, spillage (and subsequent corrosion issues) common to the wet-cell battery: chemically they are the same as wet (non sealed) batteries except that the antimony in

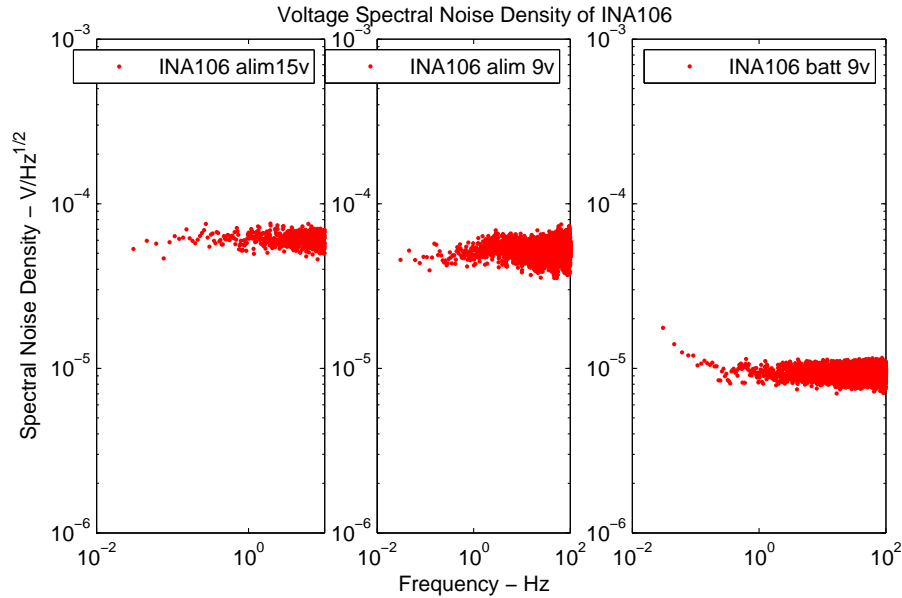


Figure 3.8: *Comparison of the noise generated from the IC INA106 with different type of voltage supply: note the best performance of the battery*

the lead plates is replaced by calcium. This preserves the mechanical characteristics but renders the construction far less prone to gassing. There are no problem related to the electrolysis of water because the requested output current is very low (about 30 mA).

Because of the low noise performance and of the portability, we have choose the battery to perform our measurement. Obviously with a non-switching supplier with a correct stabilization we can have performance very similar to the battery, but in this case we can't have the portability.

Our choice is to use two 12-Volt lead-acid battery (the common car battery) because of their low cost, high durability (about two months with the continuous consumption of our circuitry), easy commercial availability and great diffusion in geophysics and geotechnical laboratory. The voltage of this battery is about 12 V

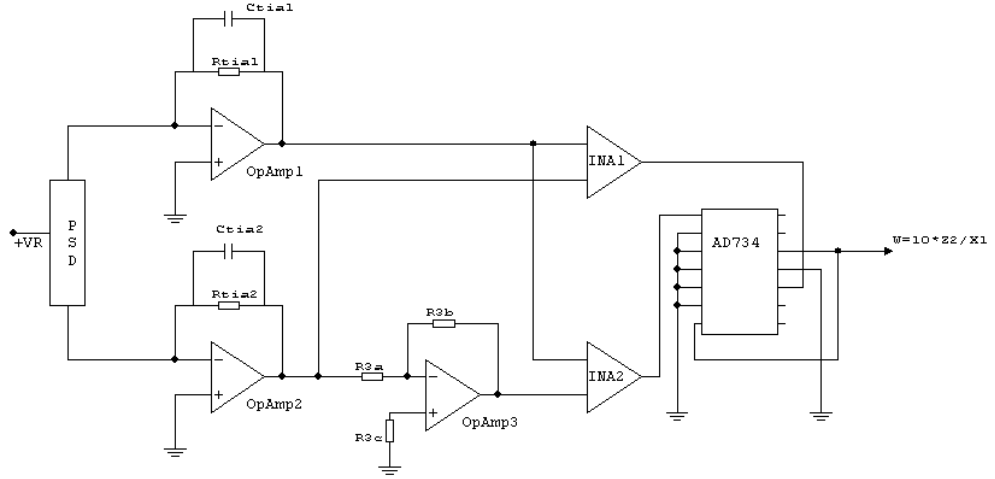


Figure 3.9: *Electronic schematic of the reading circuit.*

($V \in [12.00, 12.65] V$), that is compliant with our integrated circuits specifics.

3.6 Reading amplifier

The reading electronics would to convert the current signal generated by the PSD into a tension signal, to use this last to correct the motion of the folded pendulum with an appropriate control circuit, making the accelerometer. The schematic of the reading circuit is shown in figure 3.9 and we note that it has a part to convert the signal in a tension signal and a part, after a series of analog manipulation, that use a divider to have a signal independent from the light source power.

3.6.1 Generality on noise reduction

As we see from the schematics of the readout circuitry (figure 3.9), the reading circuit is made with a chain constituted of more than one stage. To obtain the maximum signal to noise ratio at the end of the chain we need to amplify with the maximum gain on the first stage: in fact when we amplify a signal with a certain gain on the

first stage we have a certain signal to noise ratio SNR ; in the following steps we only can degenerate the SNR , because if we amplify, in the second stage, the signal output from the first stage we amplify the noise of the first stage also. Analytically we can express this concept defining the *noise factor* N as

$$N = \frac{SNR_{in}}{SNR_{out}} \quad (3.17)$$

with the signal to noise ratio SNR in input and output of each stage expressed in decibel, and calculate the noise factor, of a system with n devices in cascade, with the *Friis formula*:

$$N_{tot} = N_1 + \frac{N_2 - 1}{G_1} + \frac{N_3 - 1}{G_1 \cdot G_2} + \frac{N_4 - 1}{G_1 \cdot G_2 \cdot G_3} + \dots + \frac{N_n - 1}{G_1 \cdot G_2 \cdot \dots \cdot G_{n-1}} \quad (3.18)$$

where N_{tot} is the noise factor on the last stage and G_i ($i = 1, 2, \dots, n$) is the gain of the i -th stage. From this formula we can immediately see that the best noise performance is achieved with the gain on the first stage⁵.

3.6.2 Amplifier noise

As explained in the introduction of this section, the aim of the amplifier electronics is to convert the current signal outcoming from the PSD into a tension signal (*current-tension converter*). Our electronic schematics is constituted of more than one stage (see figure 3.9). From the schematics we see that we use three operational amplifiers (specifically the *OP27* provided by *Analog Devices*, [4]) and two differential amplifiers (one *INA105* and one *INA106* differential amplifier, both from *Burr-Brown*, [12]). The first stage makes the current-tension converter, and the other stages are the amplifier and some other circuits that make some operations on the signal, as an integrated analog divider circuit that we use to make the output

⁵For example if we consider a system with three stages it is convenient to have maximum gain on the first stage and the minimum gain on the last stage.

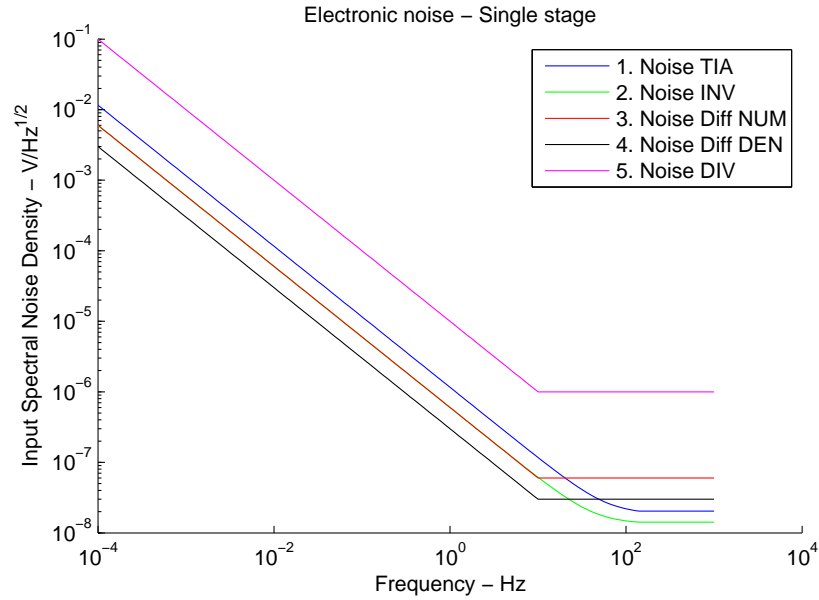


Figure 3.10: *Input voltage noise density of the single stages of the reading amplifiers. The noise is calculated considering the noise of the single amplifier integrated with the interactions of the various resistor on the input, if present.*

signal independent from the light power fluctuations (*AD734* from *Analog Devices*). Every electronic signal have random fluctuation, $n(t)$, around an expected value, $s(t)$: these fluctuation is the noise that affect the signal.

In most cases the distribution of the noise is a good approximation of a gaussian function centered on the signal value in absence of noise, that is equivalent to say that mean value of the noise has a null value. The entity of the fluctuation is characterized by the standard deviation, σ , calculated, from signal $s(T)$ generated form the noise, with a mean on the deviation: this value is the noise power, $\overline{n(t)^2}$.

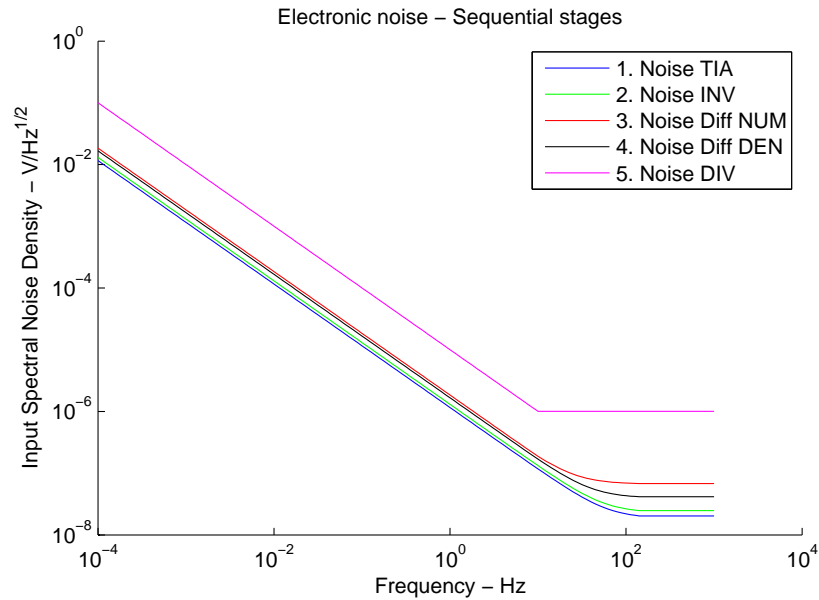


Figure 3.11: *Input voltage noise density of the reading amplifier at the various stages. The noise of every stages is calculated by considering the noise of the previous stages.*

3.6.3 Operational amplifier noise

The noise that produces an operational amplifier can be represented schematically as the noise generated by a tension generator and by a current generator. This noise can be divided into three part: *thermal noise*, *1/f noise* and *shot noise*.

Generally for an operational amplifier is specified the *corner frequency*, that is the frequency at which the *1/f* noise is more greater than the other noise: in this way we can observe that generally the voltage noise curve is given by a decreasing curve (*1/f*) followed, for frequency higher than the corner frequency, by an horizontal curve (a constant noise), white noise like (see figure 3.12). For our OP27 operational amplifier⁶ the voltage noise corner frequency is 2.7 Hz , and the noise for frequency

⁶See [6] for datasheet.

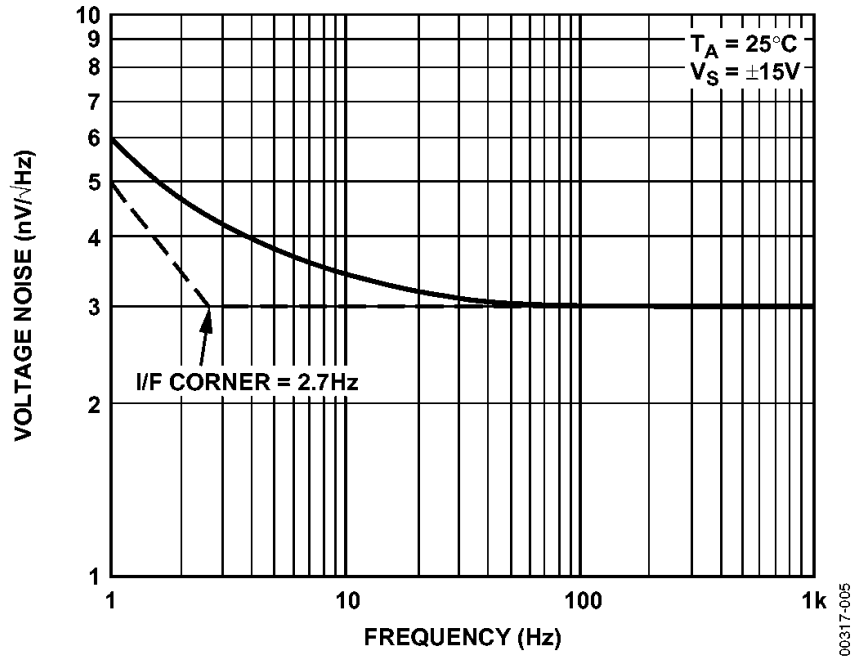


Figure 3.12: *OP27 operational amplifier noise voltage versus frequency: note the frequency corner. From OP27 datasheet [6]*

greater than the corner frequency is $V_n = 3\text{ nV}/\sqrt{\text{Hz}}$. In the same manner is defined a corner for the current noise, and, from the datasheet, we see that the variation of the current have a corner frequency at 140 Hz , above of which we have a noise of $0.4\text{ pA}/\sqrt{\text{Hz}}$.

To have the voltage noise for this transimpedance amplifier, we must convert this noise current in a voltage noise, following the transfer function of the schematic of this stage. Note that the contribute of the current noise is strongly dependent by the resistor, being the gain proportional to the resistor and then to the output voltage. Because the corner frequency for the current is higher than the corner frequency for the voltage, and in the datasheet is not indicated the value for our interest frequencies, for our numerical evaluation of the noise, we have set the value for the current noise to a value higher than high frequency limit, extrapolating it to the

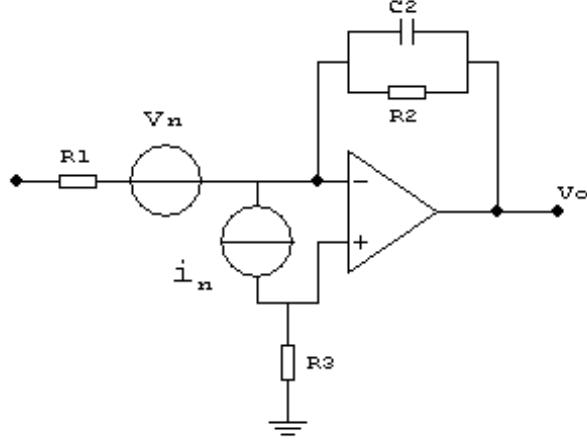


Figure 3.13: *Schematic of the general circuit for the noise analysis.*

lower frequency, and for high frequency value, we have assigned an approximative value of $I_n = 2\text{pA}/\sqrt{\text{Hz}}$ to overestimate the noise.

To describe the noise of an operational amplifier used in our work, in general, we can use the schematic represented in figure 3.13 in which we see the most general operational amplifier configuration to describe our readout schematics: the generators, that we see in figure, are substitutable by an equivalent noise generator V_{ne} , that is:

$$V_{ne}^2 = V_n^2 + I_n^2 R_t^2 \quad (3.19)$$

where $R_t = R_3 + (R_1 || R_2)$ is the thermal resistance that affect the amplifier⁷ and V_n and I_n as defined above. To this term we add the thermal noise generated from the resistors, so the equation 3.19 became

$$V_{ne}^2 = V_n^2 + I_n^2 R_n^2 + 4K_B T R_t \quad (3.20)$$

with K_B the Boltzmann constant and T the temperature.

So we can analyze directly the noise at frequency greater than 2.7 Hz (where the

⁷This sum is valid only if we assume that the generator are statistically independent.

noise is constant), obtaining (using the equation 3.20)

$$V_{ne} = \sqrt{V_n^2 + I_n^2 R_n^2 + 4K_B T R_t} \quad (3.21)$$

In this way we need to know the only value of the resistors that we used in our single stages of the general configuration to get the noise generated by the single operational amplifier and then by all the electronics.

A capacitor, in parallel to the resistor on the feedback of the amplifier, makes a low-pass filter whose cut-off frequency is given by

$$f_c = \frac{1}{2\pi R_2 C_2} \quad (3.22)$$

so the noise band became⁸

$$B = 1.57 \cdot f_c \quad (3.23)$$

In table 3.1 there is a report of the *input voltage noise* of the operational amplifiers used in our circuit⁹; only for the OP27 is specified the corner frequency (2.7 Hz), so with the other integrated circuits we suppose that the corner frequency is 10 Hz. For all the IC we have approximated the noise curve to a white noise for frequency above the corner frequency and 1/f noise from frequency under the corner frequency: in the figure 3.14 there are the curves drawn with this approximations.

To represent the noise on the reading circuit at any frequencies, we have reported the results in the figures 3.10 and 3.11. In the figure 3.10 is plotted the curve of the input voltage noise density of the single stage constituting the chain, considering the noise generated by the configuration of the amplifier as explained in the numerical example in the following sections, where:

⁸We remember that for a first order filter the equivalent noise band is obtained by multiplying the band for the factor 1.57 (see B.4 for more details).

⁹The values reported are all *referred to input* (RTI).

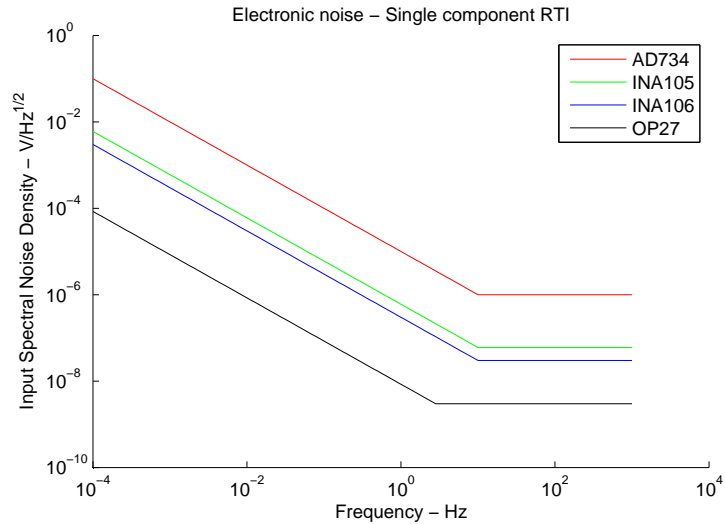


Figure 3.14: *Input voltage noise density of the single components (RTI)*

- *Noise TIA* is the transimpedance amplifier noise,
- *Noise INV* is the noise of the inverting amplifier,
- *Noise Diff NUM* is the noise of the differential amplifier at “the numerator” (the INA106 integrated circuit),
- *Noise Diff DEN* is the noise of the differential amplifier at “the denominator” (the INA105 integrated circuit),
- *Noise DIV* is the noise of the integrated divider circuit differential (AD734).

To have an idea of the absolute noise of the single stage, no interaction with the other component of the circuit are considered. Note, in comparison to the figure 3.14, that the noise is higher when we add the resistors.

In the figure 3.11 are plotted the input voltage noise density at the “sequential”

	Specification	Density		
		$f_0 = 10Hz$ nV/\sqrt{Hz}	$f_0 = 100Hz$ nV/\sqrt{Hz}	$f_0 = 1kHz$ nV/\sqrt{Hz}
Operational amplifier	μV p-p			
OP27	0.08 $f \in [0.1, 10]Hz$	3.5	3.0	3.0
OPA227P	0.09 $f \in [0.1, 10]Hz$	3.5	3	3
INA105	2.4 $f \in [0.1, 10]Hz$	-	-	60
INA106	1.0 $f \in [0.1, 10]Hz$	-	-	30
INA114	1.4 $f \in [0.1, 10]Hz$	15	11	11
AD734 DIV	-	-	1 000	1 000

Table 3.1: Input Voltage Noise of differential amplifiers used

stage¹⁰ summing the noise due to the interaction with the other components of the circuit (that generate noise) that affects the signal “before” that the signal is coming in this stage (in this way the noise of the first stage is equal to the noise of the first stage *single component*, the noise of the second stage is the noise of the second stage *single component* summed to the noise of the first stage *single component*, and so on); we can note that, while the signal is propagate along the circuit, crossing the various stages, the noise increase.

In any case we see that the greater noise of the circuit is represented by the analog divider noise, that fix the higher limit for total noise, being greater than the noise of the ADC (see figure 3.16 to have an idea of the ADC noise compared to the theoretical TIA noise with an high feedback resistor).

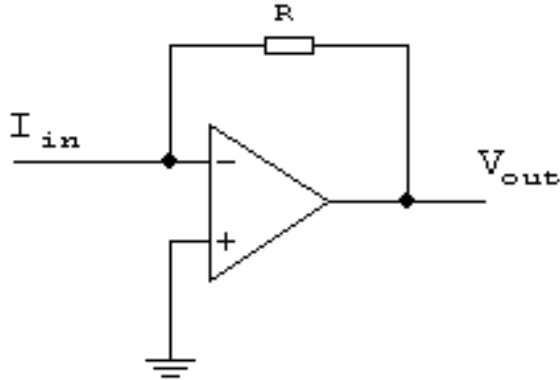


Figure 3.15: A *transimpedance amplifier* to convert the current signal generated in a tension signal.

3.6.4 Transimpedance amplifier

The output of the PSD is a *current signal*¹¹, so, to have a *tension signal*, we need to use a *current-tension converter* that in our case is constituted by a circuit based on an operational amplifier transimpedance schema (TIA). The configuration is that shown in figure 3.15, where we see that an input current I_{in} produces, via an operational amplifier, a tension signal V_{out} . The operational amplifier's input is connected to the signal source (in our case the photodiode) and the inverting input directly to the ground; the output of the operational amplifier is connected in series

¹⁰The acronyms of the legend are the same of that in the figure 3.10 but in this case are indicated also the number of the stage, because the figure shows the global theoretical noise at that stage.

¹¹The projectual choice that the output of this this sensor is a current signal, that must be converted to a tension signal, must not be considered a limitation (since we need of an ulterior electronic stage), because if we have, for example, a long cable to connect the sensor to the amplifier we can have a voltage loss along the cable, having a different tension in input to the readout circuit. In fact a lots of sensor give the output signal in current (very common is the $4 - 20\text{ mA}$ standard, for which we note that the minimum is not *zero* to avoid misreading in case of a broken wire or bad contact).

with the input voltage on the next stage of the chain.

With this schema the value of tension is equal to $V_{out} = -R_{TIA}I_{in}$, with R_{TIA} the feedback resistor.

In this configuration, with the non-inverting input connected directly to the ground, the inverting input is a virtual ground, and we have no problem due to the bias current because the only tension can be generated by the photodiode (about a tenths of volt).

The signal to noise ratio, SNR , that we have in the output of the transimpedance amplifier, depends on the feedback resistance R_{TIA} , and is given by

$$SNR \doteq \frac{U_P}{U_N} = \frac{U_P}{\sqrt{U_{PSDnoise}^2 + 2 \cdot U_{TIAnoise}^2}} = \frac{I_P \cdot R_{TIA}}{\sqrt{(I_N \cdot R_{TIA})^2 + 2 \cdot U_{TIAnoise}^2}} \quad (3.24)$$

where in the last equation we have used the equation 3.15 for the noise generated from the photocurrent of the photodiode.

Transimpedance amplifier noise

To evaluate the noise of the first stage of the amplifier, we use the curve shown in the figure 3.12 (or fig. 3.14). The noise is a specific of construction of the operational amplifier: in our schema we have used an *OP27* (Analog Devices), so we see that the value depends from the frequency (see section 3.6.3): for high frequency (above the various corner frequencies) we have that the noise is constant and assumes the value (using the equation 3.21)

$$V_{noiseTIA} = \sqrt{V_{noiseOP27}^2 + A_{noiseOP27}^2 R_{TIA}^2 + 4 * K_B * T * R_{TIA}} = 20 nV \sqrt{Hz} \quad (3.25)$$

For the range of frequency of our interest we have drawn the voltage input noise density in figures 3.10 and 3.11¹².

¹²Note that on the first stage the sequential stage noise and the single stage noise are the same.

Transimpedance SNR

The signal to noise ratio is evaluated with the use of the equation 3.24. The parameter that we use (with our apparatus) are:

R_{TIA}	$= 20.500k\Omega$	Feedback resistance
I_{Ph}	$= 260 \mu A$	Photogenerated current
I_N	$= 9.15 \cdot 10^{-10} A$	Total noise
U_{TIA}	$= 0.1 \mu V$	from the figure 3.12

As for the noise, we note that the term $U_{TIAnoise}$ depends on the frequency: we choose, as upper value, the noise at $f = 0.01 Hz$ so we setting the noise $U_{TIA} = 0.1 \mu V$, having $SNR = 284 \cdot 10^3$:

Consideration on the transimpedance amplifier noise

As explained in the section 3.6.1 it is very important to reduce the noise on this first stage, to have the minimum reachable noise on the rest of the circuit. Other motivation on the optimization of the noise for this stage can be found if we think to use a digital processing to manipulate the signal to obtain a digital divider instead of an analog divider (as described in this work). So it is very useful to analyze the noise in the best condition. To do this analysis we have measured simply the noise generated by an OP27 amplifier¹³ in transimpedance configuration with a feedback resistor of $260 K\Omega$ in parallel with a capacitor of $150 pF$ ¹⁴. The noise measurement has been done with the input terminal in open circuit¹⁵, and making a digital acquisition with a common ADC of 16 bit with sampling frequency $F_s =$

¹³We have used the OPA227P from Burr-Brown[12].

¹⁴In this configuration we have a low-pass filter with cut-off frequency equal to $f_c = 4 kHz$

¹⁵If we imagine to short circuit the input we have inevitably little current on the inverting input and, being the amplitude ratio theoretically infinite, a saturation on the output of the amplifier

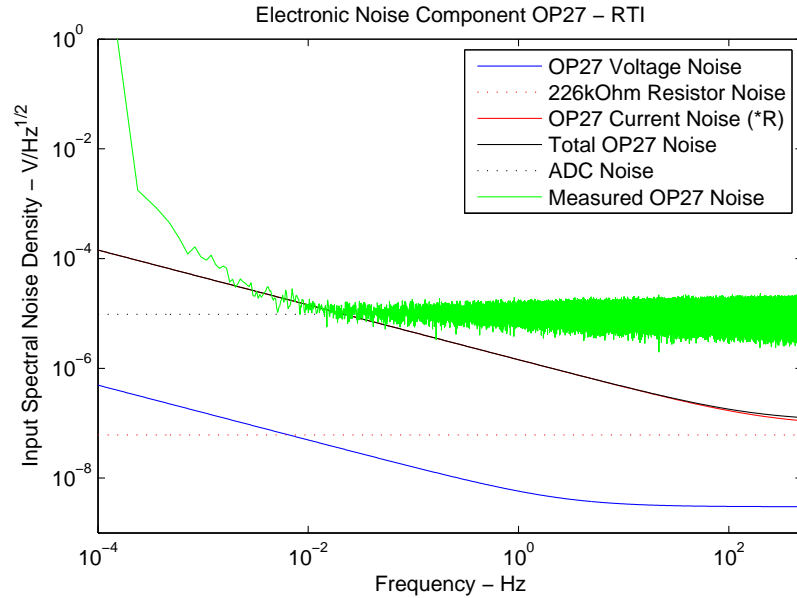


Figure 3.16: *Measured noise of the transimpedance amplifier (OP27) in comparison with the ADC 16 bit theoretical noise.*

1000 Hz. The results are shown in figure 3.16: in this figure we see the theoretical noise of the amplifier (continuous black line) as a sum of the voltage noise spectral density of the OP27 (blu line), the contribution of the feedback resistors (red dotted line) and the, most relevant, current noise spectral density of the OP27 multiplied the resistor R to have the corresponding volt value (the continuous red line, just a little under the total OP27 noise). Note that, with this feedback resistor (a very high value), all the various noise source produce a noise smaller than the noise due to the current noise multiplied for the resistor.

The measured value on the output of the amplifier is given with the green line and the ADC limit with the black dotted line¹⁶. As we can see we must to distinguish

¹⁶The quantization noise is being calculated as $E = \frac{V_R}{2^{16}} \cdot \sqrt{\frac{1}{F_s}} = 9.65 \cdot 10^{-6} V / \sqrt{Hz}$ where V_R is the range in volt of the ADC equal to $V_R = 20 \text{ volt}$ and the sampling frequency is $F_s = 1 \text{ kHz}$.

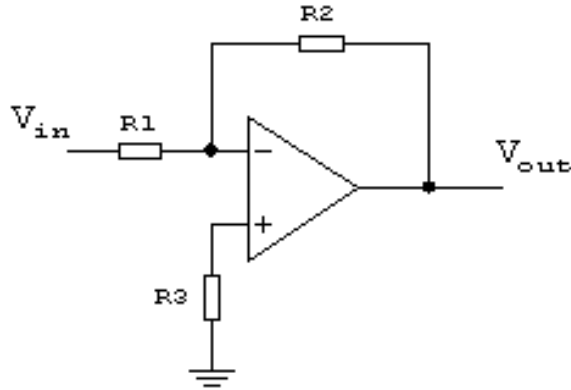


Figure 3.17: *Schematic of an inverting operational amplifier.*

the case in “high” frequency where the only limit on the noise is given by the ADC¹⁷ and case in low frequency where the limit is given by the amplifier itself. So in low frequency we have a not improvable limit due to the electronic characteristic of the component used.

3.6.5 Inverting amplifier

To normalize the signal (see section 3.6.7) we need to make the summation of the signal on the denominator of the divider. To make the sum we use an INA differential amplifier (see section 3.6.6 and 3.6.7) by inverting the signal in output of one of the two TIA amplifier.

To evaluate the noise that introduce the inverting amplifier in the chain, we use the concept explained in the section 3.6.3. The noise voltage and noise current is described in the datasheet of the OP27 and in the section 3.6.3: the new parameter

¹⁷A simple calculation give us, for an ADC of 18 bit in the same condition, a value of $2.41 \cdot 10^{-6} V/\sqrt{Hz}$.

is given from the value of R_t , that we remember is

$$R_t = R_3 + (R_1 \parallel R_2) \quad (3.26)$$

and, following the figure 3.17, by setting the value for the resistors as $R_1 = 10 K\Omega$, $R_2 = 10 K\Omega$ and $R_3 = 5.63 K\Omega$, we have $R_t = 10.63 K\Omega$. For high frequency, by using the equation 3.21 we have that the noise is:

$$\begin{aligned} V_{ne} &= \\ &= \left[\begin{array}{ccc} V_n^2 & + & I_n^2 \cdot R_n^2 \\ & + & 4 \cdot K_B T \cdot R_t \end{array} \right]^{\frac{1}{2}} \\ &= \left[\begin{array}{ccc} (3 \cdot 10^{-9})^2 & + & (2 \cdot 10^{-12})^2 \cdot (10.63 \cdot 10^3)^2 \\ & + & 4 \cdot 1.38 \cdot 10^{-23} \cdot 298.15 \cdot 10.63 \cdot 10^3 \end{array} \right]^{\frac{1}{2}} V/\sqrt{Hz} \\ &= 2.5 \cdot 10^{-8} V/\sqrt{Hz} = 25 nV/\sqrt{Hz} \end{aligned} \quad (3.27)$$

while the noise voltage density is given in the figure 3.10 for the single stage and in the figure 3.11 at the output of inverting amplifier inserted in the circuit.

3.6.6 Differential amplifier

To use the divider we must have at the numerator a signal that is the difference of the voltage given by the two transimpedance amplifiers and as denominator the sum of them. The sum on the denominator is made up by inverting the tension value of one transimpedance amplifier and than by using a differential amplifier, an *INA105* [13] (from *Burr-Brown*, [12]): in this way we make a sum, $V_1 - (-V_2) = V_1 + V_2$. The difference on the numerator is made up directly with a differential integrated amplifier, $V_1 - V_2$, and in our case, to have a greater resolution, we use the *INA106* [14]

(also from *Burr-Brown*, [12]) that has the peculiarity with respect the INA105 to multiply the difference for a factor equal to 10, to have $10 \cdot (V_1 - V_2)$.

Differential amplifier noise

For the single stage on the numerator the evaluated noise is the noise of the INA106, while the noise in the circuit can be calculated by using the equation 3.21, so we have for the numerator:

$$V_{noisediffNUM} = \sqrt{2 \cdot V_{noiseTIA}^2 + V_{noiseINA106}^2} \quad (3.28)$$

whose plot is shown in figure 3.11. In the equation 3.28 we note that have summed the noise of the single stage (the noise of the INA106) to the noise at the output of both the TIA amplifiers.

For the denominator we apply the same formula with the INA105, having the noise of the INA105 for the single stage and the noise in the circuit (equation 3.21):

$$V_{noisediffDEN} = \sqrt{V_{noiseTIA}^2 + V_{noiseINV}^2 + V_{noiseINA105}^2} \quad (3.29)$$

that is plotted in figure 3.11. In the equation 3.29 we have summed the noise of the single stage (the noise of the INA106) to the noise of the first TIA amplifier and to the noise of the inverting amplifier.

3.6.7 Divider

The last stage of the chain is constituted from an *AD734*, an integrated circuit¹⁸ that we use in a configuration as *divider*. With the divider we have a signal independent from the light source power: in fact by normalizing the amplitude of the signal with

¹⁸Provided from Analog Device, [7].

respect to the sum of the two output of the PSD, we make the output of the reading circuit independent from the variation of the power of the light. The output of the transimpedance amplifier is a voltage that is proportional to the position of the light beam, so, for a given position of the folded pendulum, if we indicate with V_1 the tension signal in the output of the first transimpedance amplifier and with V_2 the value of the signal of the second transimpedance amplifier, we can obtain the absolute position of the FP as $P = V_1 - V_2$.

Now, if we imagine that the light source accomplish a variation of the power, for example by a K factor, the position became $P' = KV_1 - KV_2 = K \cdot (V_1 - V_2)$: in this way cannot know if a variation of P depends on a variation of FP position or by a variation of the light power. To make up for remedy of this mistake, we divide P' with respect the sum of the tensions so we have

$$P = \frac{V_1 - V_2}{V_1 + V_2}$$

and if we imagine to have a variation of the light power we'll have

$$P' = \frac{K(V_1 - V_2)}{K(V_1 + V_2)} = \frac{V_1 - V_2}{V_1 + V_2}$$

so we became independent from the light power.

We can expect other variation, more than the light incident power, that justify the use of a divider when we use the system as seismometer: in this case the oscillation of the test mass is very considerable and we can have a displacement of the spot light on the PSD very large: theoretically this displacement must be horizontally, but sperimentally we can have a little vertical component, so the total incident light power can vary with the variation of the horizontal position. In any case the dimension of the spot light is not hard defined, because it is a gaussian spot with a width of about¹⁹ 0.1 mm (see Appendix A for detail). Being the amplitude of the PSD

¹⁹ Because of the presence of a light focuser collimator, the beam outcoming from the fiber is

equal to 1 mm, we have a residual light out of the sensitive surface of about 0.1 % that can vary, in case of horizontal-vertical misalignment, during the oscillation, so there is always a little contribute due to the misalignment that we cannot directly control.

Divider noise

As mentioned in the previous section, to accomplish the division we use the AD734. From the datasheet we can see that the AD734 has several configuration that permits a lots of operation; in particular there are two methods to use it as divider: the first is to use it as multiplier in a feedback loop, while the second use the capability of varying the scaling voltage (see [7]). In any case we must be careful to the denominator that must have a tension higher of about 0.1 volt²⁰, but in the second one we must have that the numerator must be $Numerator < 1.25 \cdot Denominator$, having in this a sort of limitation on the dynamics of the signal, so we use the first method.

Because we have chosen to use the divider in a configuration as multiplier, we use the specific of the AD734 as multiplier, that are provided in the range of frequency $f \in [10^2, 10^6]$ (see table 3.1). By using the equation 3.21 we have the curve shown in the figure 3.11: as we can see the noise generated by AD734 is greater than the other noise and it is this component that is responsible of the higher noise of the circuit.

described by a “cone”, so the waist is depending from the optical distance between the collimator and the PSD.

²⁰With our schema this is not a problem because the output of the transimpedance amplifier has always a value greater than about one volt, so the denominator, that is the sum of the two tension signal never be less of 0.1 volt.

3.7 The better choice

As we have seen in this chapter the limitation on the readout is the noise of the analog readout circuit. The limitation is due to the analog divider noise. To decrease this noise we can use a digital divider, and if we make some little variation on the circuit we can improve greatly the dynamic of the reading circuit.

To do this necessarily we must use an ADC in the readout chain (in the analog circuit the ADC is the last component, and it is used only if we want to digitalize the signal). The circuit can remain substantially the same, but same operation can be done numerically.

By analyzing the first stage of the stage of the circuit, we see that it is constituted by a transimpedance amplifier: this choice cannot be varied, because it is necessary to make the transduction from the signal current to the noise current. But if we increase the value of the feedback resistor we can have a greater value for the signal outcoming from the TIA amplifiers. The greater value is depending also from the light source (in fact is obviously related to the power of the light) and on the efficiency and physical dimension of the PSD, this last, fixing the lower value for the current²¹. Being our input ADC range $[-10\text{ V}, +10\text{ V}]$ the optimum is reached when the dynamic of the folded pendulum give an input value for the ADC that cover all the available range, and this can be done principally by choosing the displacement dynamic of the FP (that is depending on the use as seismometer or accelerometer, remembering that, in this last case, the movements is very little), and the geometric configuration of the optical lever, together with the choice of the feedback resistor and, not last, the supply voltage of the operational amplifier, that must be higher to permit to the

²¹Seeing the figure 3.6 we see that if the motion of the folded pendulum do not move the light beam on all the surface (from left to right for example) not all the dynamic of the system in used, making a lower value for the current that is not equal to zero.

output voltage to cover the range of the ADC²².

The second stage, is to make the sum of the two signal that must be used in the denominator of the divider. Being the input of the ADC almost 10 V , an analog summation must give a result with a maximum value of 10 V (precisely -10 V having the current the negative sign); but in this way the maximum tension voltage of the transimpedance amplifier cannot be 10 V , but must be 5 V . So we can do the summation digitally, as a simple sum of the TIA output, having no problem to use the value “20” numerically.

The digital difference at the numerator of the divider is not convenient, because we lost a great dynamic in the definition of the difference, so it is useful to make an analog difference centered in 0 V (that is when the FP is in the low potential position). In this way the value of the analog differential amplifier can be also amplified to an arbitrary value (we have used an INA114 with a resistor gain of $2050\ \Omega$, that makes gain of $G = 1 + 50\text{ k}\Omega/R \approx 25$), matching the range of the ADC.

The divider is digital.

We can summarize this concept by indicating as ADC_{TIA1} and ADC_{TIA2} the signals digitized respectively by the TIA1 and the TIA2 analog output of the TIA amplifiers, and ADC_{Diff} the output of the differential operational amplifier digitized by a third channel, having the normalized signal as:

$$Position = \frac{ADC_{Diff}}{ADC_{TIA1} + ADC_{TIA2}} \quad (3.30)$$

²²For example if the supply voltage is $\pm 9\text{ V}$ the output voltage can be maximum $\approx \pm 8\text{ V}$ and in this case we have loss in the dynamics of about 20%.

Chapter 4

The accelerometer

Usually many instruments work by treating the measured value as a disturbance, and measuring the input required to nullify that disturbance. Also in our case we use this approach, where the disturbances are the forces applied to the test mass by the movements of the Earth's surface. This method allows a non-linear measurement (of the disturbance) to be replaced by a linear measurement (of the *balancing* action); this in turn allows the construction of systems with very high dynamic range and good linearity. A particular case of this type is acceleration measurement.

4.1 Force balanced accelerometer

In this type of system, the force applied to the system results in an acceleration to a test mass. The mass displacement is sensed, and an opposing (restoring) force is applied to nullify the acceleration. The mass therefore moves in only a small zone around the null point since some small motion is needed in order to detect that the mass tries to move (a little movement necessary to sense the displacement): this permits the use of large masses with weak suspensions (to enhance sensitivity) and reduces the need for a long range of travel for such test mass. Central to this system

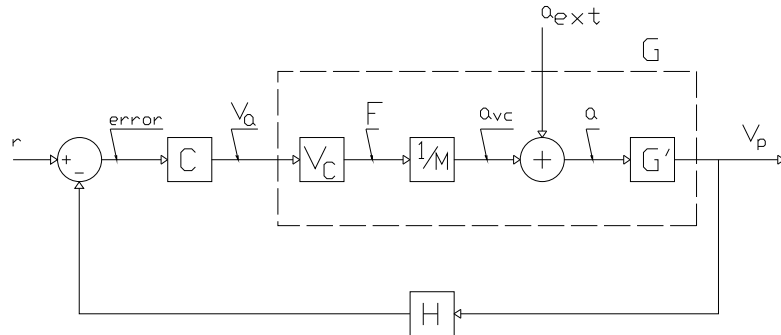


Figure 4.1: *Schematic drawing of the feedback control design.*

is the displacement sensor, that must have high resolution and wide bandwidth, but it does not require a wide range, as if the system is working correctly, the mass should not move at all¹.

In our force-balance system, we use the optical position sensor to detect the displacement and a voice coil to actuate a balancing force. To generate the correct signal to send to the actuator we have made a control system that has, as input, the signal from the reading circuit, while the output is opportunely amplified and sent to the voice coil. The voice coil, fixed to the ground², acts on a magnet fixed to the

¹For this reason it is possible to use a PSD sensor with a little dimension, having a lower noise, or, as we'll see later, a different system based on an interferometric readout.

²This described is a second version of the system: the first one had the voice-coil on the oscillating mass, but this solution was not exactly mechanical reproducible because there was problem with the two wires that carry the current to the voice coil; in fact these wires connect mechanically the oscillating mass to the ground introducing a further damping factor that depends by the geometrical form of the wire, and that can be very different from a version to another: in this way we have a not exactly reproducible system, depending the quality factor on the random curvature ratio of the wires. On the other part by putting the magnet on the oscillating part we have a loss of generality, having an "oscillating magnet" that can interact with the ferromagnetic

test mass, so when we introduce a current in the wire it is generated a force on the oscillating mass that tends to lockup the oscillating mass. By measuring the current, we have a measure linearly proportional to the external acceleration, so the sensor directly measures acceleration, because a measure of the current give us a measure of the force, and so of the acceleration: in our case we must measure directly the voltage on the voice coil to obtain a value that is proportional to the acceleration of the ground, and after a calibration we can have the measurement of the acceleration.

The figure 4.1 shows a logical schematic of the Force Balance Accelerometer, FBA: the logical block C design the control network, V_C represent the voice coil actuator, G' the mechanical system and H the transducer for the feedback.

G is the direct action block that include the actuator and the mechanical system: note that the external acceleration acts on this block; the $1/M$ block has the logical function to convert the force acting on the oscillating mass into an acceleration. The other symbols assume the following means:

r is the reference signal (for our application it is constant, and equal to $r = 0$ when we calibrate the system to have zero volt in out when it is in its equilibrium position);

$error$ is the error signal, that is the “input” for the controller (note that if the system is in an equilibrium position and there is no external acceleration the error signal is $error = 0$);

V_a , is a tension signal that represent the acceleration correction signal: it is this signal that we read to know the disturbance/external acceleration value;

F is the force actuated by the voice coil;

a_{VC} the corresponding acceleration deriving from the voice coil;

a_{ext} the external acceleration that is considered as a disturbance, summed to the material around, resulting in changing of the potential of the system.

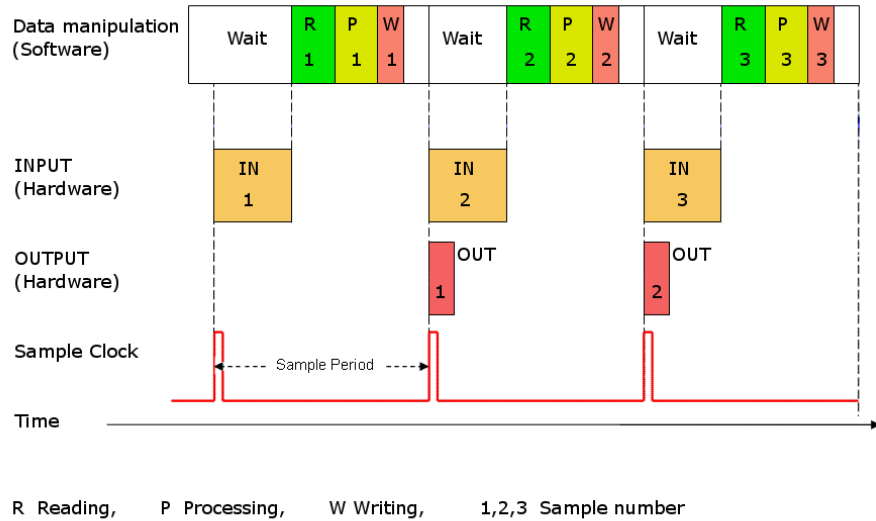


Figure 4.2: *Schematic of the intrinsic lag time of a digital control unit.*

acceleration of the actuator that must to be nullified;
 a the total acceleration incoming into the mechanic;
 V_P a tension signal that represent the position.

4.2 Digital and analog controller

To realize the control system we can follow two type of implementation, a digital controller or an analog controller. The substantial difference is on the presence of a processor unit to calculate the feedback action in the numerical implementation. The effects are the same in both the cases, but it is easiest to use the analog one because of its simplicity for the realization, requiring only operational amplifiers and some passive components (such as resistors and capacitors). On the other part it is preferable to search the time constant in a numerical way: in fact it is more

simple to find the time constant in a digital implementation (we must change only the numerical value in our program and observe the behaviour of the system) rather than in the analog way (changing the time constant necessitate to change the resistors and capacitors physically on the circuit). So, it is a good idea to choose the configuration and the time constants, implementing it with a numerical program designed to follow our specification, and experiment immediately the variation of the parameters.

To do this, it is of primary importance to have a real-time system, because the various time constants that characterize the control action must have exactly the time requested at the time of the execution. It is also necessary to have a sufficient speed for the CPU to manage the data in the correct time, generally related to the bandwidth of control requested by the project.

By seeing the schema in figure 4.2 we can see that for a digital control implementation we have always a lag time; in particular in figure we can see that the various process are synchronized by the sample clock. The first interval of time is requested by the sampling process ($IN1$ for the first event, $IN2$ for the second event and so on); when the digitalization is completed, the value is read ($R1$), processed ($P1$) and then wrote ($W1$) to the DAC ($OUT1$). As we can see the operations cannot be completed in the same time, so we have, as a consequence, necessarily also a lag time for the actuation of the control signal. For example if we consider a clock frequency of 1 kHz we have a time delay for the actuation of 1 ms ; a real-time processing assure a constant computing time ($R + P + W$ time equal constant³), so if we have that the computing time is less than $SamplePeriod - time(IN)$ we can have a correct control signal, respecting the assigned time constants, except for the time delay of

³Often we can have an *in-time processing*, where the time of the computing time is not constant but less than the time requested by the project, ensuring to complete the computing in time to actuate the control action requested for the next clock.

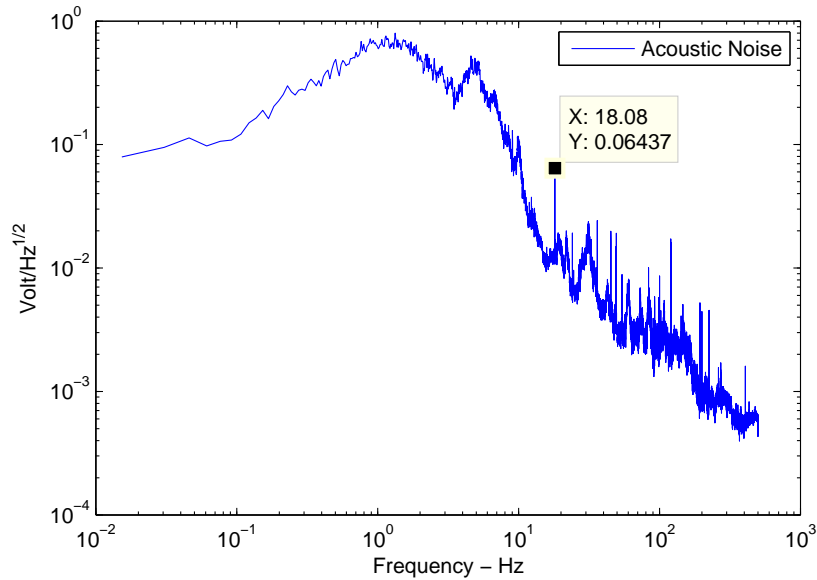


Figure 4.3: *Acoustic noise that affect the measured transfer function.*

a sample period (latency time).

In general to have a good control of the system we must have a good position signal outcoming from readout system. In the chapter relative to the readout we have seen how to minimize the noise in the analog and digital cases and how can be optimized readout circuitry having chosen the control type. The implementation based on the analog system give us a dynamic lower than the digital one (principally due to the high noise of the divider integrated circuit), but has a good portability due to the little dimension of the circuitry, while the digital control need of real time computing that, at the moment, increase the dimensions and limite the portability; the analog one has also a low cost with respect the digital one, so we have chose to implement a version of the control system also analogically.

4.2.1 Open-loop transfer function analysis

When we project the control system we make a function that “transform” the signal in an opportune way that generate an output that nullify the movement of the oscillating mass. To do this we must consider the dynamical characteristics of the system to control, that are summarized by the open loop transfer function of the mechanic.

The parameters of the control system are strongly dependent from the characteristic of the system to control, so the parameters can vary to the variation of the geometry of the mechanical system. Specifically if we vary the distribution of the masses, by moving the calibration masses, we necessarily must re-parametrize the transfer function of the corrector network. For this reason the control design must be done after that we have chosen the mass distribution.

We remember that this transfer function is obtained by exciting the oscillating mass with the voice-coil actuator, having in this way the typical transfer function of a second order mechanical system. By analyzing the open loop transfer function shown in this figure, we see that the response is flat in low frequency and decrease “linearly” (the decreasing obviously is not linear, but have the aspect of a linear decreasing in the Bode graph) in high frequency, with a rate of 40 dB/decade ; we note a principal peak, corresponding to the resonance frequency (characteristic of a second order system) with its corresponding phase shift; we see also a secondary peak, not well defined with a corresponding spread in phase at frequencies in the interval $f \in [17.2, 18.7]$: after several measurement (also validated with other instruments) we can conclude that this is an acoustic effect because by analyzing a spectrum of the acoustic noise in our lab (see figure 4.3) we have a peak at this frequency⁴; other transfer function measurement around that interval of frequency

⁴On the vertical axis is reported a value in *volt*: our system was not calibrated for an exact correspondence from acoustic sound pressure level and the output value in volt of the microphonic

(not reported in this thesis work) has given different frequency or no peak, depending on the ambient characteristics of the laboratories in which we have installed the sensor.

4.3 Feedback control design

As mentioned introducing this chapter the control system work on the FBA principle, principally because it permits a good linearity on the response in acceleration. The control system must be parametrized with correct time characteristics, depending on a specific system configuration to control; for example, we have seen that by adding a calibration mass we can vary the resonance frequency⁵ and by varying the weight of the calibration mass we can vary the mechanical quality factor⁶ that generate a different (and in our case, with a similar form until the system don't became instable) open loop transfer function, with different frequency and different width of the peak of resonance. For this reason in this thesis work we have chose to work with the folded pendulum without calibration mass, having the mechanical system some "default" characteristics that are simply reproducible.

So the system on which act with our control system is that described by the transfer function shown in figure 2.22; by observing the Bode magnitude graph of the response of the system we see that the response of the system is the typical response of a second order mechanical oscillator: at low frequency we have a constant gain, while, for frequency higher than the resonance frequency, the gain decrease to the increasing of the frequency; at the resonance frequency we have a very high peak in system, because with this graph we would only give a qualitative idea of the acoustic measurement, so we have considered unnecessary to calibrate the microphone.

⁵See section 2.1.6 for more details.

⁶See section 2.5 for more details.

the Bode magnitude graph ($f_0 = 721 \text{ mHz}$) due to its high quality factor Q .

Phase lead parameter

By using the FBA principle, the system will have a delay, a limited upper frequency response, and some additional phase compensation is required to assure stability (for example to avoid undesired oscillations); this can be done by including a phase-lead circuit [35], but the global frequency of the entire system (mechanical and feedback parts) is increased, so the global system have a frequency greater than the mechanical one [17]. To better understand this concept we can imagine that if the oscillating mass is not in the reference point (displacement due to an external acceleration that perturbs the system from its equilibrium position) and to nullify the displacement we use, in our control system, a force only proportional to the error position, we have that this force is equal to zero only when the error is zero: but in this way we have that, due to the inertia of the oscillating mass, when this last goes on the other side of the reference point, the error and the force change versus, pushing further the oscillating mass that reach the other side, generating an oscillation of the system (a situation similar to a mass constrained with a spring), having a second order system not damped. The presence of a phase-leading parameter operate the correction taking into account the position error and the derivative of the position error, having that the correction action is reinforced when the position error is high and is weaken when it is decreased: in this way the actuation force change its sign within a leading time respect to the condition of null error, having also a restoring force when the oscillating mass cross the zero position, giving the same effect of a dissipative phenomena.

Null position error

Another choice is to fix a pole in the origin obtaining a system *type 1*: given a general analytical representation of the transfer function in a factorized form with time constant:

$$G(s) = K \frac{1}{s^\gamma} \frac{(1 + \tau_{z1}s)(1 + \tau_{z2}s) \dots \left(1 + 2\delta_{z1} \frac{s}{\omega_{zn1} + \frac{s^2}{\omega_{zn1}^2}}\right) \left(1 + 2\delta_{z2} \frac{s}{\omega_{zn2} + \frac{s^2}{\omega_{zn2}^2}}\right) \dots}{(1 + \tau_{p1}s)(1 + \tau_{p2}s) \dots \left(1 + 2\delta_{p1} \frac{s}{\omega_{pn1} + \frac{s^2}{\omega_{pn1}^2}}\right) \left(1 + 2\delta_{p2} \frac{s}{\omega_{pn2} + \frac{s^2}{\omega_{pn2}^2}}\right) \dots} \quad (4.1)$$

with a pole in the origin we has the term $1/s^\gamma$ with $\gamma = 1$; this system has the main characteristic to have the regime position error equal to zero; we must remember that our reference signal (see figure 4.1) is always constant (and set to zero during the calibration with a correct levelling of the folded pendulum and centering of the optical lever), so if we not use a pole in the origin the control system is unable to reach the zero value for the position of the oscillating mass [28].

4.3.1 Corrector

Summarizing, our choose are a pole at 0 Hz to have a null position error, two zeros at 0.200 Hz before the resonance peak to dump it and two poles at 44 Hz used as low-pass filter to eliminate the high frequency disturb. The transfer function of this corrector is shown in figure 4.4 and the closed loop Bode in figure 4.5.

4.3.2 PID control design

To implement the control system we have implemented a corrector network with a PID controller. The design of the network, shown in figure 4.6, is based on a PID controller (Proportional-Integrative-Derivative) whose implementation is made up

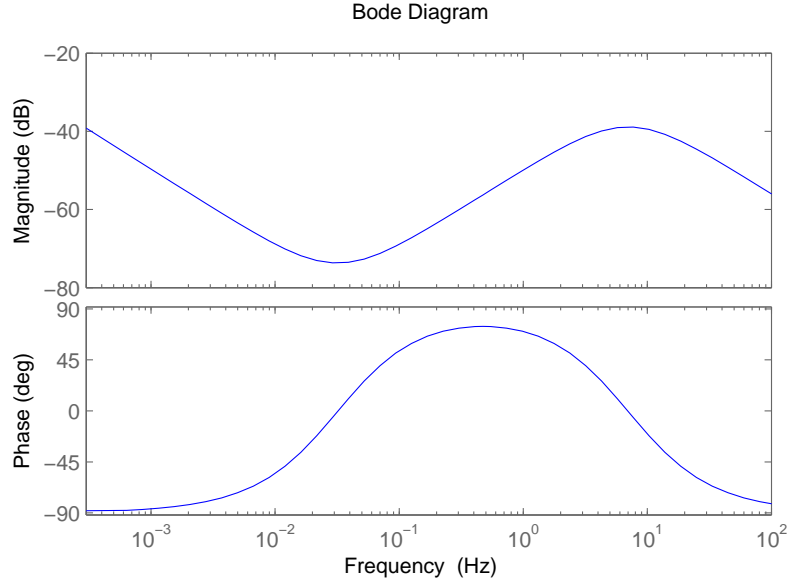


Figure 4.4: *The transfer function of the analog corrector.*

with an operational amplifier, designed as “OpAmp5” in figure. The other operational amplifiers, “OpAmp6” and “OpAmp7”, make a low-pass second order filter to attenuate the high frequency disturbance, while the last amplifier, “OpAmp8” is a buffer that acts only as a current driver for the voice-coil. Because the cut-off frequency of the low-pass filter is high enough, we study only the PID part of the control, that acts with frequency lowest the resonance frequency. By indicating on the amplifier “OpAmp5” with prefix $-a$ the group of the direct inverted input impedance, with $-b$ the feedback impedance and with $-c$ a mix of them, we have that the corrector has a transfer function given by⁷

$$C(s) = -\frac{(1 + s\tau_a)(1 + s\tau_b)}{(s\tau_c)} \quad (4.2)$$

⁷See also Appendix B for details.

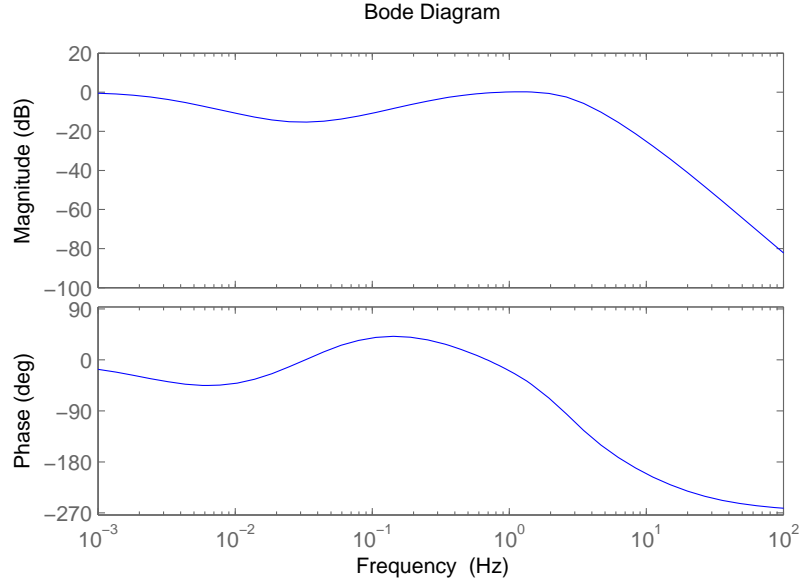


Figure 4.5: *The closed loop Bode transfer function.*

where the variuos groups are constituted by the components:

$$\begin{aligned}
 \tau_a &= R_{5a}C_{5a} \\
 \tau_b &= R_{5b}C_{5b} \\
 \tau_c &= R_{5a}C_{5b}
 \end{aligned}
 \tag{4.3}$$

The equation 4.2 can be written as

$$G(s) = -R_{5b}C_{5a} \frac{\left(\frac{1}{R_{5a}C_{5a}} + s\right)\left(\frac{1}{R_{5b}C_{5b}} + s\right)}{(s)}
 \tag{4.4}$$

that makes an evidence of the nature of the poles and zeros and their positioning on the frequency axis with the direct value of the resistive and capacitive elements.

The analog PID implementation

The analog implementation is based on an electronical circuit that makes a filter with several operational amplifiers (see figure 4.6). The input of the signal is directly the output of the analog divider circuit (discussed in section 3.6). As already

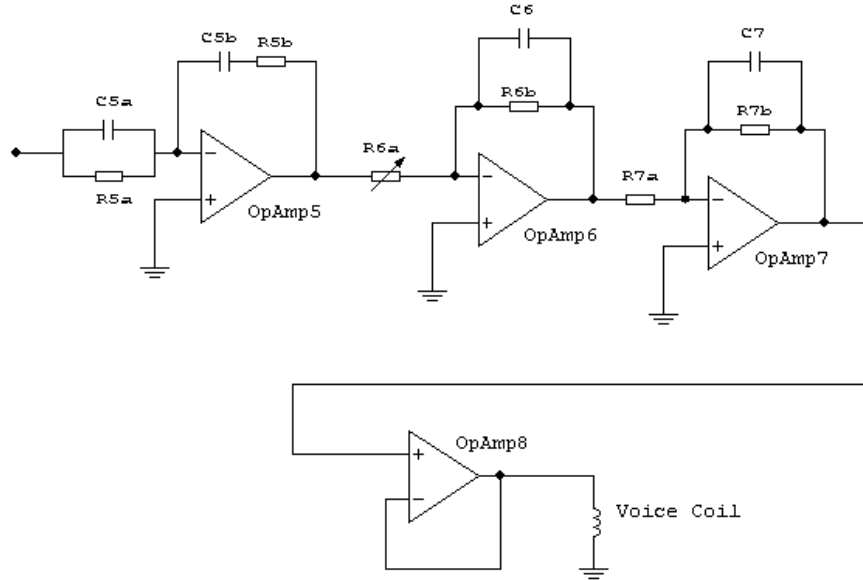


Figure 4.6: *Schematic of the analog control circuit.*

discussed the control system has a pole in the origin (at 0 Hz), two zeros at the frequency of 200 mHz and two poles at 44 Hz . To have this time constants we have set the values of the resistors and capacitors as:

$R_{5a} = R_{5b}$	$=$	$800\text{ k}\Omega$
$C_{5a} = C_{5b}$	$=$	$1\ \mu\text{F}$
R_{6a}	$=$	$2.1\text{ k}\Omega$
$R_{6b} = R_{7b}$	$=$	$3\ 650\ \Omega$
$C_6 = C_7$	$=$	$1\ \mu\text{F}$

The double pole in high frequency (that can be considered as a “double” low-pass filter) is implemented with two active RC circuit in series, each based on an operational amplifier having a resistor and a capacitor on the feedback; a resistor on the inverting input permits to have a known (fixed) gain for one of the low-pass

filter, and inserting a trimmer, R_{6a} , on the other operational amplifier we have a variable gain with which we can vary the compressive gain of the analog corrector network.

4.4 Calibration of the accelerometer

Being the accelerometer based on a FBA schema it has a flat response down to DC, and so a static response to static changes in the acceleration: that is if we have a permanent tilt we will have a permanent output. This characteristic can be used to calibrate the accelerometer, having an absolute and constant acceleration to refer, as the gravity acceleration. On this characteristics is based the tilt method: we tilt the FP by a known angle and measure the resulting gravity component, that is the constant acceleration that we consider. In closed loop the output of the accelerometer is given by

$$V_{out} = \frac{m}{\beta} (g \sin \theta + \ddot{x})$$

where m is the test mass, β is the response of the feedback actuator and θ is the tilt angle. To calibrate the accelerometer we have fixed the folded pendulum on a platform (the base that we can see in the picture in figure 2.19) that have three point of contact with a levelled plane. Each point of contact consist of micrometrical screws, so we can adjust the platform level to have the best levelling and then tilt it, along the direction of interest, with respect to the axis that vary the g gravity component. So tilting the platform we can measure the factor m/β observing the changes in DC output tension signal with respect the variation of θ . To measure the tilt of the platform we have disposed it in a way that, by tilting only one screw, we had the tilt in the interest direction; the screw has a forward pass equal to 0.25 mm

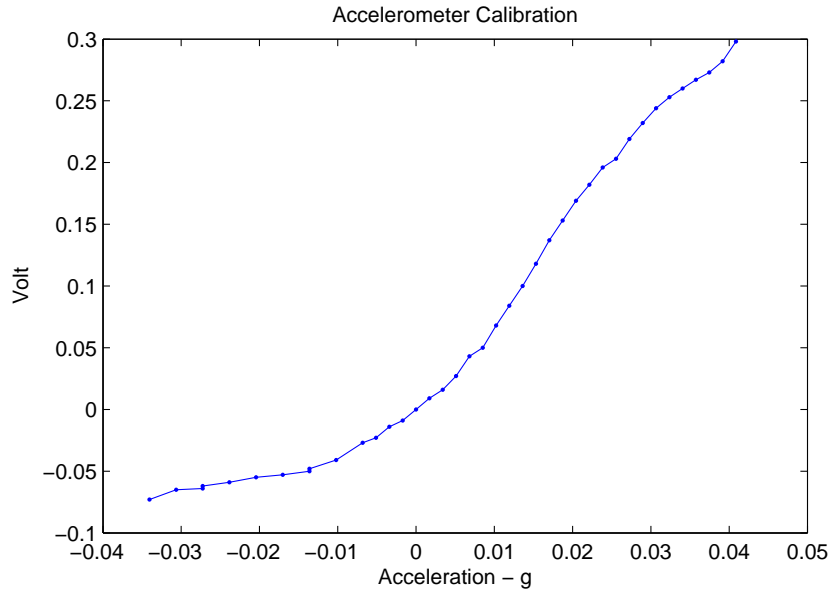


Figure 4.7: *Accelerometer response to acceleration in term of the voltage applied to the voice-coil actuator.*

for each round⁸, so by counting each round (or fraction of round) we had a measure of the tilt. At this point the angle was been evaluated as $\theta = \arctan(b/a)$, where b is the height variation (related to the number of round of the screw) and a the distance from the adjustable screw and the other fixed point of contact.

The figure 4.7 shows the corresponding value of the tension applied on the voice coil with respect the acceleration in the horizontal direction. The range chosen for the acceleration is the maximum reachable by the driver acting on the voice coil (the setup is that of the analog controller, described in section 4.3.2).

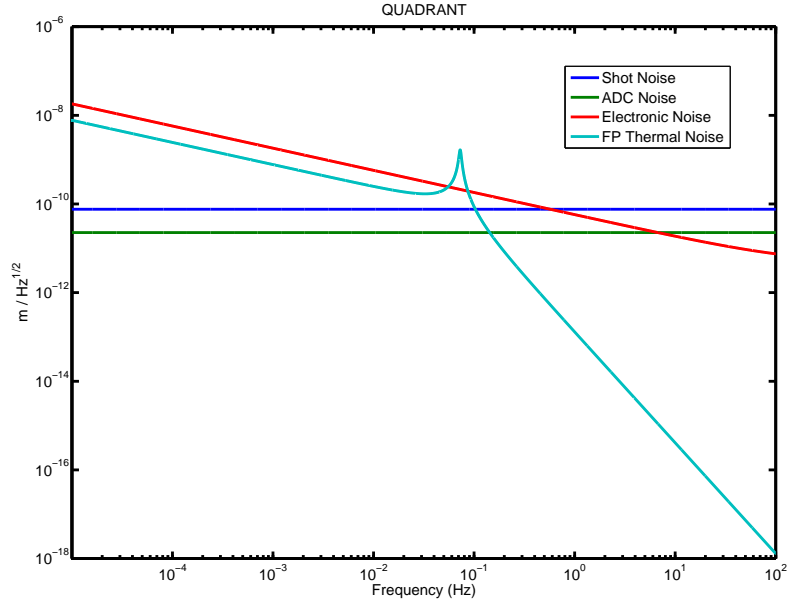


Figure 4.8: *Theoretical noise curves for optical lever with quadrant photodiode readout.*

4.5 Sensitivity Curve

The theoretical sensitivity curve of the monolithic FP sensor is defined by three main noise sources: internal thermal noise, readout noise and electronic noise. The internal thermal noise is dependent on the material and on the mechanical design (see section 2.1.5), while the readout noise and electronic noise are, instead, related to the external devices used to acquire the output signal. The readout noise is strongly dependent by the used system: in the section 3.3.3 we have seen the characteristics of two sensors (a PSD and a quadrant photodiode) used with an optical lever, from which we have calculate the best performance of the quadrant photodiode. In the figure 4.8 we see a comparison of the noise considered in the readout chain whose

⁸By rotating the screw of 28 round we have a variation of the height equal to 7 mm, so one round is equal to 1 round = 7.00/28 mm = 0.25 mm/round.

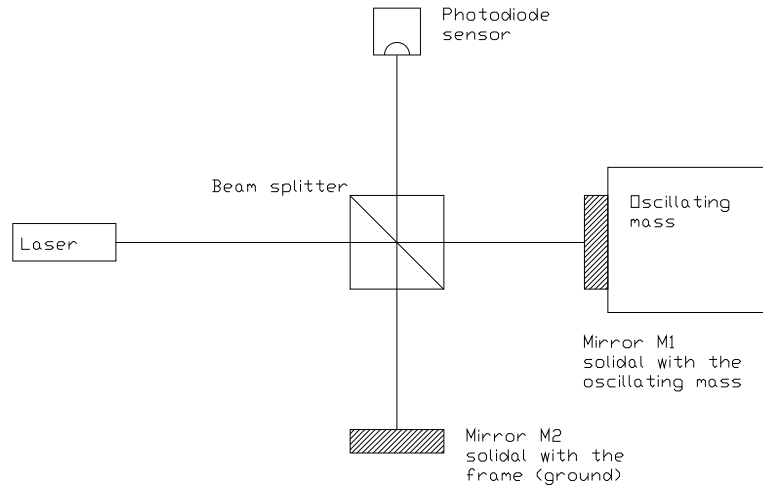


Figure 4.9: *Skecth of the Michelson interferometer using a mirror solidal to the oscillating mass.*

values are been calibrated and expressed in meters: the thermal, ADC, shot and electronic noise; we can see that the great limitations is given from the shot noise and the electronic noise, both dependent from the optical lever readout system.

4.5.1 Interferometric readout

Basing the readout on an interferometric readout we can have a great improvement on the noise. In the figure 4.9 we have skecthed a Michelson interferometer: a laser beam pass through a beam splitter that split the beam in two orthogonal directions and this two beam, reflected by the two mirror ($M1$ and $M2$) generate interference on the sensor photodiode. By fixing the mirror $M1$ to the oscillating mass, and the mirror $M2$ to the frame of the folded pendulum (that is solidal with the ground) we have that the interference fringes moves with respect the oscillating mass movements having, in this way, an high sensitivity for the readout. Comparing the noise obtained with the interferometer in figure 4.10 with the noise in figure 4.8

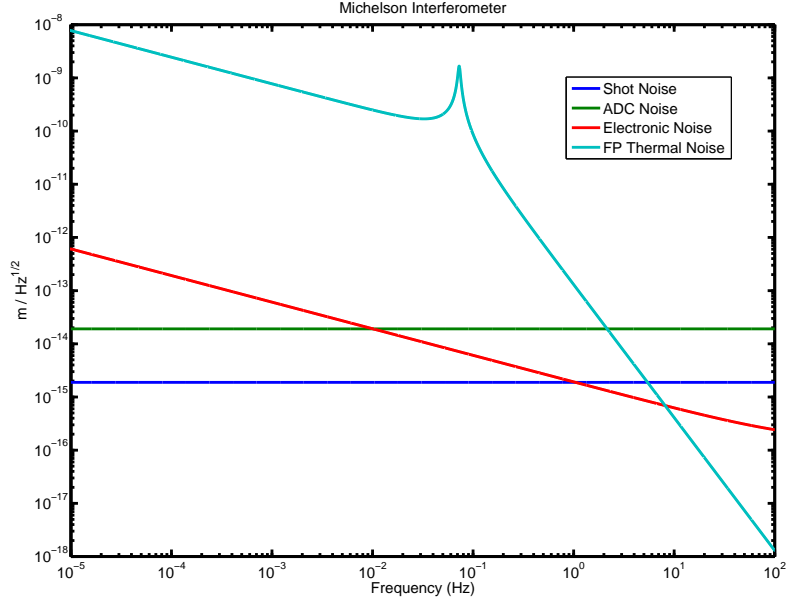


Figure 4.10: *Theoretical noise curves for Michelson interferometer readout.*

we can see that the readout noise have an improvement of a 3 ÷ 4 magnitude order, eliminating the limitations due to the shot noise.

To compare the sensitivity of the FP seismometer with other geophysical instruments, we reported in figure 4.11 the sensitivity of the STS-2 by Streckeisen, that represents the state-of-art of the low frequency seismic sensors [31]. This figure shows that the monolithic FP sensor has already a sensitivity comparable or better (with interferometric readout) of the STS-2 in the band $10^{-3} \div 10 \text{ Hz}$. We reported the Peterson New Low Noise Model (NLNM) [10], that is the minimum Earth's noise; from a collection of seismic data from 75 sites located around the world, Peterson found that there is a characteristics Earth's noise that can be described by two curves that limiting the upper and the lower of this noise; the lower limit delineate a minimum level of earth noise: noise levels below the NLNM curve

are never, or extremely rarely, observed.

All these tests were performed in air and with no thermal stabilization, evaluated at a temperature $T = 300\text{ }^\circ K$, and are obtained with the transfer function of the folded pendulum with a resonance frequency $f_0 = 70\text{ }mHz$.

It is interesting to investigate the sensitivity as accelerometer with different read-out systems, and compare this values with the commercial products. In this case force actuator keeps dynamically the oscillating mass at the equilibrium position, corresponding to the zero point of the PSD (or quadrant photodiode) and to a dark interference fringe of the Michelson interferometer. The transfer function to refer is the closed-loop one, defined as the test mass displacement with respect to the ground, $x_p(\omega) - x_s(\omega)$, as a function of the ground acceleration, $a_s(\omega)$:

$$\frac{x_p(\omega) - x_s(\omega)}{a_s(\omega)} = \frac{1 - A_c}{\omega_0^2 - \omega^2} \quad (4.5)$$

where the ground acceleration is defined as

$$a_s(\omega) = \omega^2 x_s(\omega) \quad (4.6)$$

The figure 4.12 shows the sensitivities as accelerometer with the optical lever readout (based on the PSD and quadrant photodiode sensor) and the interferometer readout, together the STS-2 sensitivity. As it was expected, also in this case we see the improvement with the interferometer readout.

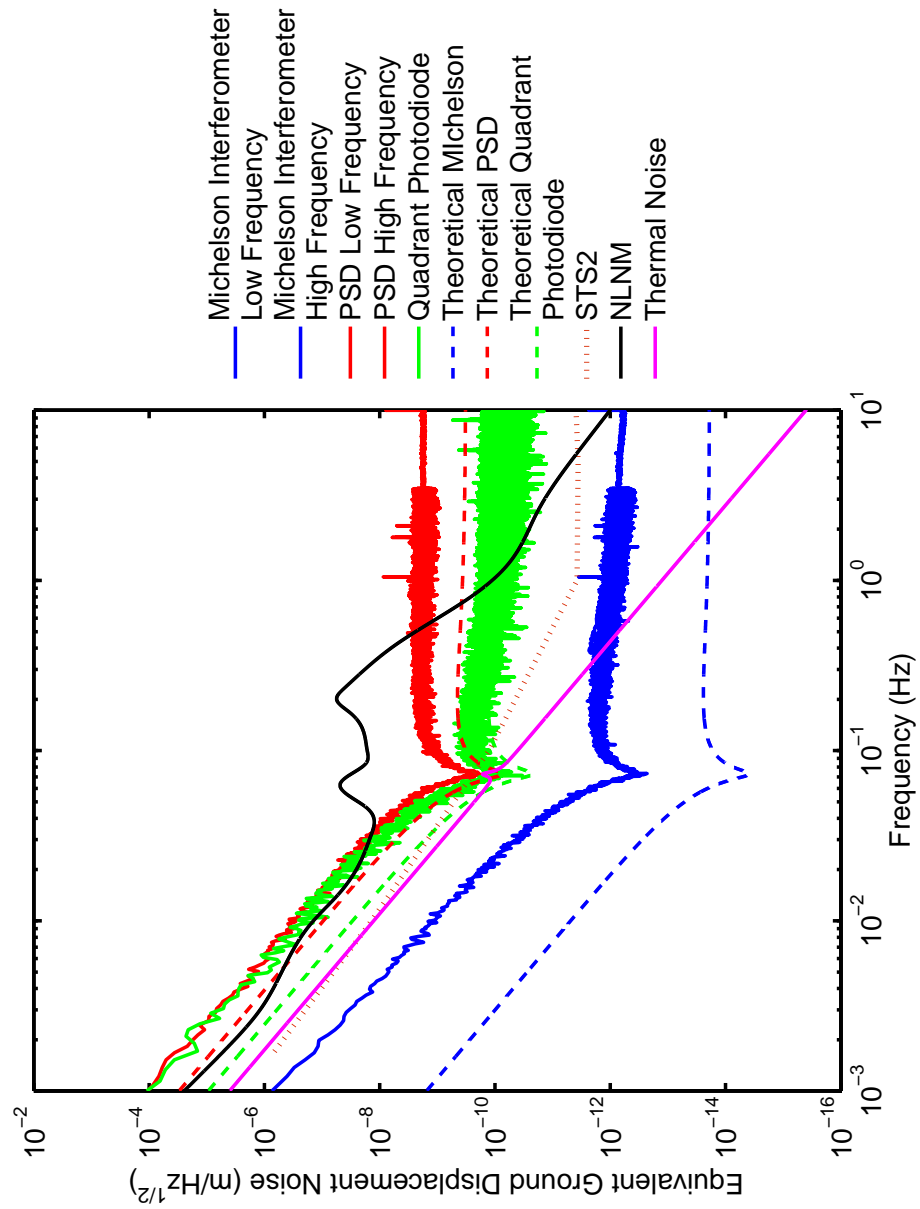


Figure 4.11: *Theoretical and experimental sensitivity curves of the seismometer with different readout systems and comparison with Streckeisen STS-2.*

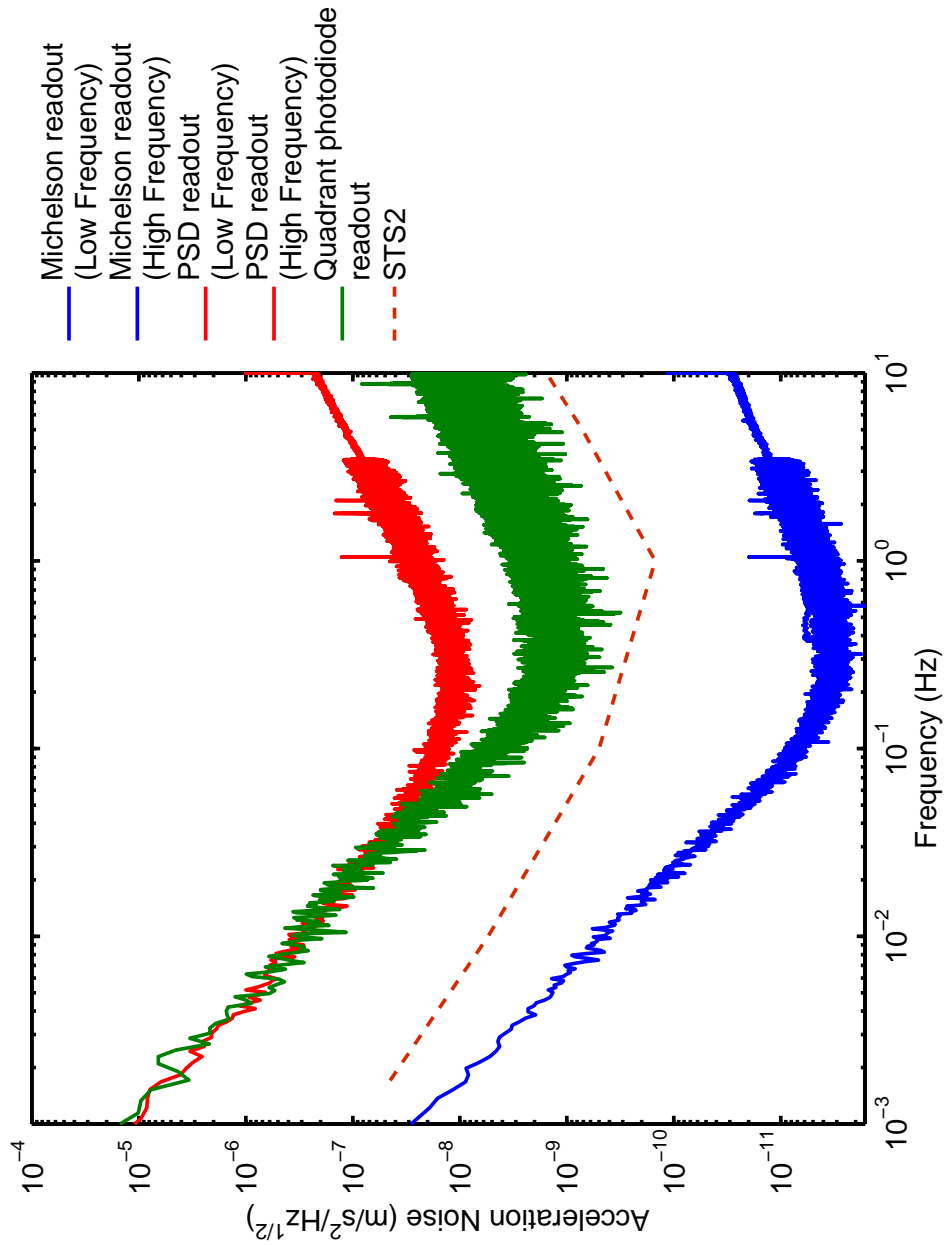


Figure 4.12: *Sensitivity curves of the accelerometer with different readout systems and comparison with Streckeisen STS-2.*

Conclusions

The work that we present is related to the technologic development of a new kind of seismic sensor, optimized for very low frequency and having a sensitivity best of the actual commercial instrument and very little dimensions. A similar instrument can give a contribute, in the low frequency band measurement, to the seismic zonation of a country: to have a more accurate mapping of seismic hazard, it is necessary to have a kind of sensors which can record with high accuracy and in a broad frequency band; in particular at low frequency, where much of the energy is released during an earthquake, we can sense teleseismic signals with periods ranging from hours to seconds. Having this target, we have developed a new oscillating mechanical system with tunable resonance frequency and high quality factor. The system is based on a folded pendulum design having a monolithic structure to reduce the thermal noise, realized with electro-discharge machining of a block of aluminum.

Summary of the work

The resonant frequency of the system is about 720 mHz , but it is possible to tune the resonance frequency down to 70 mHz , by adding a calibration mass on the oscillating part of the folded pendulum. Because of the monolithic structure of the system, the mechanical noise of the system is very low (see figure 4.8): the system has several part in suspension and it is possible to realize a monolithic structure with the

realization of some flexible hinges. Previous version of the folded pendulum had circular hinges, and with this new version, we have adopted elliptical hinges, that have best performance in terms of durability (with this design the hinge receive a lower stress with the same deformation of the older one), giving a lower frequency to the entire system also (see the FEM simulation relative to this study, see section 2.2.3). The lower stress of the material due to the new hinge design, has permitted the introduction of other variation with respect the previous version, by increasing the space between the oscillating part and the frame (fixed to ground), having a greater displacement of the oscillating mass (useful in the seismometer configuration), that has as good improvement to eliminate the air gap in this space; in this way we have reduced the dissipative effect due to the air flowing, having in air a greater mechanical quality factor, Q , with the possibility to reach the value of about $Q \approx 140$ at resonance frequency of about $f_0 \simeq 800 \text{ mHz}$ and a $Q \approx 10$ at a resonance frequency of $f_0 = 70 \text{ mHz}$. Some in vacuum measurement demonstrate that the quality factor increase of a factor ten at pressure of $P = 10^{-4} \text{ mbar}$.

Furthermore, with the adopted design, the system has almost a purely uniaxial response, with a cross-coupling ranging from 10^{-4} to 10^{-3} with respect to all the other degree of freedom.

We have also introduced a new readout system, based on an optical lever: a light source solidal to the ground generate a light beam that is reflected by a mirror solidal to the oscillating mass; when there is a movement of the oscillating mass due to the ground shaking, the light beam is deflected and a sensor, based on a position sensing device photodiode, solidal with the frame, sense the movement by detecting the light beam position. A dedicated electronics generate a voltage signal proportional to the light position, and so to the mass displacement, taking into account, and eliminating, the various noise of this approach (like laser power fluctuation, misalignment, etc.), giving a total noise very low, in comparison to other

readout system. However a new interferometric readout system has been developed, that permits to obtain a sensitivity, for the global system, in the band $10^{-3} \div 10 \text{ Hz}$, better than other systems, like the Streckeisen STS-2, that represents the state-of-art of the low frequency seismic sensors.

With a voice-coil acting on a magnet, we can apply a force on the oscillating mass. We have realized an analog (and digital) feedback control circuit, that, by using the position signal can generate a signal, that conveniently manipulated, can drive the voice-coil to “immobilize” the oscillating mass, having in this way an accelerometer, with the possibility to measure directly the acceleration of the ground.

By summarizing with this work we have:

- designed and realized the monolithic part of the sensor;
- tested a calibration procedure to tune the resonance frequency, reaching the lower frequency of 70 mHz
- realized and tested an optical readout system, with an analogic reading circuitry
- estimated the sensitivity curve with different readout system in open-loop
- realized and tested an analogic control system to realize, in closed-loop, the accelerometer with the optical lever readout

Future Development

A development of the system can be made with an improvement on the mechanical part, on the read out and then on the control system to close the loop to have an accelerometer. The parameter and the implementation of this last one is depending by the two other, but the development of the mechanical part, can be made

independently from the development of the the readout and viceversa. An improvement of the readout can be made up by changing the philosophy of the circuitry, by passing from the analog operation (to obtain the divider) to the digital one, having in this way a totally numeric readout and control system (the only analog part is consituted by the two transimpedance amplifiers and one instrumentation amplifier, see section 3.6.4), while introducing the interferometric readout we can have a great improvement on the sensitivity of the system.

Another great improvement is reached with a new project of the mechanical part, that allows a greater quality factor and a more stable system in low frequency (under 300 mHz).

Mechanical improvement and simulation with FEA analysis

Of great utility is the study on the finite elements analysis: a knowledge of the correct procedures can give an instrument that permits to compute the solution of the dynamic of the folded pendulum. As already mentioned in the section 2.6, there are several problem on this type of analysis, but if we can have simulation method to calculate the response of the system with high accuracy, we can save a lot of time by sparing the realization of a piece before to know the improvement of the project. Actually we have made some experiment but we had only qualitative value of the resonant frequency; in fact the experimental value had a sistematic error of about 500 % with respect the simulated one, although we have the correct trend on several data.

With aid of the simulation we can obtain a good project design to have a system that has a natural very low frequency with a minimal stress of the joint; we remember that the higher is the joint's width the higher is the stiffness of the joint, so the natural frequency of the folded pendulum is higher because of the elastic restoring force. On the other part a little width make the joint more fragile, so we can have the

rupture of the joint, obtaining a not reliable system. In this optics the simulations is a useful way to search the correct trade-off between the width and the resonance frequency.

Readout and control improvement

As discussed in the introduction of this chapter, it can be performed an ulterior improvement on the readout and control system. As shown in the figure 4.11 we can see that with an interferometric readout we can reach a level of sensitivity better of several magnitude orders: on this point we have developed the interferometer readout, based on an optical laser source with a compact apparatus constituting the interferometer. With this interferometric readout we can improve the use as accelerometer by developing a new control system. To do this it is necessary also to use the optical level readout: in fact in a first step the optical lever provides the error signal for the FP in order to reduce, within an interferometric fringe, the movement of the mirror fixed with the inertial mass; in a second step the interferometric signal is used then as an error signal for the control. In this last phase the Michelson interferometer (also described in figure 4.9), far better of the optical lever, provides a more accurate error signal, and it allows the locking of the test mass position with respect to the frame.

Actually, with the optical lever, the digital divider (see section 3.6.7) is implemented with a real-time computer VME based, but it is possible to use a PC with a specific operating system, or some commercial product based on FPGA microcontroller. Because of the low complexity of the execution of the operations, we can make a digital divider using a PIC (Programmable Interface Controller); this type of implementation can be used because of the low frequency of the signal to elaborate, that not require great velocity in computing. In this case we can use a circuit like that described in section 3.7, actually used with a PC in off-line analysis (obviously

not used with control system).

It possible to use the numerical solution with the control system also, just implementing the actual control system on the PIC.

Bibliography

- [1] Acernese F., De Rosa R., Giordano G., Romano R. and Barone F. (2007)
Mechanical Monolithic Sensor for low frequency seismic noise measurement
Proc. SPIE Vol 6529 65292B-1
- [2] Acernese F., De Rosa R., Giordano G., Romano R. and Barone F. (2007)
Mechanical monolithic accelerometer for suspension inertial damping and low frequency seismic noise Proc. Amaldi 2007
- [3] Acernese F., De Rosa R., Giordano G., Romano R. and Barone F. (2008)
Mechanical monolithic horizontal sensor for low frequency seismic noise measurement Review of Scientific Instruments 79, 074501 2008 (DOI 10.1063/1.2943415)
- [4] Analog Devices[©] - <http://www.analog.com> (2008)
- [5] Borman P., (2002), *New manual of seismological observatory practice*, Geoforschungszentrum Potsdam
- [6] Analog devices[©] OP27, *Low Noise, Precision Operational Amplifier* datasheet, rev. F, 2006
- [7] Analog Devices[©] AD734, *10MHz, 4-Quadrant Multiplier/Divider* datasheet, rev. C

- [8] Aki K. and Richards P. G., (2002) *Quantitative Seismology*, University Scientific Books
- [9] F. Barone, A. Brillet, C.N. Man, F. Fusco, R. De Rosa, L. Di Fiore, A. Grado, L. Milano, G. Russo, *Digital alignment system for laser beam*, Physics Letter A, Elsevier, 193, (19 September 1994), pp.15-20
- [10] Berger J., Davis P. (2005) *Ambient Earth Noise: A Survey of the Global Seismographic Network*, 2005 IRIR 5-Year Proposal, 38
- [11] Bertolini A. et al., (2006), *Nuclear Instrument and Method*, No. 556, p. 616
- [12] Burr-Brown[©], <http://www.ti.com> (2008)
- [13] Burr-Brown[©] INA105, *Precision Unity Gain Differential Amplifier* datasheet, Texas Instrument, August 1993
- [14] Burr-Brown[©] INA106, *Precision Gain = 10 Differential Amplifier* datasheet, Texas Instrument, October 2003
- [15] Comsol[©] Multiphysics user's Guide (2007)
- [16] Fergusson E. S., (1962), *US Nat. Museum Bull.*, No. 228, p. 185
- [17] Havskov J. and Alguacil G. (2002), *Instrumentation in earthquake seismology*, preliminary version, June 2002, pp.46-51
- [18] Hamamatsu[©], <http://www.hamamatsu.com> (2008)
- [19] Horowitz P. and Hill W. (1990) *The Art of electronics*, 2nd edition, Cambridge University Press
- [20] Labview[©] National Instruments
- [21] L. D. Landau and E. M. Lifshitz, (1986) *Theory of Elasticity*, Pergamon, Oxford

- [22] Lay T. and Wallace T.C., (1995) *Modern global seismology*, Academic press
- [23] Linear Technology[©] - <http://www.linear.com> (2008)
- [24] Linear Technology[©] LT1028, (1992) *Ultralow Noise Precision High Speed Op Amps* datasheet, rev. A
- [25] Liu J., (2000) *PhD Thesis*, University of Western Australia
- [26] Liu J., Ju L. and Blair D.G. (1997) *Vibration isolation performance of an ultra-low frequency folded pendulum resonator*, Physics Letters A, Elsevier, 228, (14 april 1997), pp.243-349
- [27] Liu J., Winterflood J. and Blair D.G. (1997) *Transfer function of an ultra-low frequency vibration isolation system*, Rev. Sci. Instrument., Vol. 66, No. 5, May 1995, pp.3216-3218
- [28] Marro G. (2004) *Controlli Automatici*, Bologna, Zanichelli Editore
- [29] Mencuccini C. and Silvestrini V. (1992) *Fisica I Meccanica Termodinamica*, Napoli, Liguori Editore
- [30] Milotti E. (1994) *Linear processes that produce 1/f or flicker noise*, Phys. Rev. E 51 pp.3087-3103
- [31] Nakayama Y. et al. (2004) *Performances test of STS-2 seismometers with various data loggers*, proceedings of IWAA2004, CERN, Geneva, 4-7 October 2004
- [32] Saulson P. R. (1990) *Thermal noise in mechanical experiments*, Physical Review D - Particles and fields, 3rd series, Vol. 42, No. 8, 15 october 1990, pp. 2437-2445
- [33] Stuart, T. et al. (1997) *Elliptical flexure hinges*, Review of Scientific Instruments 68 (3)

- [34] Tseytlin Y. M. (2002) *Notch flexure hinges: an effective theory*, Rev. Sci. Instrum., Vol. 73, No. 9, September 2002, pp. 3363-3368
- [35] Usher M.J., Burch R.F. and Guralp C. (1979) *Wide-band feedback seismometers*, Physics of the Earth and Planetary Interiors
- [36] Acernese F., De Rosa R., Giordano G., Romano R., Barone F., (2008) *Mechanical monolithic accelerometer for suspension inertial damping and low frequency seismic noise measurements*, Amaldi
- [37] Doebelin, E. O. (2005) *Strumenti e metodi di misura*, McGraw-Hill

Appendix A

Work hints

A.1 Structural specification of the folded pendulum

All the mechanical specification are summarized in the table A.1, in which we have indicated the physical characteristics of the system (dimension and weight of the most significative parts), while in the table A.2 the physical mechanical measurements on the prototype that reports some value in different configuration.

The mechanical open loop transfer function is reported in the section 2.3.1 with the comment on the method used for the measurements.

A.2 Spot light waist

We have measured the gaussian spot light waist of the SLED at different distance. Because of the presence of a light focuser collimator, the beam outcoming from the fiber is described by a “cone”, so the waist is depending from the optical distance between the collimator and the PSD surface. We have measured the dimension of

Material	Aluminum 7075/T6
Hinge type	elliptical, $\epsilon = 3.2$
Oscillating central mass	760 g
Pendulum mass	80 g
Inverted pendulum mass	72 g
Pendulum length (l_{p1})	81.5 mm
Inverted pendulum length (l_{p2})	81.5 mm
Pendulum arm length (l_1)	81.5 mm
Inverted pendulum arm length (l_2)	99.8 mm
Dimension	$140 \times 134 \times 40 \text{mm}^3$
Total weight	914 g

Table A.1: Mechanical specification of the realized prototype.

Frequency with no calibration mass	$721 \pm 1 \text{ mHz}$
Minimum reached resonance frequency	70 mHz
Vertical to horizontal coupling	$10^{-4} \div 10^{-3}$
Quality factor in air at $f_0 = 721 \text{ mHz}$	130 ± 10
Quality factor in air at $f_0 = 450 \text{ mHz}$	80 ± 10
Quality factor in air at $f_0 = 70 \text{ mHz}$	12 ± 1
Quality factor in vacuum (10^{-4} bar) at $f_0 = 450 \text{ mHz}$	500 ± 50

Table A.2: Mechanical behaviour.

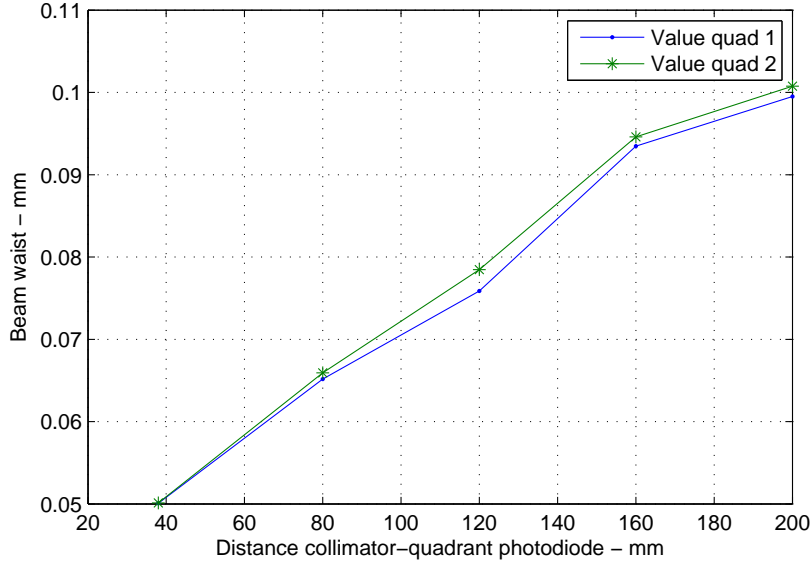


Figure A.1: *Incident spot light waist dimension.*

the spot light by using a quadrant photodiode, obtaining two different value (one for each quadrant) and the value is shown in figure A.1. The value of the waist is the width of the gaussian function that describe the incident spot light.

A.3 Cross talk of the electronic circuit

When the accelerometer was in the vacuum chamber, we have noted that the measurement was affected by great cross talk from the voice-coil signal. The effect is shown the figure A.2 in which we can see four graph that point out this problem. The variables $V1$ and $V2$ are the signal outcoming from the two transimpedance operational amplifier, V_{Coil} is the voltage signal sent to the voice-coil actuator (in this csae a white noise) and x is the position signal $(V1 - V2)/(V1 + V2)$ obtained following the equation 3.30 (see section 3.7).

On the upper-left of the figure we can see the transfer function (module and phase)

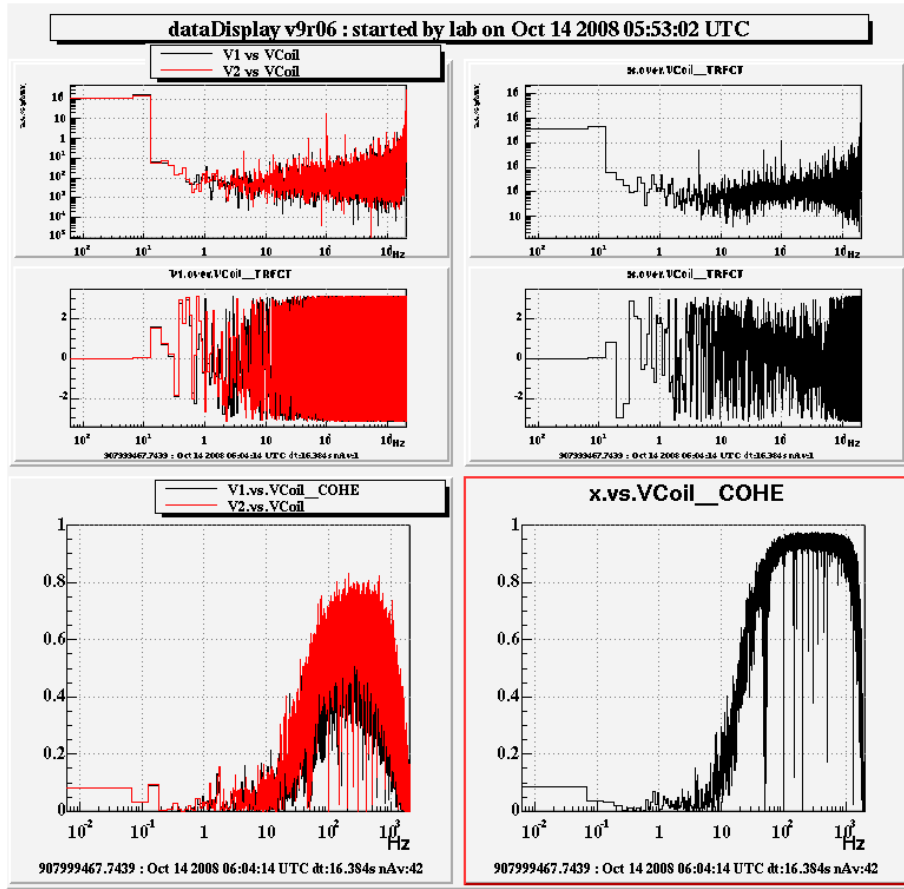


Figure A.2: *Transfer functions and coherence of various signal showing the cross talk between all the signal.*

V1 (and V2 in red) versus $VCoil$, while on the down-left the coherence of these two signal; on the upper-right the transfer function of x versus $VCoil$ and on the down-right the relative coherence. By a rapid analysis of the coherence we can see that upon the frequency of about 20 Hz we see that the coherence increase to 1 for all the signal, while the transfer function (that should be a simple horizontal line) has an increasing of the module upon 20 Hz and the phase (that should be a random distribution of the point) show a decreasing from π to 0 rad .

The problem was due to the cross talk from the cable of the voice-coil signal versus

the PSD cable signal, because in this type of measure, having the necessity to pass the cable into the vacuum chamber, we have made a vacuum connector that allow to pass the signal in and out the chamber, and the variuos cable was very near each other: this circumstance has created the pick up of the voice-coil signal (that have a great current) on the signal of the PSD.

The problem was been resolved by a new cabling with coaxial cable and BNC connector.

Acronym	Meaning
BB	Broadband, related to the frequency band of an instrument
FBA	Force Balance Accelerometer
FEA	Finite Elements Analysis
FP	Folded Pendulum
IC	Integrated Circuit
LED	Ligth Emitting Diode
NLNM	New Low Noise Model of the Peterson's noise model
OS	Operating System
Q	Mechanical Quality factor, see section 2.4
PID	Proportional-Integrative-Derivative automatic control design
SLED	Super Luminescent light Emitting Diode
SM	Single Mode
SP	Short Period, related to the frequency band of an instrument
TIA	TransImpedance operational Amplifier converter
VI	Virtual Instrument, a special application of <i>Labview</i> [20]
VBB	Very Broadband, related to the frequency band of an instrument

Table A.3: Less common acronyms used in this thesis work.

A.4 Acronyms

Less common acronyms used in this thesis work are shown in table A.3.

Appendix B

Mathematical hints

B.1 Transfer function of a PID feedback control

Given the the schema design of an analogic pid controller, shown in the figure B.1, where Z_a is the impedance on the inverting input

$$\begin{aligned}\frac{1}{Z_a} &= \frac{1}{Z_{R_{5a}}} + \frac{1}{Z_{C_{5a}}} \\ &= \frac{1}{R_{5a}} + \frac{1}{j\omega C_{5a}} \\ &= \frac{j\omega R_{5a}C_{5a} + 1}{R_{5a}}\end{aligned}\tag{B.1}$$

and Z_b the impedance on the feedback

$$\begin{aligned}Z_b &= Z_{R_{5b}} + Z_{C_{5b}} \\ &= R_{5b} + \frac{1}{j\omega C_{5b}} \\ &= \frac{j\omega R_{5b}C_{5b} + 1}{j\omega C_{5b}}\end{aligned}\tag{B.2}$$

we have

$$\begin{aligned}G(\omega) &= -\frac{Z_2}{Z_1} \\ &= -\frac{j\omega R_{5b}C_{5b} + 1}{j\omega C_{5b}} \cdot \frac{j\omega R_{5a}C_{5a} + 1}{R_{5a}} \\ &= -\frac{(1 + j\omega R_{5b}C_{5b})(1 + j\omega R_{5a}C_{5a})}{j\omega R_{5a}C_{5b}}\end{aligned}\tag{B.3}$$

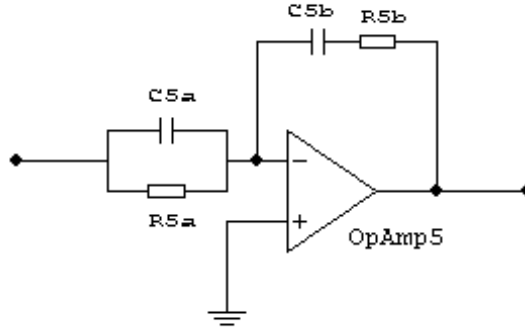


Figure B.1: *Electronic schema of an analog PID controller.*

By setting $s = j\omega$ we have that

$$\begin{aligned}
 G(s) &= -\frac{(1+j\tau_a)(1+j\tau_b)}{j\tau_c} \\
 &= -\frac{\tau_a(\frac{1}{\tau_1}+s)\tau_b(\frac{1}{\tau_b}+s)}{s\tau_c} \\
 &= -\frac{\tau_a\tau_b}{\tau_c} \frac{(\frac{1}{\tau_1}+s)(\frac{1}{\tau_b}+s)}{s} \\
 &= -\frac{R_{5a}C_{5a}R_{5b}C_{5b}}{R_{5a}C_{5b}} \frac{(\frac{1}{R_{5a}C_{5a}}+s)(\frac{1}{R_{5b}C_{5b}}+s)}{(s)} \\
 &= -R_{5b}C_{5a} \frac{(\frac{1}{R_{5a}C_{5a}}+s)(\frac{1}{R_{5b}C_{5b}}+s)}{(s)}
 \end{aligned} \tag{B.4}$$

where

$$\begin{aligned}
 \tau_a &= R_{5a}C_{5a} \\
 \tau_b &= R_{5b}C_{5b} \\
 \tau_c &= R_{5a}C_{5b}
 \end{aligned} \tag{B.5}$$

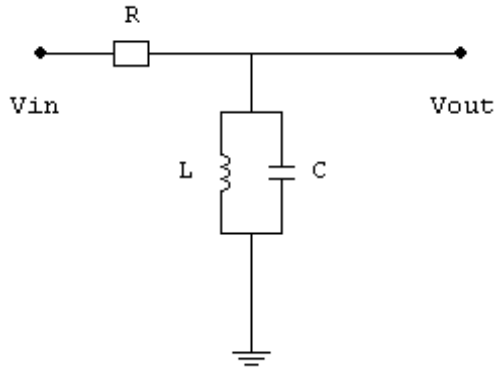


Figure B.2: *LC resonance circuit.*

B.2 Quality factor: an electric approach

Consider the circuit shown in figure B.2: it is an *RLC* circuits with an *LC* bandpass filter. The reactance of the *LC* part at frequency f is:

$$\frac{1}{Z_{LC}} = \frac{1}{Z_L} + \frac{1}{Z_C} = \frac{1}{j\omega L} + j\omega C = \frac{j}{\frac{1}{\omega L} - \omega C} = \frac{j\omega L}{1 - \omega^2 LC} \quad (\text{B.6})$$

from which we have that $Z_{LC} = \infty$ if $\omega = 1/\sqrt{LC}$. Considering the the combination of the *LC* part with *R* it forms a voltage divider: because of the opposite behaviors of the inductor and the capacitor the impedance of the parallel circuit *LC* goes to infinity at the *resonance frequency* $f_0 = 1/2\pi\sqrt{LC}$, giving a peak in the response at this frequency, as shown in figure B.3; obviously the same consideration are valid for the pulsation ω (*rad/s*) remembering that $\omega = 2\pi f$ (that is $\omega_0 = 1/\sqrt{LC}$).

Pratically the losses of the inductor and capacitor limit the sharpness of the peak; a *Q* spoiling resistor *R* is added to reduce the sharpness at resonance peak. This circuit is known as a parallel *LC* resonance circuit. The *quality factor Q* is

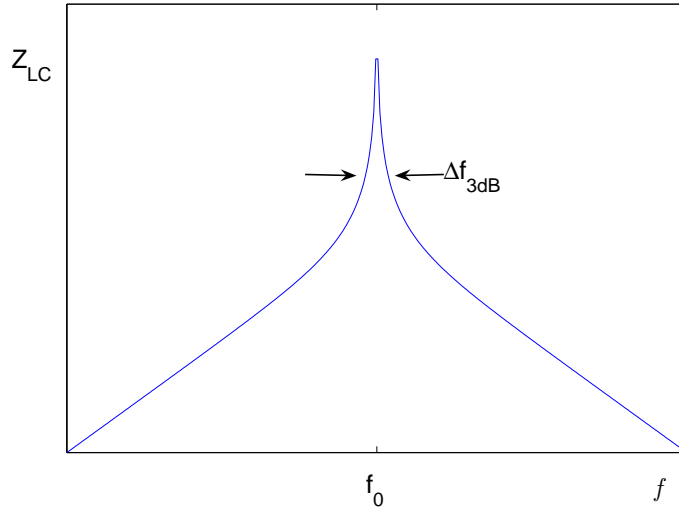


Figure B.3: *Peak of LC resonance circuit*

a measure of the sharpness of the peak and it is equal to the resonance frequency divided by the width of the the peak at the $-3dB$ points, $Q = f_0 / \Delta f_{3dB}$. So for a parallel RLC circuit $Q = \omega_0 RC$ [19].

B.3 The dB unity

The ratio of the power of two signal can be expressed in *bel* as

$$bel = \log \frac{P_2}{P_1}$$

where P_2 and P_1 are the two power. For example we can consider the case of the power dissipated by two resistor, where this ratio became:

$$bel = \log \frac{V_2^2/R}{V_1^2/R} = \log \frac{V_2^2}{V_1^2} = 2 \log \frac{V_2}{V_1}$$

The *bel* is a unity too big, so commonly is used the *decibel*, dB , so the ratio became:

$$1 dB \doteq 20 \log \frac{V_2}{V_1}$$

As we can see the decibel is a ratio so it is important to define a value as a reference for the ratio.

Commonly we use the decibel also to define the dynamics of a system; for example if we consider a 16 bit ADC, it has a dynamics equal to 96.33 dB ¹: in fact if we fix as 1 the more little number that we can represent with a such ADC (corresponding to the minimum value in volt that we want to digitize), the maximum number is $2^{16} = 65\,536$, so the ratio became:

$$20 \log \frac{65\,536}{1} \approx 96.33 \text{ dB}$$

In the same way we can say that a 18 bit ADC has a dynamics of 108.37 dB .

B.4 Equivalent noise band

Consider a linear system represented by a quadripole characterized by the transfer function

$$A(f) = \frac{V_o}{V_i}$$

where V_i is the input signal and V_o the output signal. Now consider a white noise whose spectral density is v_n in input to the quadripole (that we suppose with no noise); the effective value of the noise voltage on the output depends by the transfer function of the quadripole. Because of the uniform spectral density, the noise band of the system is not the band of the transfer function but it that of the ideal filter whose square tranfer function cover the same area of the square module of the quadripole transfer function (see figure B.4).

The effective value of the output noise of the filter is [30]

$$V_{no}^2 = \int_0^\infty |A(f)|^2 v_n^2 df = v_n^2 \int_0^\infty |A(f)|^2 df$$

¹This consideration assume that we use a PCM method and have an uniform quantization for the tension value.

Filter order	Noise band
1	$1.57 \cdot B$
2	$1.11 \cdot B$
3	$1.05 \cdot B$
4	$1.025 \cdot B$

Table B.1: Equivalent noise band and filter order

By substituting on ideal filter (low-pass or band-pass) whose equivalent band is B_{Eq} and gain in middle band A_0 , the effective value of the output noise is

$$V_{no,B}^2 = v_n^2 \cdot |A_0|^2 \cdot B_{Eq} \quad (\text{B.7})$$

where B_{Eq} is the equivalent band noise when $V_{no,B}^2 = V_{no}^2$, that is

$$B_{Eq} = \frac{1}{|A_0|^2} \int_0^\infty |A(f)|^2 df$$

So to evaluate the output noise of a linear filter that has on the input a white noise source [19] we must consider his equivalent noise band and the gain in the middle band, that is, from the equation B.7:

$$V_{no}^2 = v_n^2 \cdot |A_0|^2 \cdot B_{Eq}$$

where the band noise can be evaluate on depending of the filter order as indicated in the table² B.1

²Note from the table that when the order of the filter is higher the factor tends to 1 because the shape of the band tends to become rectangular

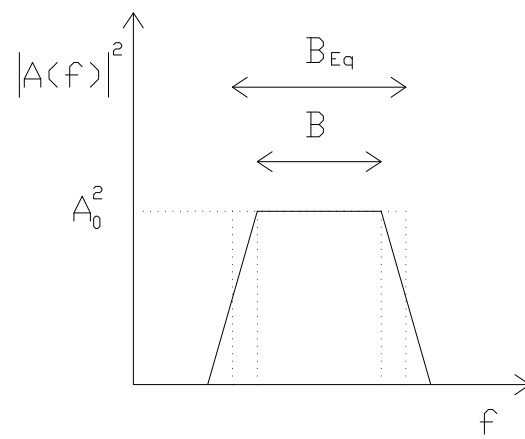


Figure B.4: *Equivalent band sketch.*

Ringraziamenti

Tanto per cominciare ringrazio tutti coloro che hanno collaborato direttamente e indirettamente a questo lavoro.

In particolare desidero innanzitutto ringraziare Emilia, per la pazienza avuta nel sopportarmi nei momenti difficili;

Fabrizio Barone, che con le sue battutine mi mette sempre di buon umore, e mi ha insegnato come si affrontano i problemi piu' disparati, come si risolvono e come gli si dá senso, stimolandomi a dare sempre il meglio di me stesso,

Leopoldo Milano per l'ottimismo e la rasserenazione che a ogni incontro mi ha sempre dato "che la pace sia con noi", oltre che per le dritte datomi nei momenti di indecisione,

Fausto Acernese per il suo continuo interessamento alla mia attività di ricerca,

Rosario De Rosa per la fiducia mostratami nonché Fabio Garufi per avermi aiutato a sciogliere tanti piccoli dubbi.

Non potrei non ringraziare i miei genitori che mi hanno aiutato appoggiando le mie scelte, mia nonna Caterina per i suoi saggi consigli, zio Antonio per avermi seguito sempre con interesse, la signora Punziano per i suoi panini, zia Carmela per la fiducia posta nelle mie iniziative, mia cugina Caterina per aver seguito le mie pratiche burocratiche, Barbara per avermi prestato il suo computer per scrivere parte di questo lavoro, Alfonso Boiano per il suo perenne interessamento alle mie attività tecnico-scientifiche oltre che per i preziosi discorsi fatti che mi hanno sempre culturalmente

arricchito, Angelo Marcone, per il suo ottimismo, per l'appoggio datomi, e per tutti i libri che mi ha prestato (e che prima o poi dovrò restituirgli!), Enzo Schiavo per avermi dato giusti consigli, Pierluigi per le sue meticolose analisi dei fatti, Italo Bastianelli per i suoi pazienti insegnamenti che mi hanno inconsapevolmente introdotto ai fenomeni oscillatori, Pino Passeggio per il suo sorriso nel vedermi impegnato in questa attività, Giacomo Sapere, Polti, Ferdinando e tutti i colleghi dell'ufficio per il loro supporto morale, ma soprattutto il mio gatto Tim, per avermi introdotto sorridendo allo studio della Fisica, che mi ha fatto capire che è meglio rilassarsi piuttosto che scervellarsi, perché se qualcosa è complicato vuol dire che la soluzione è altrove!

...e non se la prendano a male coloro che non ho menzionato, perché tutti hanno partecipato, chi piú chi meno, con le loro parole e con la loro presenza.